DEVELOPMENT OF THE ATOM LASER

MATTHEW JEPPESEN

A thesis submitted for the degree of
Doctor of Philosophy of The Australian National University

March 2009

Matthew Jeppesen: *Development of the atom laser*
A thesis submitted for the degree of
Doctor of Philosophy of The Australian National University

Previous page: atom laser oscillating as it falls downward in an angled waveguide.

DECLARATION

This is to certify that this thesis comprises only my original work, except where due acknowledgement has been made in the text, and has not been submitted in whole or in part for a degree in any university.

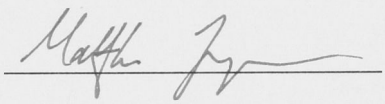

Matthew Jeppesen

Canberra, March 2009

Dedicated to my parents, Marianne and Peter

ACKNOWLEDGMENTS

There are some people I would like to thank ...

My supervisor, John Close. He has been an excellent teacher, a wise counsel, and a great boss.

Nick Robins has been my supervisor in the lab. Nick is an amazing experimentalist, always cheerful and helpful, and an all round inspiration.

Cristina Figl, who I have worked with in the lab since my first day, and who has been helping me since then too.

All the people in our group at the ANU, who have been great colleagues to work with, and who have become great friends: Simon Haine, Mattias Johnsson, Julien Dugué, Graham Dennis, Paul Summers, Oliver Topic, Paul Altin, Finnian Lattimore, Michael Hush, Rachel Poldy, John Debs, and Daniel Döring.

All the people at the ÉNS, who made my time in Paris so much fun and so rewarding: Antoine Couvert, Gaël Reinaudi, Renaud Mathevet, Thomasz Kawalec, Armin Ridinger, Thomas Salez, Gianluca Gattobiggio, and David Guéry-Odelin. I'll say it again: Vous êtes super les mecs!

All the people at the ANU who have particularly helped me over the years: Hans Bachor, Craig Savage, Ben Buchler, Joe Hope, Damien Hughes, Huma Cheema, Ruth Wilson, and Gaye Carney.

Russell Anderson, who has been a great colleauge and collaborator in cold atoms, ever since together we started to study them in Honours.

My family in Canberra: Trixie and Roger, who made me feel so welcome, and Barbara, Chris, Ed, Julia, and Joel, for helping me out so many times.

My brother and sister, Simon and Cara, and my parents, Marianne and Peter, for all you've done.

Zoe, for much love and support.

To all of you, thanks.

ABSTRACT

This thesis reports work on developing the atom laser as a tool for precision measurement.

The improved beam quality and reduced divergence of an atom laser produced by an optical Raman transition (compared to one produced by an RF transition) is demonstrated with both experimental and theoretical results. The improvement in the beam quality of the atom laser (M^2) is greater than a factor of 10 for experiments with tight trapping potentials (greater than $2\pi \times 300$ Hz). The analysis shows that Raman outcoupling can produce atom lasers whose quality is only limited by the wave function shape of the condensate that produces them, typically a factor of 1.3 above the diffraction (Heisenberg) limit.

Measurements have been done on the spatial mode of an optically guided and quasi-monomode atom laser, in all spin projection states ($m_F = -1, 0$ and $+1$) of $F = 1$ in rubidium 87. The atom laser source is a Bose-Einstein condensate (BEC) in a crossed dipole trap, purified to any one spin projection state by a spin-distillation process applied during the evaporation to BEC. The atom laser is outcoupled by an inhomogenous magnetic field, applied along the waveguide axis. The mean excitation number in the transverse modes is $\langle n \rangle = 0.65 \pm 0.05$ for $m_F = 0$ and $\langle n \rangle = 0.8 \pm 0.3$ for the low-field seeker $m_F = -1$.

A pumped atom laser has been produced. This involves coherently and irreversibly adding atoms to a Bose-Einstein condensate whilst an atom laser is outcoupled. Two spatially separated Bose–Einstein condensates of rubidium 87 in different internal hyperfine states were used, one providing a source of ultra cold atoms, and one acting as the lasing mode into which atoms were pumped.

PUBLICATIONS

The articles indicated by ⟨ have been particularly emphasised in this thesis.

⟨ M. Jeppesen, J. Dugué, G. D. Dennis, C. Figl, N. P. Robins, and J. D. Close. Approaching the Heisenberg limit in an atom laser. *Physical Review A*. 77:063618, 2008

⟨ N. P. Robins, C. Figl, M. Jeppesen, G. D. Dennis, and J. D. Close. A pumped atom laser. *Nature Physics*, 4(9):731–736, 2008.

⟨ A. Couvert, M. Jeppesen, T. Kawalec, G. Reinaudi, R. Mathevet, and D. Guéry-Odelin. A quasi-monomode guided atom-laser from an all-optical Bose-Einstein condensate. *EPL (Europhysics Letters)*, 83(5):50001, 2008.

J. Dugué, G. Dennis, M. Jeppesen, M. T. Johnsson, C. Figl, N. P. Robins, and J. D. Close. A multibeam atom laser: Coherent atom beam splitting from a single far-detuned laser. *Physical Review A*, 77:031603, 2008.

J. Dugué, N. P. Robins, C. Figl, M. Jeppesen, P. Summers, M. T. Johnsson, J. J. Hope, and J. D. Close. Investigation and comparison of multistate and two-state atom laser-output couplers. *Physical Review A*, 75(5):053602, May 2007.

M. Johnsson, S. Haine, J. Hope, N. Robins, C. Figl, M. Jeppesen, J. Dugué, and J. D. Close. Semiclassical limits to the linewidth of an atom laser. *Physical Review A*, 75(4):043618, 2007.

N. P. Robins, C. Figl, S. A. Haine, A. K. Morrison, M. Jeppesen, J. J. Hope, and J. D. Close. Achieving Peak Brightness in an Atom Laser. *Physical Review Letters*, 96(14):140403, 2006.

C. Figl, L. Longchambon, M. Jeppesen, M. Kruger, H. A. Bachor, N. P. Robins, and J. D. Close. Demonstration and characterization of a detector for minimally destructive detection of Bose condensed atoms in real time. *Applied Optics*, 45:3415–3419, May 2006.

CONTENTS

LIST OF FIGURES

LIST OF TABLES

ACRONYMS

AOM	acousto-optic modulator
BEC	Bose-Einstein condensate
EIT	electromagnetically induced transparency
GP	Gross-Pitaevskii (equation)
MOT	magneto-optical trap
RF	radio frequency
RMS	root-mean-square ($\sqrt{\langle x^2\rangle - \langle x\rangle^2}$)
TOF	time of flight
TOP	time-orbiting potential (magnetic trap)
QUIC	quadrupole Ioffe configuration (magnetic trap)
UHV	ultra high vacuum (pressure less than 10^{-10} torr)
WKB	Wentzel–Kramers–Brillouin (approximation)

INSTITUTIONS

ACQAO	Australian Research Council Centre for Quantum-Atom Optics
ANU	Australian National University
ÉNS	École Normale Supérieure
ISO	International Organization for Standardization

LCF	Laboratoire Charles Fabry (de l'Institut d'Optique)
LKB	Laboratoire Kastler Brossel
JPL	Jet Propulsion Laboratory at the California Insitute of Technology
MIT	Massachusetts Institute of Technology
NIST	National Insitute of Standards and Technology

INTRODUCTION

1

INTRODUCTION

An *atom laser* is a beam in which many atoms occupy a single quantum mode, just as an *optical laser* is a beam of light in which many photons occupy a single quantum mode. As a consequence, both may be approximated as a classical wave with well-defined amplitude and phase, and both have similar quantum statistics and the properties of brightness, directionality, coherence. These properties, and others such as their mass and sensitivity to electromagnetic fields, give atom lasers great potential to be useful in precision measurement, and in studies of fundamental physics (as optical lasers have already been). However, the techniques to produce and manipulate atom lasers have not yet been sufficiently developed. This thesis describes work on improving the spatial mode and flux of atom lasers, and on producing a pumped atom laser, with the goal of making precision measurements.

~

Precision measurement is important. Where you are now, where you are going to, how fast you are going there, how much time has elapsed, even what gravitational and electric and magnetic fields you are travelling through: the ability to measure all these leads to technologies that improve our lives, and improve our understanding of the natural world.

For instance, the precision measurement of position and velocity provided by navigation satellites, such as the Global Positioning System (GPS),

make it possible for millions of people to fly around the world every day in safety and comfort. These systems rely for their function on the precision measurement of time, provided by atomic clocks [1].

Another instance is the advance in medical research through improved imaging techniques, such as Magnetic Resonance Imaging (MRI). This relies on the precision measurement of many quantities including magnetic fields [2]. Yet another instance is the detection of valuable minerals, buried far below the Earth's surface, more easily, cheaply, and without the need for drilling, made possible through the precision measurement of gravitational gradients with remote sensing aircraft [3].

This thesis concentrates on developing a particular technology, *atom lasers*, for use in precision measurement, through the technique of *atom interferometry*. Atom lasers have potential for use in several types of precision measurement, including the measurement of:

- rotations,
- accelerations,
- magnetic fields,
- gravitational fields, and
- the gradients of all those fields.

The remainder of this introduction will give some background to both atom lasers and atom interferometry.

1.1 ATOM LASERS

What is an atom laser? And in what sense is it a laser?

To answer these questions, it is necessary to define a laser. This is not easy to do; there is no universally accepted definition. Different physicists hold different opinions about what the definition should be and what features are and are not essential. The reasons for this are partly historical; as lasers have developed, so the definition has broadened and changed.

The definition of a laser (atomic or optical) adopted in this thesis is that proposed by Howard Wiseman, who argued that the definition of a laser should rely upon the properties of the beam itself, not upon the type of particles which comprise it, nor upon the internal structure of the system that produces it. Wiseman proposed that a laser be defined as a beam with a large number of bosons in a single mode, so that:

> the output of a laser is well approximated by a classical wave of fixed intensity and phase [4].

The properties of directionality, brightness, monochromaticity, coherence, and quantum statistics, are either direct consequences of this or are in part derived from it. Therefore, these features are shared by both optical lasers and atom lasers.

Currently, typical atom lasers contain about one million atoms, and range in length from several microns to several meters. Their transverse spatial mode ranges from gaussian in the ideal case, to any combination of hermite-gaussian modes. Figure 1.1 shows absorption images of atom lasers, created by illuminating the atoms with resonant light and recording the shadow of the atoms produced as they scatter the light.

Many of the well known features of an optical laser have a counterpart in an atom laser. This is because they share the same defining feature—many bosons in a single mode—and to produce this requires a similar structure in both cases. For example, optical lasers have as their source a resonator (a cavity), usually two or more highly reflective mirrors, inside which there is an intense electromagnetic field, with many photons in an eigenmode of the cavity. For light, this eigenmode is a highly excited mode of the cavity. This has its analogy in the source of the atom laser, which contains many atoms in the ground state eigenmode of a confining potential. An optical laser leaves the cavity through partially reflective mirrors, which allow some light to leak out without changing the mode. This has its counterpart in the process which transfers atoms from the confining potential to the beam. Some features of an optical laser are not present (such as a population inversion). All of features, similar and dissimilar, are merely useful for arriving at the output beam, not a defining feature of the laser itself. The important detail—the chief reason why optical lasers have been so successful in precision measurement, and why atom lasers have such great potential—is that, again, each contains a large number of bosons in a single mode (or a small number of modes), and is well approximated by a classical wave.

All atom lasers produced so far have used a Bose-Einstein condensate (BEC) as their source, including those developed for this thesis. There is a good reason for this. As discussed above, an atom laser needs many atoms in one quantum mode. Conveniently, this is what occurs when a BEC is created. The process of extracting the atom laser from the BEC (known as outcoupling) then needs only to preserve this concentration of atoms in a single mode, not create it.

1.2 BOSE-EINSTEIN CONDENSATES

The phenomenon of Bose-Einstein condensation was first predicted by Albert Einstein in 1925, using theoretical ideas developed by Satyendra Bose. It occurs when the size of the atomic de Broglie wavelength becomes comparable to the average spacing between atoms, so that the average number of particles in each quantum state (the phase space density) becomes of order unity. When this happens, the thermally accessible states of the system become saturated, and all excess density accumulates in the ground state. Einstein described it in this way:

> For each temperature, there exists a saturation density of the ideal quantum gas, such that molecules in excess of this density do not participate in the thermal agitation [5].

More precisely, for ideal gases in free space, condensation occurs when:

$$\left(\frac{\lambda_{\text{DB}}}{d}\right)^3 = \zeta(3/2) \approx 2.612, \tag{1.1}$$

where,

λ_{DB}	is the thermal de Broglie wavelength ($h/\sqrt{2\pi m k_B T}$),
$d = \rho^{-1/3}$	(where ρ is the density) is the average spacing between atoms,
ζ	is the Riemann zeta function; and where
m	is the mass of the atom,
k_B	is Boltzmann's constant,
h	is Plank's constant,
T	is the absolute temperature.

BEC was first achieved in 1995 by Carl Wieman, Eric Cornell and coworkers at JILA in Boulder, Colorado [11]. Later that year, Randall Hulet and coworkers at Rice, and Wolfgang Ketterle and coworkers at MIT, also created BECs [12–14]. In 2001, Wiemann, Cornell, and Ketterle of MIT received the Nobel prize for the achievement of Bose-Einstein condensation, and for important early experiments with the condensates themselves [15, 16].

BECs proved an exciting new material for study. Below are listed a number of the important experiments which examined and revealed their properties.

- Matter wave interference fringes from two expanding BECs were measured by Andrews et al., demonstrating the coherence of condensates [17].

- Matter wave amplification in a condensate from an input pulse atoms was demonstrated by Kozuma et al. and Inouye et al. [18, 19].
- The role of bosonic stimulation in the formation of the condensate was demonstrated by Miesner et al. [20].
- Non-linear atom optics effects in a condensate were demonstrated in the 4-wave mixing experiment by Deng et al. [21].
- Vortex lattices were observed by Abo-Shaeer et al. [22].
- The connection to condensed matter physics was demonstrated by experiments with optical lattices, such as the phase transition to a Mott insulator state [23].

Experimental realisation of atom lasers

The thesis describes the use of BECs as a source for atom lasers. The first atom laser was produced two years after the first production of BEC, by Mewes et al. in the group of Wolfgang Ketterle at MIT [6]. (See Figure 1.1). They used short pulses of radio frequency (RF) radiation, the frequency of which was swept through a resonance between the trapped condensate state $m_F = -1$ and the untrapped states. The proportion of atoms transferred depended on the pulse power and the speed of the sweep: transfer of more than 50% to $m_F = 0$ and 100% to $m_F = +1$ was achieved.

The advantage of a sweep scheme is that fluctuations in the magnetic trap have little effect, provided that the resonant frequency remains inside the sweep range. To produce a quasicontinuous or long pulse atom laser (where the energy width of the pulse is much less than that of the condensate) required a very stable magnetic trap. Such an atom laser was first achieved by Bloch et al. in the group of Tilman Esslinger at Max Planck Garching [8]. (See Figure 1.1). They used a highly stable magnetic QUIC trap, which permitted the use of a constant RF outcoupling frequency [24].

It is also possible to use a two photon Raman transition to outcouple an atom laser, which gives the atoms a momentum kick, resulting in improved spatial mode and increased brightness. The first (pulsed) Raman atom laser was reported by Hagley et al. in the group of Bill Phillips at NIST [9]. (See Figure 1.2). They used fast pulses of light to outcouple atoms from a TOP trap, timing the pulses of light to the motion of the trap (which had a magnetic bias field rotating at 20 kHz). The first quasicontinuous Raman atom laser was reported by Robins et al. in our group at the ANU [10]. (See Figure 1.2). Again, a highly stable magnetic trap permitted a constant outcoupling resonant frequency to be used.

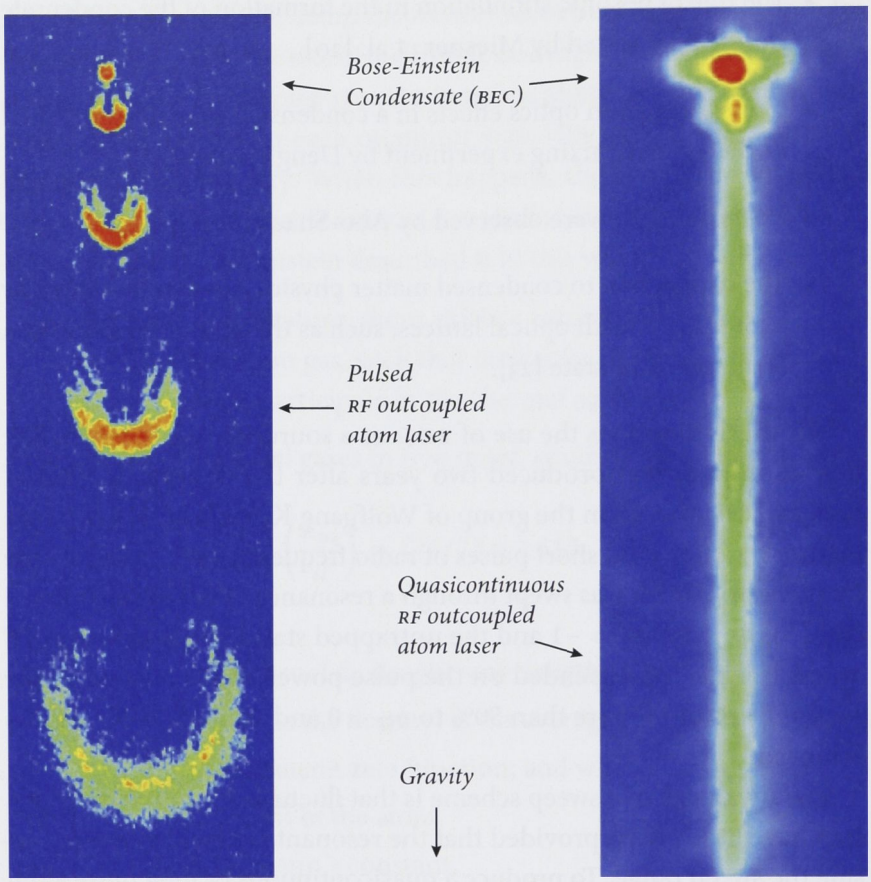

Mewes et. al., MIT 1997 *Bloch et. al., Munich 1999*

Figure 1.1: *Left:* Pulsed RF outcoupled atom laser produced by Mewes et al. (1997). Figure adapted from Reference [7]. *Right:* Quasicontinuous (long pulse) RF outcoupled atom laser produced by Bloch et al. (1999). Figure adapted from Reference [8]. These are false colour absorption (shadow) images. The different colours represent different atomic densities, with increasing density from green to yellow to red to white.

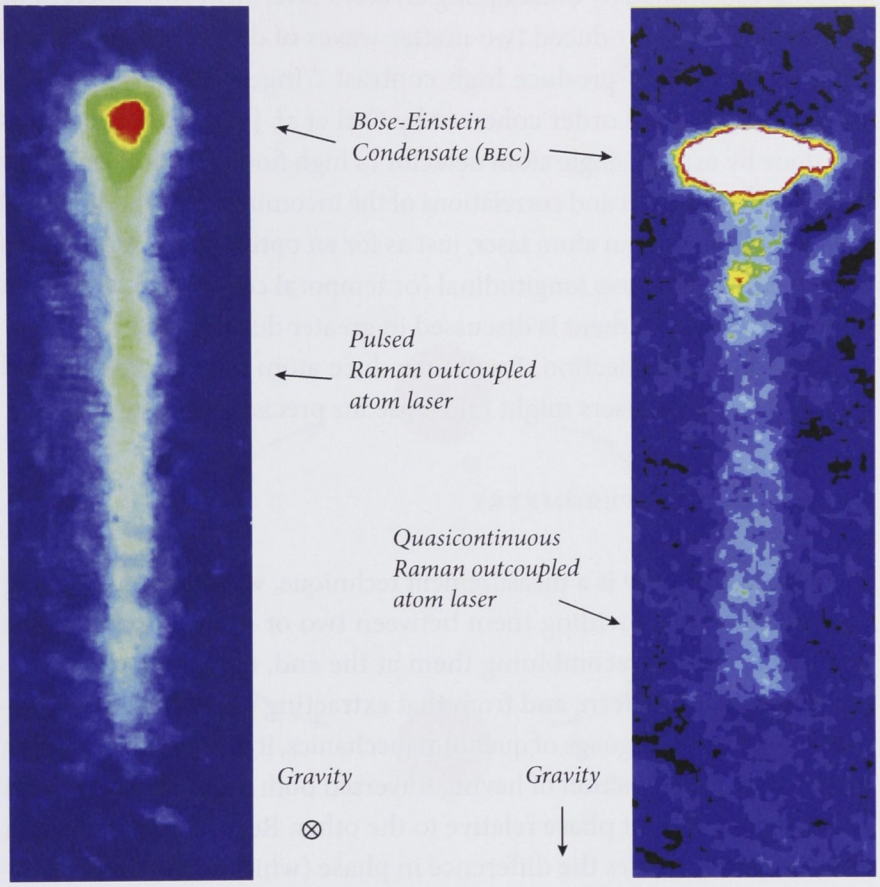

Hagley et. al., NIST 1999

Robins et. al., ANU 2006

Figure 1.2: *Left:* Pulsed Raman outcoupled atom laser produced by Hagley et al. (1999). Gravity is in the plane of the image. Raman outcoupling gives atoms an intitial momentum kick (§2.5), in this case the kick was was horizontal in direction. The outcoupling pulses were applied in rapid succession (at the 20 kHz frequency of the rotating magnetic bias field of the TOP trap) and so gaps between the pulses are not observable. Figure adapted from Reference [9]. *Right:* Quasicontinuous (long pulse) Raman outcoupled atom laser produced by Robins et al. (2006). The momentum kick was downwards in direction and the image is normally oriented (gravity is down). Figure adapted from Reference [10]. These are false colour absorption (shadow) images. The different colours represent different atomic densities, with increasing density from green to yellow to red to white.

Several experiments have confirmed important theoretical predictions about atom lasers, and demonstrated their potential. They include the demonstration of atom lasers to be first order coherent by Bloch et al. [25]. This was established by outcoupling an atom laser with two different RF frequencies. This produced two matter waves of different wavelengths which interfered to produce high contrast fringes. Atom lasers were shown to be second order coherent by Öttl et al. [26]. The experiment was done by using a single atom detector (a high finesse optical cavity) to measure the statistics and correlations of the incoming beam, and showed that $g^{(2)}(\tau) = 1$ for an atom laser, just as for an optical laser. Atom lasers were measured to have longitudinal (or temporal coherence) by Kohl et al. [27]. (This experiment is discussed in greater detail in §8.1.)

In the following section, I will introduce atom interferometry, and explain how atom lasers might find a use for precision measurement.

1.3 ATOM INTERFEROMETRY

Atom interferometry is a measurement technique, which involves taking a group of atoms, dividing them between two or more possible paths through a system, recombining them at the end, observing the resulting interference pattern, and from that extracting the desired measurement [28]. In the language of quantum mechanics, it is said that the atoms enter into a superposition of having traversed both paths, with one path acquiring a different phase relative to the other. Recombination, when done correctly, causes the difference in phase (which is not directly observable) to become a difference in another quantity which is observable. For instance, the relative number of atoms in two distinct quantum states. The two "paths" need not be physical trajectories through space, but may be any suitable internal or external quantum states.

Atom interferometry has already been very successful in the measurement of time. Beginning with the method of separated oscillatory fields, for which Norman Ramsey received the Nobel prize in 1989, atomic clocks have provided the most accurate measurement of time [29, 30]. Atomic clocks are the now accurate to one part in 10^{16} [31], have led to the redefinition of the second, and they have allowed development of such technology as satellite navigation systems and GPS [1].

Atom interferometry can be used to measure more than time. Lenef et al. have made measurements of rotations [32]. For rotations, interferometers with atoms would have a sensitivity of 11 orders of magnitude greater than those with light, if each had the same detector area and rate of flux. At the present, however, optical lasers can achieve typically 7

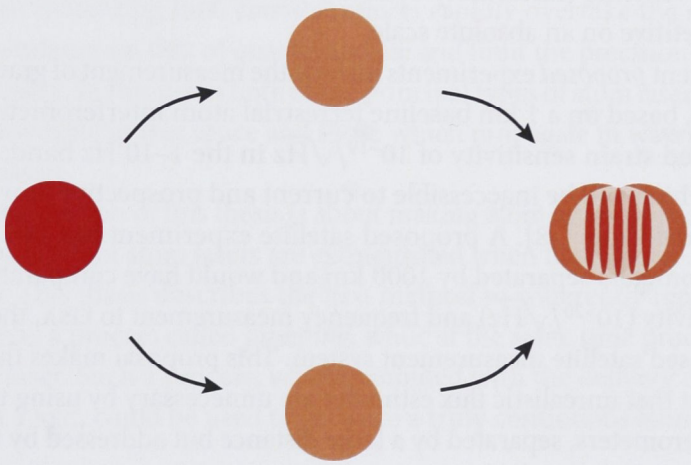

Figure 1.3: General principle of atom interferometry. A group of atoms is coherently divided between two or more possible paths through a system, such that the effect being measured affects the phase of one differently to the other. They are coherently recombined at the end, the resulting interference pattern observed, and from that the desired measurement is inferred. The two "paths" need not be physical trajectories through space, but may be any suitable internal or external quantum states.

orders of magnitude greater area and more than 10 orders of magnitude greater flux; nevertheless, the potential exists and this may change as atom lasers develop [28]. Because of their mass, atoms are useful for measurements of gravitational fields. Peters et al. have used atom interferometry to measure the local gravitational field g with a sensitivity of $2 \times 10^{-8}\, g/\sqrt{\text{Hz}}$ [33, 34]. Gravitational gradients have been measured to a sensitivity of $4 \times 10^{-9}(g/\text{m})/\sqrt{\text{Hz}}$ [35, 36]. Atoms are also sensitive to magnetic fields. Vengalattore et al. have used a spinor condensate to measure magnetic fields with sensitivity of 8.3 $\text{pT}/\sqrt{\text{Hz}}$ over an area of 120 μm^2 [37]. This is already an improvement over SQUID magnetometers for small measurement areas, and the group has proposed several improvements (faster duty cycle etc.) so that the sensitivity would be competitive on an absolute scale.

Recent *proposed* experiments include the measurement of gravitational waves, based on a 1 km baseline terrestrial atom interferometer, with a planned strain sensitivity of $10^{-19}/\sqrt{\text{Hz}}$ in the 1–10 Hz band, frequencies which will be inaccessible to current and prospective gravitational wave detectors [38]. A proposed satellite experiment has two atom interferometers separated by 1000 km and would have comparable strain sensitivity ($10^{-20}/\sqrt{\text{Hz}}$) and frequency measurement to LISA, the current proposed satellite measurement system. This proposal makes the crucial insight that unrealistic flux estimates are unnecessary by using two atom interferometers, separated by a large distance but addressed by the same laser.

With all atom interferometers, the more atoms used, the greater the measurement precision will be. This is because with all these measurements, the signal is proportional to the number of atoms. The noise is usually proportional to the square-root of the atom number (unless the quantum statistics of the source have been altered by squeezing). Therefore the all important signal-to-noise ratio is also proportional to the square-root of the atom number. Because of this, thermal atoms have been used until now, because of their greater flux of atoms compared to BEC and atom laser sources.

One problem, however, with current devices is the large velocity spread of the thermal atomic sources used. A key feature of these devices is the large momentum beam splitter (using Bragg diffraction) giving up to 24 photon recoils to the atoms [39]. The chief benefit of the large momentum kicks is the long measurement time that is made possible. These beam splitters have a very narrow velocity resonance, meaning that only a small fraction of the large thermal atom flux is addressable. The proposed next

generation devices will use Bose condensed sources because of their low (Heisenberg limited) momentum spread.

1.4 ABOUT THIS THESIS

The first two sections of this thesis describe improvements to the spatial mode of atom lasers. The *spatial mode* refers to the physical form of the quantum state: the wavefunction for atom lasers or the electric field for optical lasers. A good spatial mode may be a "classical" effect (it concerns single-particle quantum mechanics) but for atom interferometry it is an important one. Classical effects contribute noise that scales linearly with flux. With increasing flux, classical effects rapidly overtake the square root dependence on flux of quantum noise and limit the precision of any measurement. In this thesis both of the principal types of atom laser, those which propagate in free space and those which propagate in waveguides, are discussed.

The final section of this thesis is about making atom lasers operate continuously. Current atom lasers are extinguished when their source, a BEC, is empty. This thesis describes the first method to coherently replenish that source, a process called *pumping*, while at the same time producing an atom laser. Such a process, when combined with the delivery of cold atoms to a BEC, could be used to produce a truly continuous atom laser.

Part I

FREE SPACE ATOM LASERS

2

SPATIAL MODE

In this chapter I, discuss the spatial mode of atom lasers. I consider these questions:

A. Why is the spatial mode important?

B. How can this be quantified?

C. Is it currently a problem?

D. How may it be improved?

2.1 WHY IS THE SPATIAL MODE IMPORTANT?

A physics experiment may be done for one of two reasons. It may be done to observe some new phenomenon, and learn something fundamental about nature. In this case, it is necessary that the magnitude of the phenomenon be greater than the magnitude of the noise, so that the phenomenon may be successfully observed and correctly identified. The extent to which it is greater, however, is not important.

An experiment may also be done in order to know a particular quantity precisely. This may be of fundamental interest, such as the charge of an electron, or it may be of practical interest, such as a person's current position and velocity. For a precision measurement, the fundamental consideration is the *sensitivity* of the measurement: that is, the level of

exactness to which the particular quantity may be determined. The sensitivity of a measurement is determined by the relative magnitude of the signal derived from this quantity and of the background noise: the *signal-to-noise ratio*.

The reason that the spatial mode of an atom laser beam — or an optical laser beam — is important is because it affects the sensitivity of any measurement made with that beam. It is true that this is a "classical effect" (it concerns single particle quantum mechanics). Classical sources of noise are sometimes considered less fundamental than quantum sources of noise, such as the quantum number fluctuations of the beam (the *shot noise*). However, the experimenter's goal is simply to maximise the signal-to-noise ratio of the measurement. Standard quantum noise scales with the square root of the flux, and classical noise scales linearly with the flux. As flux increases, classical effects quickly become the dominant source of noise, and therefore it is important to be able to deal with them.

A quantitative discussion

I will now discuss this in a more quantitative way. Consider an interferometric measurement made with N particles (atoms or photons) divided equally between two beams. The signal is:

$$\text{Signal} = V\phi N, \tag{2.1}$$

where ϕ is the phase (this is the limit for small phases) and V is the fringe visibility, which quantifies how well the two beams are mode matched to each other. This is discussed in more detail below, but briefly, is 1 if the mode matching is perfect, it is 0 if the two beams do not interfere at all (for example, if they have orthogonal electric field polarisations (for optical lasers), or are physically separated from one another), or it may be any value in between.

What is the magnitude of the noise in such a measurement? Let us imagine that there are two main sources of noise. First, that the source has conventional Poissonian number fluctuations (quantum shot noise) and is not squeezed. The magnitude of the noise due to these fluctuations will therefore be $\sqrt{N}$. Second, let us imagine that, during the measurement, the position of one beam fluctuates with respect to the other by a displacement d which is perpendicular to their propagation. This displacement could be due to a mirror moving (for optical lasers) or fluctuating magnetic fields (for atom lasers) or indeed many possible reasons. Other than this fluctuating displacement, the spatial modes of the two beams are identical. The visibility V will therefore be a function only of the displacement, $V = V(d)$.

Let us further imagine that the interferometer can be aligned to oscillate around the position of ideal mode matching, that is $\langle d \rangle = 0$. Therefore $\langle V \rangle = 1$, and the first derivative of V with respect to the displacement is zero (since it is at a maximum), but the second derivative is not. The magnitude of the noise due to this displacement is therefore $(1/2)(\partial^2 V/\partial d^2)(\Delta d)^2 \phi N$ where $(\Delta d)^2$ is the variance in the displacement. Since the two noise sources (shot noise and shaking noise) are uncorrelated, we shall add their magnitudes in quadrature. The total signal-to-noise ratio is therefore:

$$\frac{\text{Signal}}{\text{Noise}} = \frac{\phi N}{\sqrt{\left(\frac{1}{2}\frac{\partial^2 V}{\partial d^2}(\Delta d)^2 \phi N\right)^2 + N}}. \tag{2.2}$$

There are therefore two limits to be considered, that of large and small particle number (or large and small flux — in this thesis I often refer to particle number as flux, because it is clear and concise, with the understanding that there is certain measurement time involved which would determine the bandwidth.) In these two limits, the signal-to-noise ratio is:

$$\frac{\text{Signal}}{\text{Noise}} = \begin{cases} \phi\sqrt{N}, & N \text{ small} \\ 1/\left(\frac{1}{2}\frac{\partial^2 V}{\partial d^2}(\Delta d)^2\right), & N \text{ large} \end{cases} \tag{2.3}$$

Note that in the large N regime, the signal-to-noise ratio is independent of the flux and also of the signal strength. For a given variance in the displacement, it depends only on $\partial^2 V/\partial d^2$. An ideal beam for this type of measurement, therefore, would have a spatial mode where the visibility did not change greatly with displacement, that is where $\partial^2 V/\partial d^2$ was small. Of course, the quantity $\partial^2 V/\partial d^2$ is not a complete description of the spatial mode quality of a beam. It describes only how easy it is to mode match a beam with itself—in general, two different beams with different spatial modes would be used. They would have a $\partial^2 V/\partial d^2$ when interfered together which would be different from that which they would have when each was interfered with itself. (However, it is *likely* that two beams each with a high (or low) $\partial^2 V/\partial d^2$ would also have a high (or low) $\partial^2 V/\partial d^2$ between them.) The maximum visibility is also not 1 in general between two different beams. Furthermore, it is artificial to consider only one type of modematching problem, such as the simple transverse displacements considered here. In general, such fluctuations would be a combination of longitudinal, transverse, and rotational displacements,

as shown in Figure 2.1. There exists no general way to quantify all these different fluctuations, but there is a single figure of merit which helps to classify them, and which helps to predict the usefulness of a beam in a precision measurement. It is the beam quality parameter M^2, and it indicates how far the beam differs from the minimum uncertainty state. I will define this quantity properly in §2.3 and discuss it in detail in §3.3. Before that, however, I will examine the case of two gaussian optical laser beams interfering, as it develops the above ideas further and elucidates several interesting and useful facts about inteferometery.

Poor modematching reduces the effective flux

There is one further point about spatial mode worth mentioning. If the two modes are different, so that perfect modematching is not possible, and the visibility V is less than one, then this is equivalent to reducing the flux by a factor V^2. That is, it reduces the signal by a factor of V, but all the flux of the beam contributes to the shot noise, so the noise remains $\sqrt{N}$, giving a signal-to-noise ratio of $V\phi\sqrt{N}$, the same as for perfectly modematched beams with flux V^2N.

2.2 AN EXAMPLE WITH OPTICAL LASER BEAMS

Some motivation

Before I present the results on atom laser beam profiles, I would like to present a short example to motivate this discussion, which fully works through the mathematics presented in brief above. This example demonstates a surprising fact about spatial modes, which is true for both optical laser beams and atom laser beams: that even though the width of a diverging beam grows larger and larger as it propagates, the absolute amount of misalignment possible for a given sensitivity *does not change*. If two laser beams with waists of 50 microns were used to make an inteference measurement, with the detector located at the position of their waists, one would obviously need to physically overlap the two beams to within a tolerence smaller than their waist—that is, to a tolerance less than 50 microns. But even if the detector was placed at a distance from the waist, so that each beam had expanded to a width of 1 meter, the two beams would still need to be overlapped to within the same tolerance—less than 50 microns! Again, this is true for both optical lasers and atom lasers. Note that using a lens to increase the waist of a beam (atomic or optical) *does* does increase the tolerance on modematching: it is always the beam waist, not the size at any particular point in the beam propagation that is important.

Let us now perform a thought experiment, the purpose of which is to measure the phase difference ϕ between two imaginary optical laser beams. The two beams are modematched together on a 50-50 beam

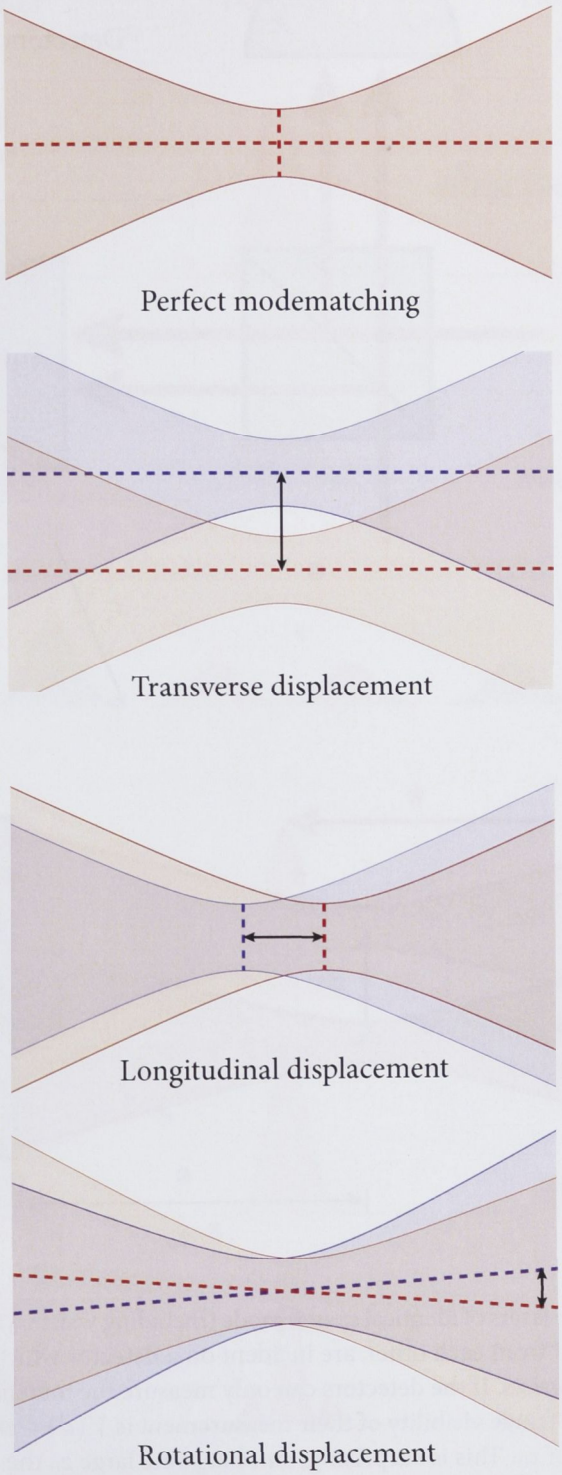

Figure 2.1: Different possible modematching problems. In general, an experiment would experience all of them simultaneously to some degree.

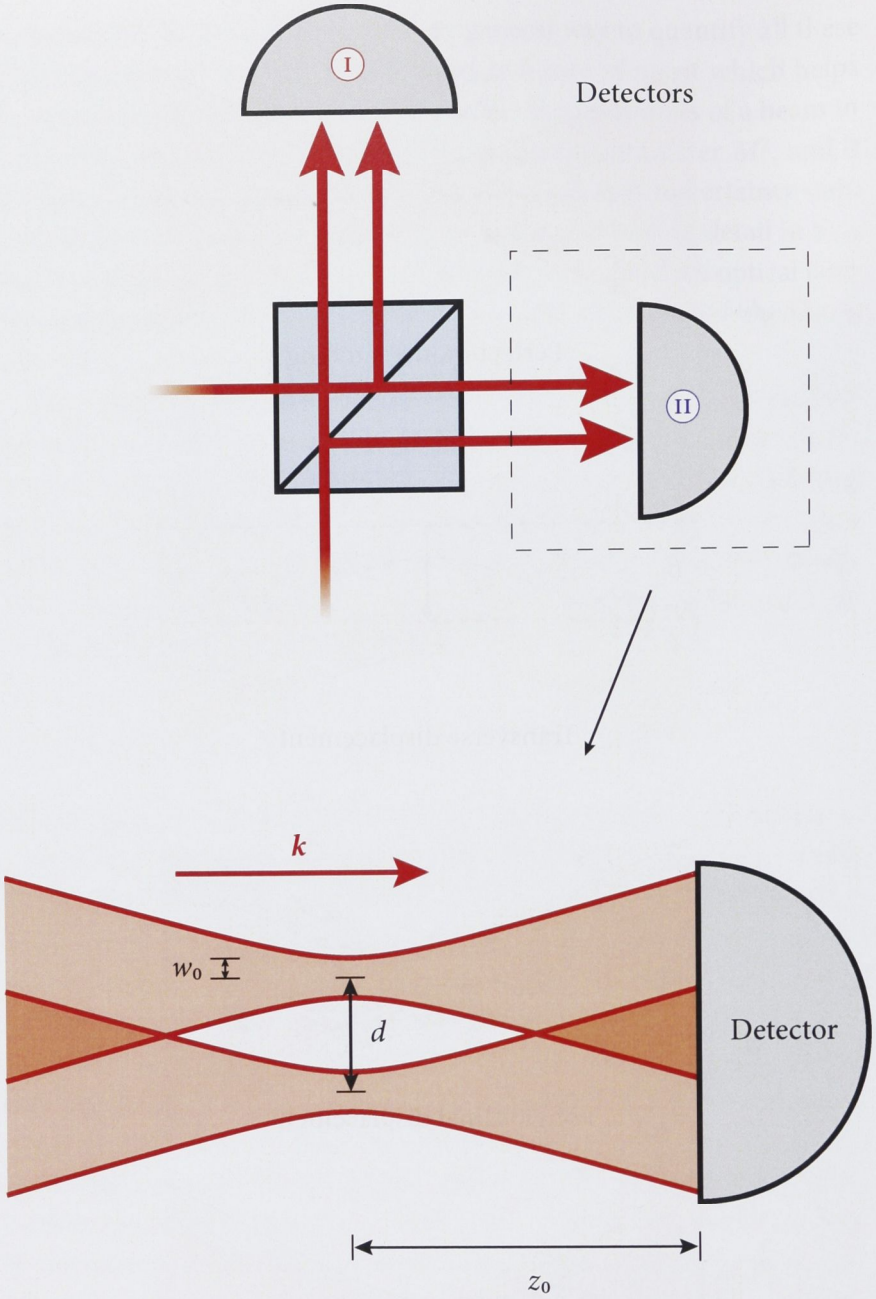

Figure 2.2: Two lasers of identical spatial mode (including waist w_0) but displaced by a distance d from each other, are incident on a detector which is a distance z_0 from their waists. If the detectors can only measure the total power incident on them, then fringe visibility of their measurement is $V(d) = \exp(-\frac{1}{2}d^2/w_0^2)$, independent of z_0. This is surprising, since at some large z_0 the displacement could be a tiny fraction of the widths of the beams at that point (yet still larger than w_0), so that the beams appeared to be completely overlapped and yet the fringe visibility would be negligible. The top part shows the lasers, beam splitter cube and both detectors. The bottow part shows a detail of the beams incident on one detector.

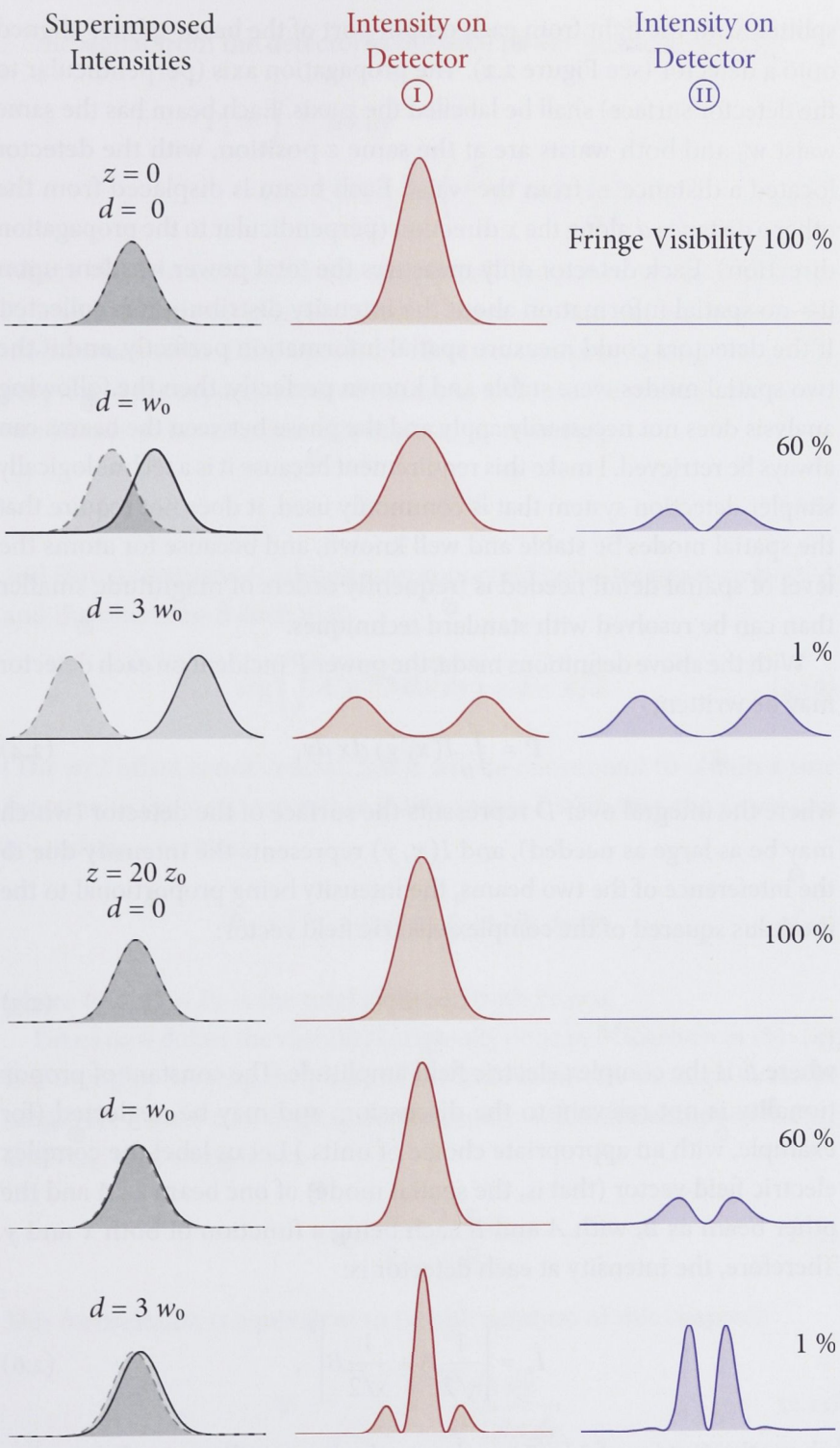

Figure 2.3: Invariance of visibility to propagation distance. The fringe visibility for all combinations of $d \in \{0, w_0, 3\,w_0\}$ and $z \in \{0, 20\,z_0\}$ are shown. The interference pattern on each detector is shown for the case $\phi = 0$ (for $\phi = \pi$, it is the same but with detectors swapped). The fringe visibility is therefore (area under red curve - area under blue curve) / (area under both). Note that for $d = 3\,w_0$ and $z = 20\,z_0$ (bottom row), the beams *appear* almost overlapped but the visibility is still 1 %. (The scale changes between the top 3 rows and the bottom 3 rows.)

splitter, with the light from each output port of the beam splitter aligned onto a detector (see Figure 2.2). The propagation axis (perpendicular to the detector surface) shall be labelled the z axis. Each beam has the same waist w_0 and both waists are at the same z position, with the detector located a distance z_0 from the waist. Each beam is displaced from the other a distance d along the x direction (perpendicular to the propagation direction). Each detector only measures the total power incident upon it—no spatial information about the intensity distribution is collected. If the detectors could measure spatial information perfectly, and if the two spatial modes were stable and known perfectly, then the following analysis does not necessarily apply and the phase between the beams can always be retrieved. I make this requirement because it is a technologically simpler detection system that is commonly used, it does not require that the spatial modes be stable and well known, and because for atoms the level of spatial detail needed is frequently orders of magnitude smaller than can be resolved with standard techniques.

With the above definitions made, the power P incident on each detector may be written:

$$P = \int_D I(x, y)\, dx\, dy, \tag{2.4}$$

where the integral over D represents the surface of the detector (which may be as large as needed), and $I(x, y)$ represents the intensity due to the inteference of the two beams, the intensity being proportional to the modulus squared of the complex electric field vector:

$$I \propto |E|^2, \tag{2.5}$$

where E is the complex electric field amplitude. The constant of proportionality is not relevant to the discussion, and may be neglected (for example, with an appropriate choice of units.) Let us label the complex electric field vector (that is, the spatial mode) of one beam as A and the other beam as B, with A and B each being a function of both x and y. Therefore, the intensity at each detector is:

$$I_{\pm} = \left| \frac{1}{\sqrt{2}} A \pm \frac{1}{\sqrt{2}} B \right|^2, \tag{2.6}$$

where the factors of $1/\sqrt{2}$ are due to the beam splitter, and the $\pm$ has sign + at one detector and − at the other detector (also due to the beam splitter [40]).

The signal from the detector is the total power incident upon it:

$$P_{\pm} = \int I_{\pm}\, dx\, dy \tag{2.7}$$

$$= \tfrac{1}{2}P_A + \tfrac{1}{2}P_B \pm \mathrm{Re}\left(\int A^* B\, dx\, dy\right). \tag{2.8}$$

Where the first two terms are simply half the power in the first beam P_A and half the power in the second beam P_B, and the last term is the interference term. (The operator * denotes complex conjugation). The purpose of the experiment is of course to measure the phase between the two beams ϕ. Let us make this explicit, by rewriting:

$$B \longrightarrow e^{i\phi} B, \tag{2.9}$$

and (for convenience) adding a unimportant constant phase to both A and the rewritten B such that:

$$\arg\left(\int A^* e^{i\phi} B\, dx\, dy\right) = \phi + \pi/2. \tag{2.10}$$

(The $\pi/2$ offset is not crucial, but it will be convenient to obtain a sine function in the next step rather than a cosine.) With this, the power can be usefully rewritten:

$$P_{\pm} = \tfrac{1}{2}P_T \pm \sin(\phi) \int |A^* B|\, dx\, dy, \tag{2.11}$$

where $P_T = P_A + P_B$ is the total power in both beams.

Let us now define the visibility (originally done by Michelson in 1891 [41]). It is found by varying the phase of the interferometer through its entire range (see Figure 2.4), finding the maximum and minimum powers $P_{\max}$ and $P_{\min}$, and using them:

$$V = \frac{P_{\max} - P_{\min}}{P_{\max} + P_{\min}}. \tag{2.12}$$

This formulation is equivalent to (in the notation of this chapter):

$$V = \frac{2\int |A^* B|\, dx\, dy}{\int (|A|^2 + |B|^2)\, dx\, dy}. \tag{2.13}$$

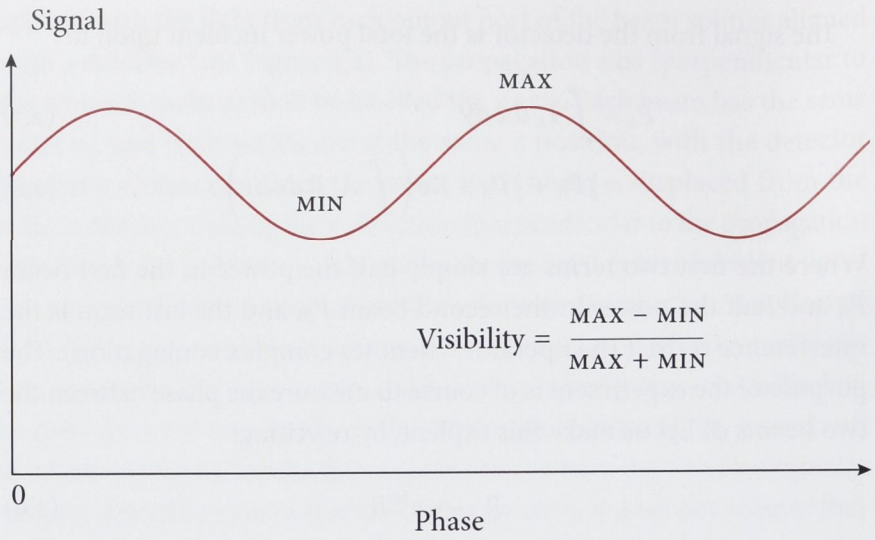

Figure 2.4: Definition of fringe visibility (or simply visibility) in an interferometric measurement. The visibility quantifies how much of the flux contributes to the interferometric signal. It is found by varying the phase of the interferometer through its range, and the minimum and maximum signals are recorded. The intensity maximum is often referred to as the *bright port* and the intensity minimum the *dark port*. When a phase of zero corresponds to a signal in the middle of its range (as in the figure above) the interferometer is said to be operating at *mid-fringe*.

Note that the visibility at one detector must always be the same as at the other (this is a consequence of energy being conserved.) Using this definition, Equation 2.11 can be rewritten:

$$P_{\pm} = \tfrac{1}{2} P_T \left(1 \pm V \sin(\phi)\right). \tag{2.14}$$

The phase is calculated by subtracting the power at one detector from the other:

$$\begin{aligned} \text{Signal} &= P_+ - P_- && (2.15)\\ &= V \sin(\phi)\, P_T && (2.16)\\ &\approx V \phi\, P_T \qquad \text{for small } \phi, && (2.17) \end{aligned}$$

thereby obtaining the expression for the signal given in Equation 2.1, after making the connection between the power in the light field and the flux of photons in it.

Until this point, we have kept the two modes A and B quite general. Let us now make them specific: as each being the lowest order gaussian beam

(also known as the TEM_{00} mode). For this beam, the complex electric field amplitude is:

$$E(\rho, z) = E_0 \frac{w_0}{w(z)} \exp\left(\frac{-\rho^2}{w^2(z)}\right) \exp\left(-ikz - ik\frac{\rho^2}{2R(z)} + i\zeta(z)\right), \tag{2.18}$$

where,

E_0	is the field amplitude,	
w_0	is the beam waist,	
z	is the axial coordinate,	
ρ	is the (transverse) radial coordinate	$\sqrt{x^2 + y^2}$,
$w(z)$	is the beam width	$w_0\sqrt{1 + z^2/z_0^2}$,
z_R	is the Rayleigh length	$\pi w_0^2/\lambda$,
$R(z)$	is the radius of curvature	$1 + z_0/z$,
k	is the wavenumber	$2\pi/\lambda$,
$\zeta(z)$	is the Gouy phase.	

Neglecting E_0 (which again is unimportant), neglecting ikz and the Guoy phase $\zeta(z)$ which will be identical in each beam at every point along the detector, and noting that the second last phase term may be rewritten:

$$\frac{k}{2R(z)} = \frac{1}{w(z)^2}\frac{z}{z_R}. \tag{2.19}$$

then the complex electric field amplitude may be rewritten:

$$E(\rho, z) = \frac{w_0}{w(z)} \exp\left(-\frac{\rho^2}{w(z)^2}\left(1 - i\frac{z}{z_R}\right).\right) \tag{2.20}$$

A and B can be explicity defined using this formulation:

$$A = E(x, y, z) \quad \text{and} \quad B = E(x - d, y, z). \tag{2.21}$$

Calculating the integral in Equation 2.13 (using standard techniques of gaussian integrals), the visibility is:

$$V(d) = \exp(-\tfrac{1}{2}d^2/w_0^2), \tag{2.22}$$

which, as discussed above, is independent of the propagation distance to the detector z_0, and in fact depends only on the waist. When the displacement is *larger* than the waist of the beam, yet *smaller* than the width of the beam, then complicated interference patterns may appear

on each detector. The form of these patterns may vary as the phase varies, whilst the power on each detector remains almost the same. An example of this in given in Figure 2.3, which shows the intensity pattern on each detector for a range of displacements and propagation distances.

Of course, for precision measurement it is typically small fluctuations in the displacement that are of concern (see §2.1). Therefore the quantity $\partial^2 V/\partial d^2$ (evaluated at $d = 0$) is the important quantity in determining the signal-to-noise of a measurement. From Equation 2.22, it can be seen that for two gaussian (TEM_{00}) beams:

$$\left.\frac{\partial^2 V}{\partial d^2}\right|_{d=0} = -\frac{1}{w_0^2}. \tag{2.23}$$

Higher order Hermite-Gaussian beams

How does this change for higher order Hermite-Gaussian modes? In general it is quite complicated. For two $n_x = 1, n_y = 0$ Hermite-Gaussian beams, the visibility is:

$$V(d) = \left(1 - d^2/{w_0}^2\right) \exp\left(-\tfrac{1}{2} d^2/w_0^2\right). \tag{2.24}$$

For two $n_x = 2, n_y = 0$ Hermite-Gaussian beams, the visibility is:

$$V(d) = \left(1 - 2\frac{d^2}{w_0^2} + \frac{d^4}{2w_0^4}\right) \exp\left(-\tfrac{1}{2} d^2/w_0^2\right). \tag{2.25}$$

The important quantity, of course, is $\partial^2 V/\partial d^2$ which for a beam which contains only the n^{th} higher order mode is:

$$\left.\frac{\partial^2 V}{\partial d^2}\right|_{d=0} = -(2n + 1)\frac{1}{w_0^2}. \tag{2.26}$$

2.3 HOW CAN THE SPATIAL MODE QUALITY BE QUANTIFIED?

There is no *completely general* way to quantify the spatial mode quality of an atom laser (or an optical laser), so that it is easy to calculate the change in signal-to-noise ratio due to every possible misalignment, or to calculate the maximum signal-to-noise ratio with two different beams. There is, however, a quantity which is *useful* in evaluating the spatial mode quality, and is a good indicator of how a beam will perform in a precision measurement. It is the beam propagation factor M^2, introduced for optical lasers by A. E. Siegman et al. and extended to atom lasers by

The beam propagation factor M^2

J.-F. Riou et al. [42, 43]. It is a measure of how far the beam deviates from the minimum uncertainty (least diffracting) state, and is defined by:

$$M^2 = \frac{2}{\hbar}\Delta x \Delta p_x, \tag{2.27}$$

where Δx is the beam width measured at the waist, and Δp_x is the transverse momentum spread. An ideal (Gaussian) beam therefore has $M^2 = 1$ along both its principal transverse axes. A non-ideal beam has an M^2 greater than 1 (see Figure 2.5).

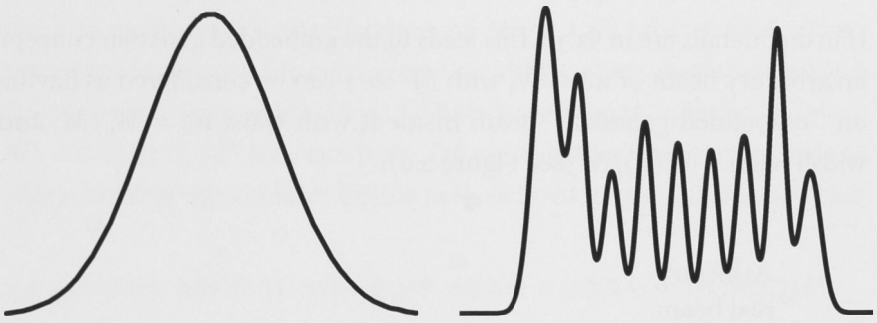

$M^2 = 1$
Excellent
spatial mode

$M^2 \gg 1$
Poor
spatial mode

Figure 2.5: Examples of beams with different spatial modes.

Why is M^2 useful?

The beam propagation factor M^2 is useful because, *usually*, the lower the M^2 value, the smaller the effect on a measurement due to imperfect modematching. The M^2 value is also practical because it does not change during propagation, even through lenses which change the waist, reflections from mirrors or simply propagation in free space. Therefore, for many systems it need only be calculated once. To be more precise, it does not change during propagation in the paraxial regime. This regime is defined in §3.3, but essentially it applies when there is a well defined direction of propagation and low divergence—in other words, it applies to almost anything that could be considered a *beam* of light or atoms, rather than a point source or a cloud expanding in all directions. Furthermore, in many experiments it is possible to change the beam waist with lenses, which reduces the effect of certain misalignments, such as the transverse displacement studied in the previous section. The M^2 value, which does not change as the beam waist is changed, makes it possible to compare beams of different sizes. M^2 is also practical because only measurements

of the intensity of the beam in question are needed to determine it; it is not necessary to make interference measurements of the beam with itself or anything else.

The M^2 values can be used in a rigorous second moment propagation law, which holds (in slightly different forms) for both light and atoms:

$$w(z)^2 = w_0^2 + M^4 \times \left(\frac{\lambda}{\pi w_0}\right)^2 (z - z_0)^2 \qquad \text{for light,} \qquad (2.28)$$

$$w(t)^2 = w_0^2 + M^4 \times \left(\frac{\hbar}{2mw_0}\right)^2 (t - t_0)^2 \qquad \text{for atoms.} \qquad (2.29)$$

(Further details are in §3.3.) This leads to the embedded gaussian concept: an arbitrary beam of waist W_0 with $M^2 \gg 1$ can be considered as having an "embedded gaussian" beam inside it with waist $w_0 = W_0/M$, and width $w(z) = W(z)/M$ (see Figure 2.6).

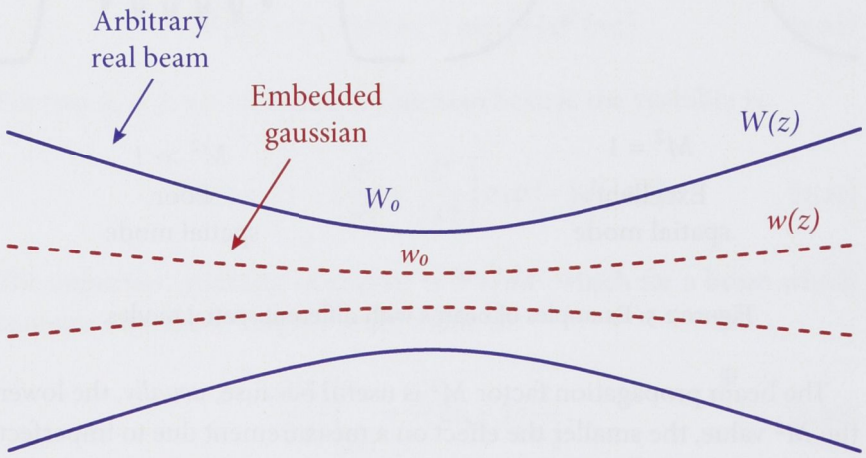

Figure 2.6: The embedded gaussian concept. An arbitrary beam of waist W_0 with $M^2 \gg 1$ can be considered as having an "embedded gaussian" beam in it. The embedded gaussian has waist $w_0 = W_0/M$, and with width $w(z) = W(z)/M$. Figure adapted from Reference 44.

One detail to note is that a real beam has two transverse axes, and therefore two M^2 values, M_x^2 and M_y^2. These can be defined rigorously along an arbitrary choice of axes x and y, but will be most useful when the principal axes of the beam are chosen. Some unusual beams have "twisting" propagation which makes characterisation using M^2 difficult; they are not considered in this thesis as they are typically not useful for interferometry [44]. When a beam has a high degree of circular symmetry, usually only one M^2 value is given. For the atom lasers studied in this

thesis, only one of the principal axes has a poor spatial mode (as shall be seen later), and so only for that axis is the M^2 value examined. (For the other principal axis, M^2 is very close to 1.)

Typical M^2 values of commercial optical lasers.

What are typical values for M^2? Amongst optical lasers, the Toptica DLX 110, a 1 W diode laser marketed to research labororatories, costing around $US 50,000 and used in many atom optics experiments including at ANU, has a manufacturer's specification of $M^2 = 1.5$ [45]. Typically, the spatial mode is improved using single-mode optical fibers or spatial filtering techniques before use. The Mephisto laser from Innolight, an ultrastable laser for precision measurement and costing around $USD 150,000, has a manufacturer's specification of $M^2 = 1.05$ [46]. A high power industrial laser used for cutting and welding (where modematching is unimportant), such as the 2 kW Yb fiber laser from IPG photonics has an $M^2 = 1.15$ [47]. M^2 is in fact part of the ISO standard for measuring and characterising optical laser beams [48], defined in ISO 11146-1:2005 [49].

2.4 IS THE SPATIAL MODE OF ATOM LASERS A PROBLEM?

The source of an atom laser is a Bose-Einstein condensate (BEC). This is a cloud of atoms with a large fraction of atoms in the quantum ground state. Typically these atoms are held in a trapping potential, and typically this potential is harmonic. The spatial mode of the ground state for such a potential is a minumum uncertainty state gaussian wavefunction (for non-interacting atoms); that is, it satisfies the equality:

$$\Delta x \Delta p_x = \frac{\hbar}{2}. \tag{2.30}$$

If an atom laser could be produced in a way which preserved this wavefunction, it would have the ideal spatial mode $M^2 = 1$.

Is this observed in current experiments with atom lasers? Many experiments have studied atom laser beam spatial mode, and they have noted that the atom laser spatial mode is poor [6, 8, 9, 50–52]. Figure 2.7 shows atom laser spatial mode measurements by Riou et al. in the group of Alain Aspect at the Laboratoire Charles Fabry (LCF) in Orsay. They clearly show a poor spatial mode, with an M^2 as high as 15 with certain parameters. The reason for this is that atoms interact with each other through collisions. This has two consequences. The first consequence is that the spatial mode of the condensate is not a minimum uncertainty gaussian, but is broadened to become approximately parabolic. The second (and more significant) consequence is that the condensate acts as a non-ideal diverging lens on the atom laser. This is discussed in more

detail in §3.1, but briefly, transfer of atoms from the trapped to the untrapped state (*outcoupling*) occurs along magnetic equipotential surfaces inside the condensate. When the atom laser is created on the outcoupling surface, it has the same excellent spatial mode as the condensate, but this is altered as it propagates through and exits the condensate, and creates caustics in the beam. These atom lasers show high spatial frequency fringes along their transverse profile, which would be a problem if they were used in a precision measurement. Anything which increases the interactions between the atoms, such as increasing the condensate atom number or the tightness of the trap only makes the problem worse.

2.5 HOW CAN THE SPATIAL MODE OF ATOM LASERS BE IMPROVED?

As mentioned in the previous section, an atom laser is produced inside the condensate along magnetic equipotential surfaces. By selecting the appropriate surface, the atom laser may be produced from any height inside the condensate. Many experiments have noted that by outcoupling atoms from the base of the condensate, the spatial mode is improved [43, 50, 52]. (This is shown dramatically in Figure 2.7, which shows atom lasers outcoupled from the top, center, and bottom of the condensate.) This is done by using a higher outcoupling frequency so that the resonant surface is at the base of the BEC. The atom laser travels less distance inside the condensate, and is therefore less affected by it. This is demonstrated in Figure 2.8. The figure shows cross sections through the condensate, and the classical trajectories of atoms travelling through them.

Outcoupling from the base of the condensate

However, outcoupling from the base of the condensate is undesirable for a number of reasons (see Figure 2.9). First, because the condensate is most dense in the center, outcoupling from the center produces the highest flux for the given coupling strength and hence classical intensity noise level [54]. Second, outcoupling from the center allows the longest operating time (for a quasicontinuous atom laser) since all the atoms can be outcoupled to completely drain the condensate. Third, outcoupling from the center minimizes the sensitivity of the outcoupling to condensate excitations or external fluctuations. For example, when outcoupling from the base of the condensate, small fluctuations in the magnetic bias field could move the outcoupling surface completely outside the condensate, turning off the atom laser.

Therefore, for precision measurement, we require a means of creating an atom laser with a high quality spatial mode whilst outcoupling from the center. This is the subject of the next two chapters. The technique we have used is to change the outcoupling method, from using an RF

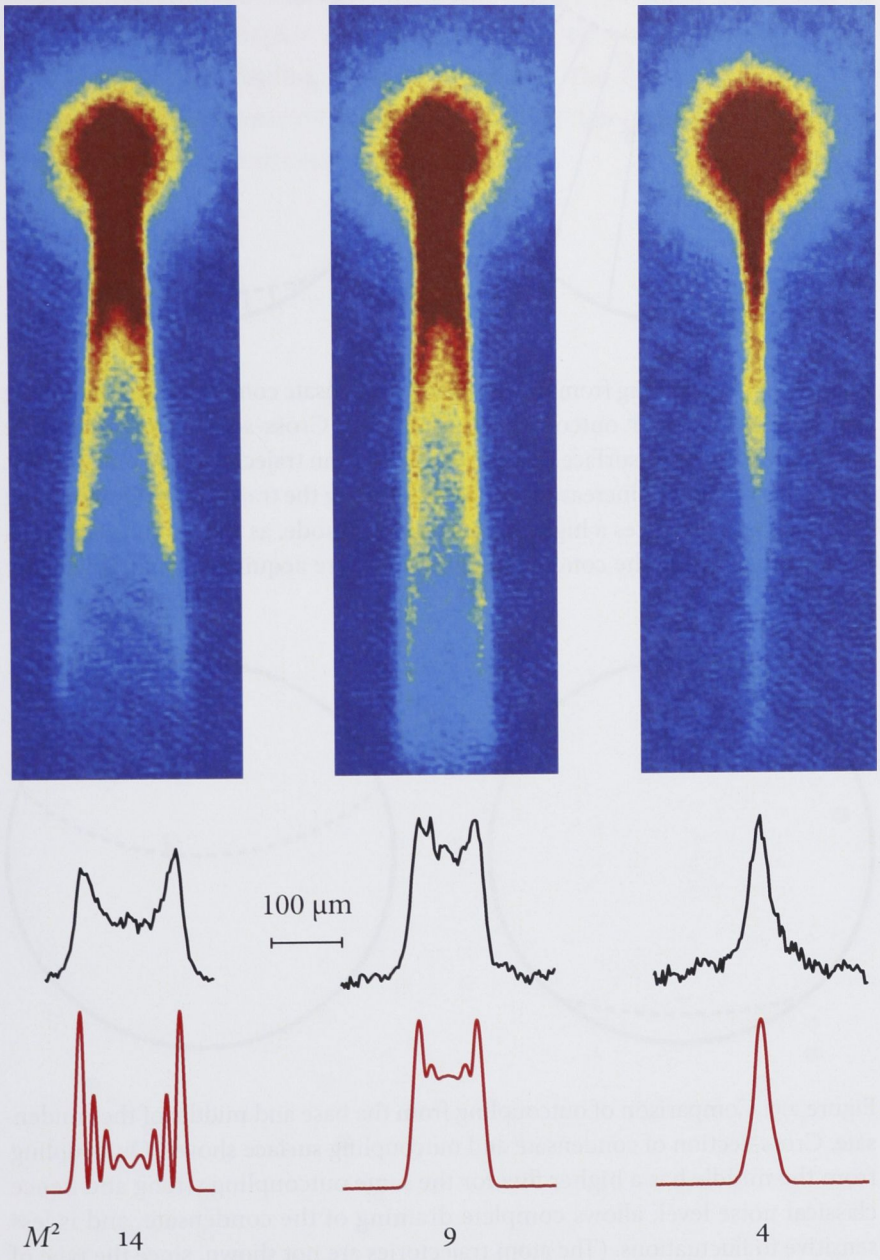

Figure 2.7: Atom lasers produced with RF outcoupling by J. F. Riou et al. at the Laboratoire Charles Fabry de l'Institut d'Optique near Paris. The top row shows absorption images, the middle row shows the density profile 600 μm below the condensate, and the bottow row shows the theoretical predictions. The left column shows an atom laser outcoupled from the top of the condensate, the central column from the middle of the condensate, and the right column fron the bottom of the condensate. Figure adapted from Reference 53.

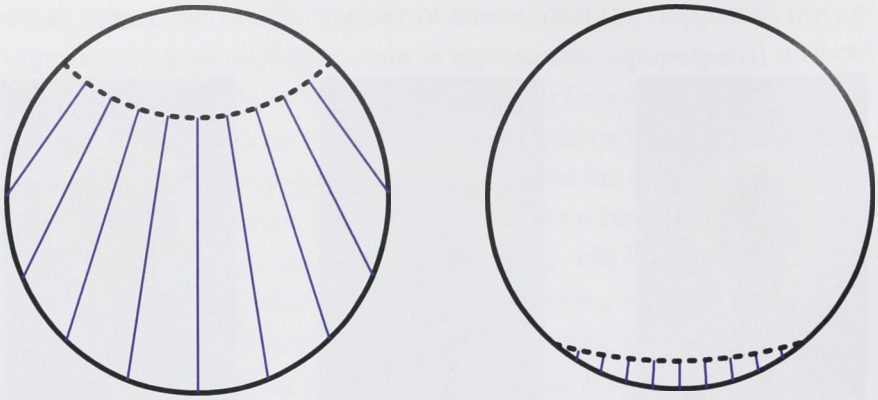

Figure 2.8: Outcoupling from the top of the condensate compared to outcoupling from the base (for RF outcoupled atom lasers). Cross-section of condensate (circles), outcoupling surface (dashed line) and atom trajectories (in blue) shown. The atoms move with increasing acceleration along the trajectories. Outcoupling from the base produces a higher quality spatial mode, as the atom laser travels less distance inside the condensate, and therefore acquires a smaller velocity spread.

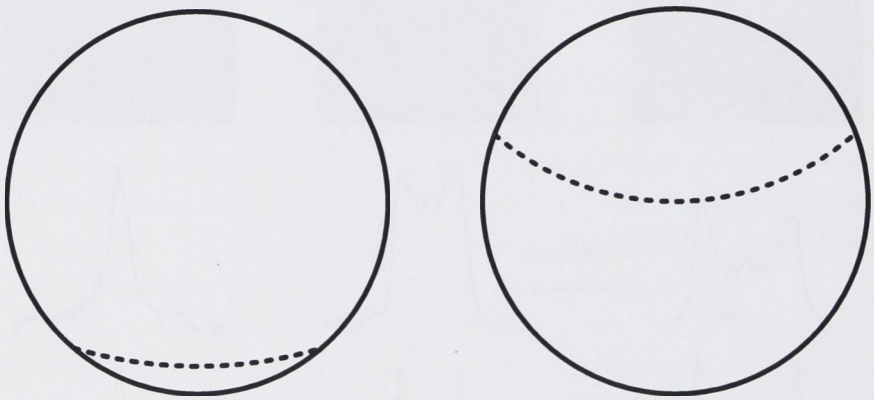

Figure 2.9: Comparison of outcoupling from the base and middle of the condensate. Cross-section of condensate and outcoupling surface shown. Outcoupling from the middle has a higher flux for the same outcoupling streng and hence classical noise level, allows complete draining of the condensate, and is less sensitive to fluctuations. (The atom trajectories are not shown, since the type of outcoupling considered here is more general).

transition to a two-photon Raman transisiton. Raman outcoupling was first proposed by Moy et al. at ANU [55]. It was first done experimentally as pulsed outcoupling by Hagley et al. at NIST [9], and continuous Raman outcoupling was first done by Robins et al. at ANU [10]. This technique improves the spatial mode because atoms are given a momentum kick of up to 5 mm/s, which accelerates them out of the condensate and the

reduces the effect of the interaction between them. In short, it permits outcoupling from the center whilst producing a high quality spatial mode.

The following chapter introduces the theory needed to understand and to model outcoupling from an atom laser. The chapter following that discusses the experiments done at ANU which demonstrate the improvements that Raman outcoupling brings.

3

CALCULATION OF THE SPATIAL MODE

In the previous chapter, I discussed the importance of spatial mode for atom lasers. In this chapter, I describe the calculations done to model the atom laser spatial mode. This was done in a three-stage process, shown in Figure 3.1, using a technique developed by J.-F. Riou et al. [56]. Each stage models the atom laser propagation in a different region.

Convention for this chapter: z is down (and a tight trapping axis), y is weak trapping axis (because it is the magnetic bias field direction), x is the horizontal strong trapping axis. The origin is the center of the condensate.

1. The first stage is the region inside the condensate, in which the WKB approximation is used, by integrating the phase along the classical trajectories. The purpose of this is to find the atom laser wavefunction and its derivative on the surface of the condensate.

2. The second stage is immediately outside the condensate, in which a Kirchoff-Fresnel integral is used, with the Green's function for the gravitational potential.

3. The third region is sufficiently below the condensate that the paraxial approximation is valid. In this regime *ABCD* matrices can be used to propagate the atom laser beam further, and the M^2 value can be found.

Assumptions made in the calculation

Several assumptions and simplifications are made in the calculation. The calculation models outcoupling which is both steady state and weak (that is, the outcoupling rate is low) [57]. The calculation assumes steady state operation of the atom laser (since it solves the time independent

Schrödinger equation), which approximates long duration, weak outcoupling [58]. Because the outcoupling is weak, we shall neglect changes to the condensate from the outcoupling process, including decreases in number. The approximations have been checked against a full 3D time dependent numberical simulation (done by Graham Dennis) which includes all these neglected effects. In addition, the electromagnetic outcoupling fields (both RF and optical) are assumed to be plane waves, a good approximation on the length scale of the condensate (order 10 μm) compared to the RF coil radius (order 1 cm) and Raman outcoupling laser beam waist (order 1 mm).

3.1 INSIDE THE CONDENSATE: CLASSICAL TRAJECTORIES

Inside the condensate, the WKB approximation is used. This is done by finding the classical trajectories of the atoms inside the condensate, from where they are produced to where they exit the condensate, and integrating the phase along that trajectory. The simulation assumes that atoms do not reenter the condensate once they have been outcoupled. This happens when atoms with low mass or in tightly confining traps, so that the gravitational sag is less than the condensate width, for example experiments with helium [59].

In the WKB approximation, the wavefunction on the edge of the condensate is related to that on the outcoupling surface by:

$$\psi(\mathbf{r}_f) = \underbrace{\frac{\partial(\mathbf{r}_f)}{\partial(\mathbf{r}_i)}}_{\text{Jacobian}} \exp\left(i\int_c \mathbf{k}\cdot d\mathbf{r}\right) \exp(i\,\mathbf{k_0}\cdot\mathbf{r}_i)\,\psi(\mathbf{r}_i) \tag{3.1}$$

where,

- ψ is the atom laser wavefunction,
- $\mathbf{r}_i$ is a coordinate on the outcoupling surface,
- $\mathbf{r}_f$ is a coordinate on the edge of the condensate,
- c is the atomic trajectory which connects $\mathbf{r}_i$ and $\mathbf{r}_f$
- $\mathbf{k}$ is the atomic wavenumber during the trajectory ($\mathbf{p}/\hbar$).
- $\mathbf{k_0}$ is the initial kick to the atom (in the case of Raman outcoupling).

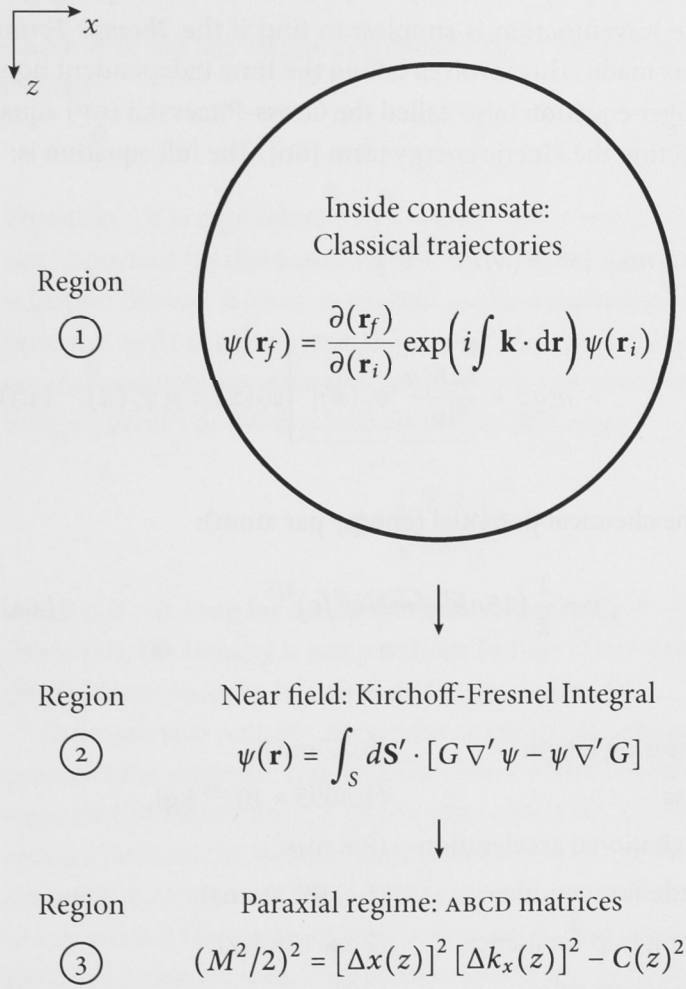

Figure 3.1: Schematic of the simulation, showing the three regimes: inside the condensate, the near field, and the far field, where the three different techniques are used.

To find the wavefunction on the outcoupling surface, we need the condensate wavefunction ψ_c, because in the weak outcoupling limit the atom laser wavefunction there is simply proportional to it:

$$\psi(\mathbf{r}_i) \propto \psi_c(\mathbf{r}_i), \tag{3.2}$$

Thomas-Fermi approximation

where the constant of proportionality is related to the outcoupling rate. The condensate wavefunction is simplest to find if the *Thomas-Fermi approximation* is made. This involves taking the time independent nonlinear Schrödinger equation (also called the Gross-Pitaevskii (GP) equation) and neglecting the kinetic energy term [60]. The full equation is:

$$\Bigg[\underbrace{-\frac{\hbar^2}{2m}\nabla^2}_{\text{Kinetic energy}} + \underbrace{\frac{1}{2}m\omega^2\left(x^2 + (y/\epsilon)^2 + z^2\right)}_{\text{Magnetic trap}} \underbrace{- mgz}_{\text{Gravity}} + \underbrace{\frac{4\pi\hbar^2 a}{m}|\psi_c(\mathbf{x})|^2}_{\text{Mean field}}\Bigg]\psi_c(\mathbf{x}) = \mu\,\psi_c(\mathbf{x}), \tag{3.3}$$

in which μ is the chemical potential (energy per atom):

$$\mu = \frac{1}{2}\left(15a\hbar^2\sqrt{m}N\omega^3/\epsilon\right)^{2/5} \tag{3.4}$$

and where,

a	is the scattering length	(5.77 nm),
m	is the mass	(1.4095×10^{-25} kg),
g	is the gravitational acceleration	(9.8 m/s^2),
N	is the condensate number	(5×10^5 atoms),
ω	is the strong trap frequency	($2\pi \times 128$ Hz),
ϵ	is the trap aspect ratio	(10).

Using this approximation, one can solve for the condensate wavefunction:

$$|\psi_c(\mathbf{x})|^2 = \frac{m}{4\pi\hbar^2 a}\Big(\mu - V(\mathbf{x})\Big), \tag{3.5}$$

where $V(\mathbf{x})$ is the gravitational, magnetic, and mean-field terms of the Hamiltonian. This can be usefully rewritten:

$$\psi_c(\mathbf{x}) = \begin{cases} \sqrt{1 - \dfrac{x^2 + (y/\epsilon)^2 + z^2}{R^2}}, & (x^2 + (y/\epsilon)^2 + z^2) < R^2, \\ 0, & \text{otherwise}, \end{cases} \tag{3.6}$$

where R is the size of the condensate (also called the Thomas-Fermi radius):

$$R = \sqrt{\frac{2\mu}{m\omega^2}}. \tag{3.7}$$

About the Thomas-Fermi approximation

Equation 3.6 is equivalent to 3.5, except for a constant factor which is not important (as discussed above). The Thomas-Fermi approximation is helpful because it gives an analytic expression for the condensate wavefunction and (as will be seen below) for the classical trajectories. It is a good approximation given the parameters of our experiment; the approximation breaks down at a distance d from the edge:

$$d = \left(\frac{\hbar^2 R}{4m\mu}\right)^{1/3}, \tag{3.8}$$

which is $d = 0.4$ μm for our parameters, compared to $R = 5.2$ μm. Beyond this point, the density is not parabolic but decreases exponentially; the precise form needs to be calculated numerically [60].

Choice of reference frame

There are two natural choices for origin of the reference frame: the center of the magnetic trap and the center of the condensate, which are separated by a distance $z_c = g/\omega^2$ (often called the *sag*). They are natural choices because the total potential has rotational symmetry around the center of the magnetic trap, and the atomic density has rotational symmetry around the center of the condensate. In this chapter, the center of the condensate is chosen to be the origin of the reference frame, which makes the atomic trajectories slightly more complicated but simplifies the remainder of the calculation.

Weak trapping axis ignored

The entire system has a high degree of translational symmetry along the weak axis of the trap (the y axis), with a trap aspect ratio ϵ of 10. Because of this, it is sufficient to study the dynamics of the system in the x-z plane (see Figure 3.2).

We can see that ignoring decreases in condensate number has only a slight affect, since $\mu \propto N^{2/5}$ and $R \propto N^{1/5}$.

Outcoupling surface

Outcoupling occurs on magnetic equipotential surfaces. This is because the Hamiltonian for the $|F = 1, m_F = 0\rangle$ atom laser state is the same as

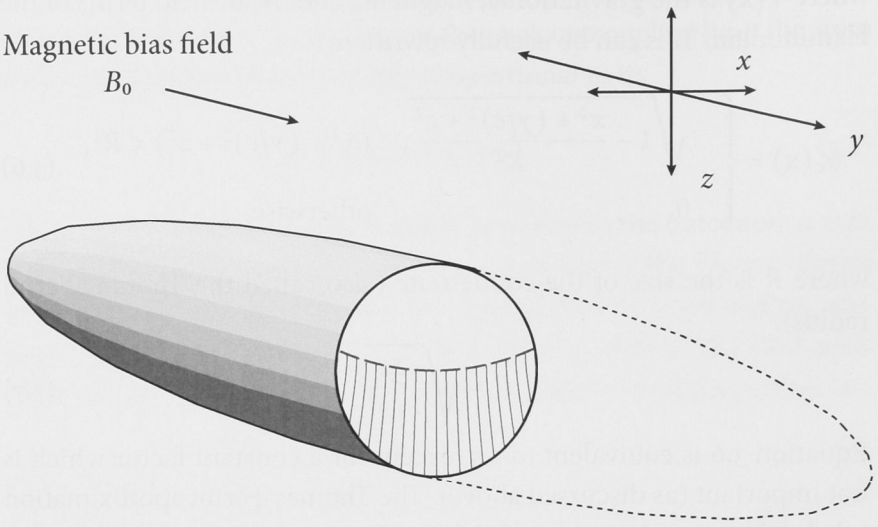

Figure 3.2: Geometry of the experiment, showing cross-section of the condensate along the two strongly confining directions. The condensate is cigar shaped, with an aspect ratio of 10 and with the long axis along the y direction. As the system has high degree of translation symmetry along that direction, only dynamics perpendicular to it need be considered.

for the $|F = 1, m_F = -1\rangle$ condensate state, *except* for the magnetic trap terms. This is true regardless of the type of outcoupling used. These equipotential surfaces are ellipsoids, and in the relevant x-z plane they have a circular cross section whose radius r_{oc} depends on the frequency of the outcoupling field [8]:

$$r_{oc} = \frac{1}{\omega}\sqrt{\frac{2(\hbar\delta - \frac{1}{2}\mu_B B_0)}{m}}, \tag{3.9}$$

where μ_B is the Bohr magneton, B_0 is the magnetic bias field (2 G), and δ is the frequency of the field for RF outcoupling or the two-photon detuning for Raman outcoupling (less the detuning due to the momentum transfer, $\hbar^2k^2/(2m) = h \times 13$ kHz). (For microwave outcoupling, or any outcoupling which changes hyperfine manifold, the hyperfine splitting (which is 6.8 GHz for ^{87}Rb) must be taken into account. Full details of the calculation, including second order Zeeman shift corrections, can be found in many places, for example the thesis of Kai Dieckmann [61, page 9].) A schematic of the condensate, outcoupling surfaces, and atom trajectories is shown in Figure 3.3.

The potential that the atoms experience inside the condensate is:

$$V_{\text{inside}} = \mu\left(1 - \frac{x^2 + (z - -z_c)^2}{R^2}\right) - mgz. \tag{3.10}$$

Classical trajectories

The trajectories in such a potential are:

$$x(t) = x_i \cosh(\omega t), \tag{3.11}$$

$$z(t) = (z_i + z_c)\cosh(\omega t) + \frac{v_{z_0}}{\omega}\sinh(\omega t) - z_c, \tag{3.12}$$

where v_{z_0} is the velocity kick due to the photon recoil (in the case of Raman outcoupling). This depends upon the angle between the Raman lasers; the maximum two photon kick is $v_{z_0} = 1.1$ cm/s. For RF outcoupling, v_{z_0} is neglible.

The outcoupling surface and the Thomas-Fermi radius of the condensate intersect at $(x_{\text{int}}, z_{\text{int}})$ (this is needed to find the limits of integeration for the Kirchoff-Fresnel integral in §3.2):

$$x_{\text{int}} = \pm\left(r_{\text{oc}}^2 - \frac{\left(r_{\text{oc}}^2 - R^2 + z_c^2\right)^2}{2z_c^2}\right)^{1/2} \tag{3.13}$$

$$z_{\text{int}} = \frac{\left(r_{\text{oc}}^2 - R^2 + z_c^2\right)}{2z_c} - z_c \tag{3.14}$$

For RF outcoupling, the trajectories are straight lines and therefore it is possible to use similar triangles to find a mapping from final position to initial position, and therefore find the escape time t_e:

$$t_e = \frac{1}{\omega}\text{arccosh}\left(\frac{(z_i + z_c)z_c + \sqrt{-(x_i z_c)^2 + (r_{\text{oc}} R)^2}}{r_{\text{oc}}^2}\right). \tag{3.15}$$

For Raman outcoupling, it is not trivial to find a mapping from initial to final position, as the trajectories are curved. We do this numerically: starting at an initial position, moving along the classical trajectory from that position, and varying the parameter t whilst numerically minimising the quantity $x^2 + z^2 - R^2$.

The wavefunction ψ is separated into an amplitude and a phase:

$$\psi = \sqrt{n}e^{i\phi}, \tag{3.16}$$

where $n = n(\mathbf{x}, t)$ is the density and $\phi = \phi(\mathbf{x}, t)$ is the phase. The derivative is therefore:

$$\nabla\psi = \left(\frac{1}{2n} + i\nabla\phi\right)\psi \tag{3.17}$$

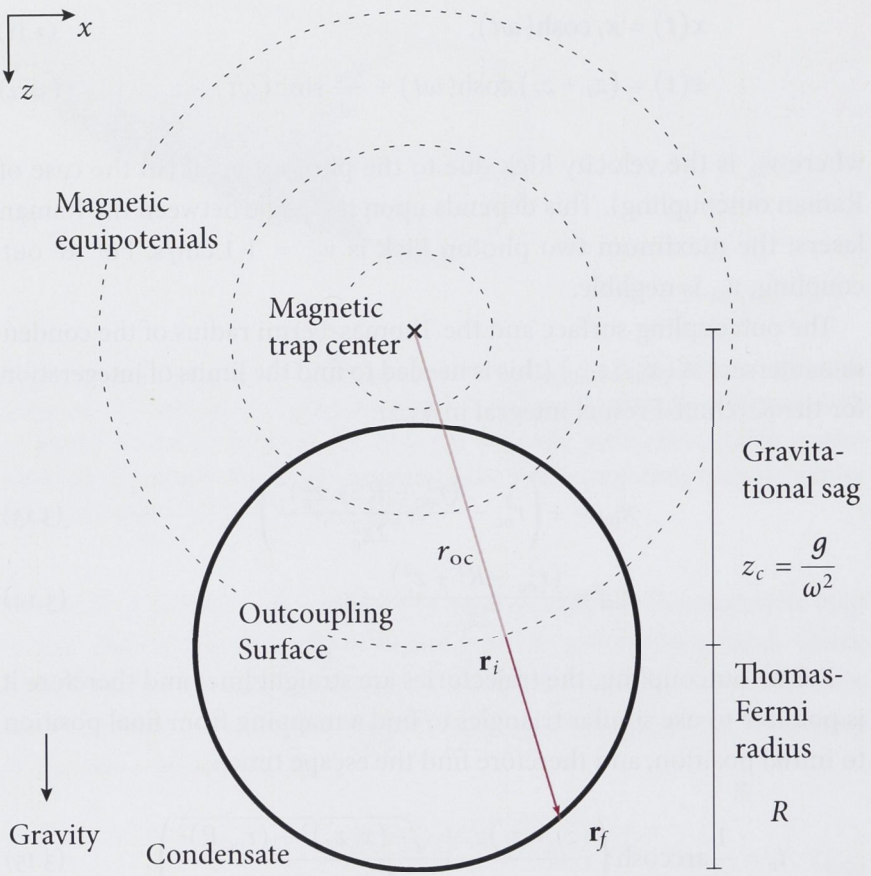

Figure 3.3: Geometry of the classical trajectories simulation, showing the magnetic trap center, gravitational sag z_c, intial position $\mathbf{r}_i$, final position $\mathbf{r}_f$. The trajectory shown is for an RF outcoupled atom, and so it is a straight line from the center of the magnetic trap. The outcoupling resonances, for both RF and Raman outcoupling, occur along magnetic equipotentials, which in the plane considered here are circles centered on the magnetic trap. The radius of the outcoupling resonance is denoted r_{oc}.

For our experiment, $\frac{1}{2n} \ll \nabla\phi$ and can be neglected.

Phase of the wavefunction

For the WKB approximation, the phase is the integral of the de Broglie wavelength along the classical trajectory:

$$\phi = \int_c \mathbf{k} \cdot \mathbf{dr} \tag{3.18}$$

$$= \int_0^{t_e} \mathbf{k}(t) \cdot \mathbf{r}'(t) dt \tag{3.19}$$

$$= \frac{m}{\hbar} \int_0^{t_e} |\mathbf{v}(t)|^2 \, dt. \tag{3.20}$$

Doing this integral gives:

$$\phi = \frac{m}{\hbar}\left(\omega^2 r_{oc}^2 \left(-\frac{t_e}{2} + \frac{\sinh(2\omega t_e)}{4\omega}\right) + v_{z_0}^2 \left(\frac{t_e}{2} + \frac{\sinh(2\omega t_e)}{4\omega}\right) + z_i v_{z_0} \sinh(\omega t_e)^2\right) \tag{3.21}$$

The gradient of the phase is:

$$\nabla\phi(\mathbf{x}, t_e) = \frac{m}{\hbar}\mathbf{v}(\mathbf{x}, t_e) \tag{3.22}$$

Jacobian determinant

We also need the Jacobian determinant, to know how an infinitesimal area in the outcoupling region maps to an infinitesimal area on the edge of the BEC. The Jacobian determinant is defined:

$$\frac{\partial(x_f, z_f)}{\partial(x_i, z_i)} = \begin{vmatrix} \frac{\partial x_f}{\partial x_i} & \frac{\partial x_f}{\partial z_i} \\ \frac{\partial z_f}{\partial x_i} & \frac{\partial z_f}{\partial z_i} \end{vmatrix} \tag{3.23}$$

We find the Jacobian by considering the trajectories of the initial points x_i and $x_i + dx_i$:

$$x_f = x_i \cosh(\omega t) \tag{3.24}$$

$$(x_f + dx_f) = (x_i + dx_i)\cosh(\omega t), \tag{3.25}$$

and subtracting one from the other gives:

$$dx_f = \cosh(\omega t) dx_i \tag{3.26}$$

And similarly for z_i and $z_i + dz_i$:

$$dz_f = \cosh(\omega t) dz_i \tag{3.27}$$

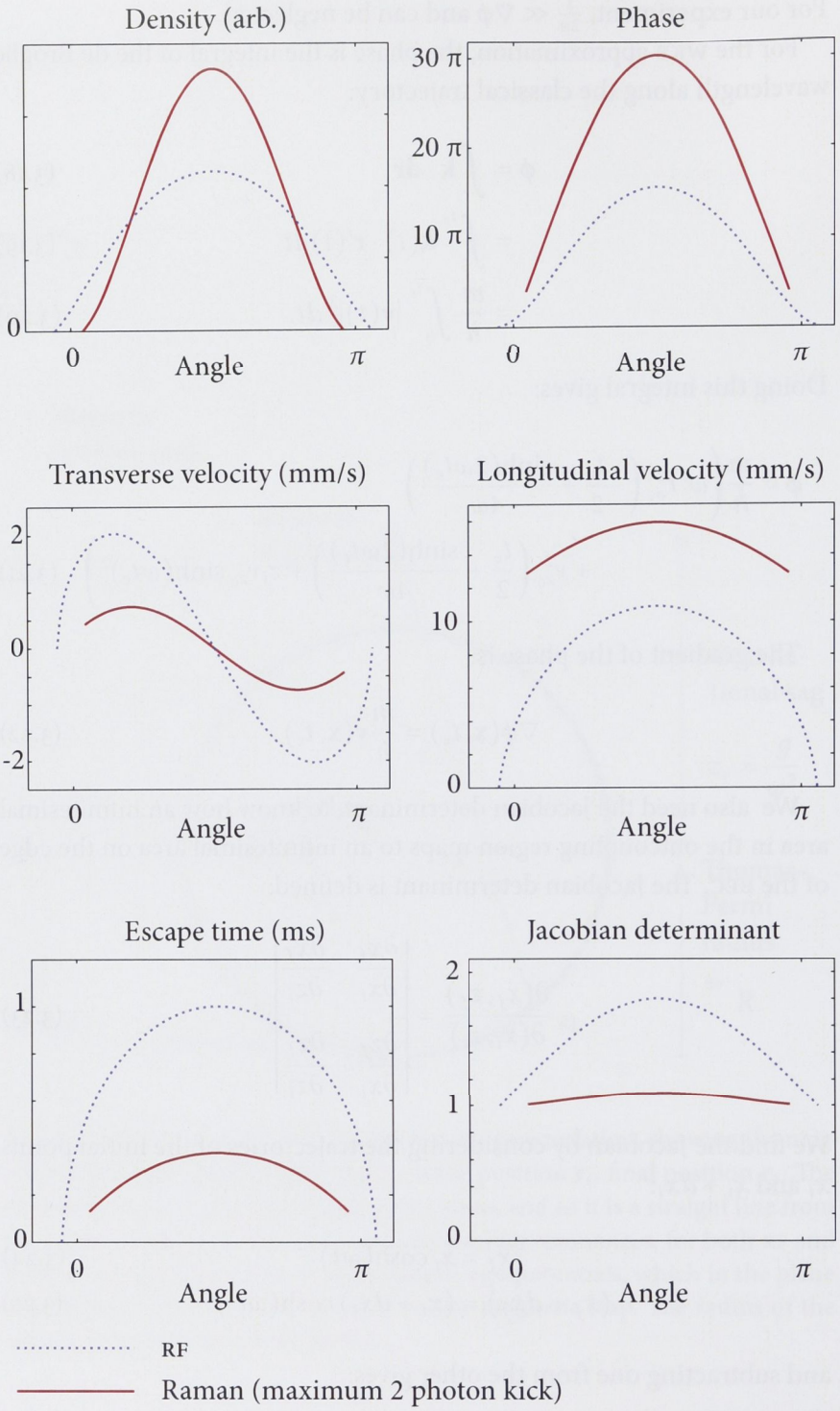

Figure 3.4: Results of the classical trajectories simulation for the edge of the condensate. Note in the second row the smaller variation in both transverse and longitudinal escape velocity for Raman outcoupling – this is the principle reason for the improved spatial mode profile.

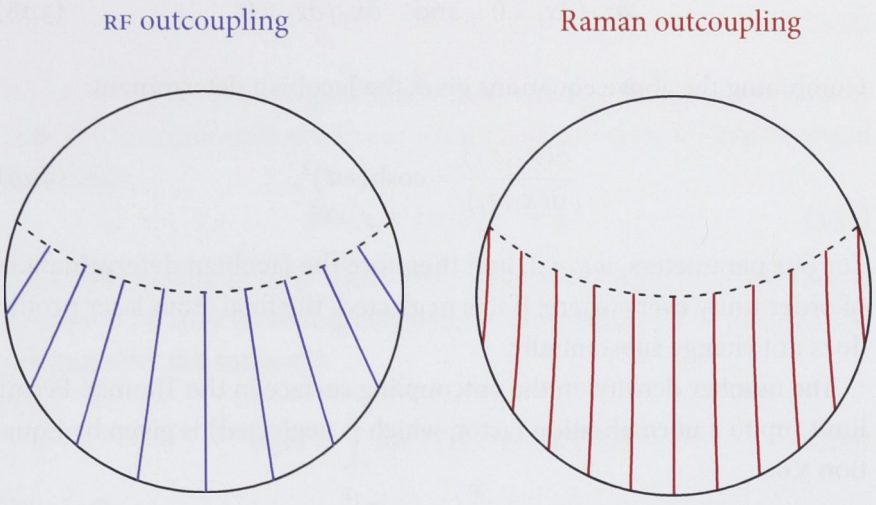

Classical trajectories — view through cross section.

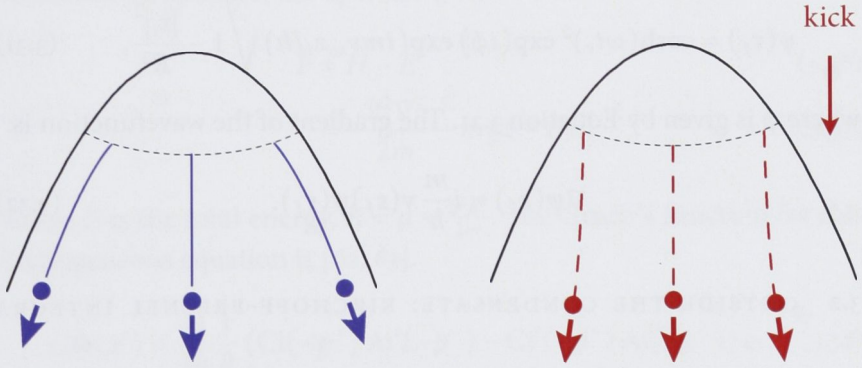

3D view of trajectories.

Figure 3.5: An intuitive explanation as to why the spatial mode of Raman atom lasers is superior to RF atom lasers. The momentum kick of the Raman transition ensures the mean field energy becomes kinetic energy from motion that is primarily in one direction only (downward), in contrast to motion through a range of directions as in RF outcoupling.

Note the mixed partial derivatives vanish, as the final x position does not depend on the inital z position, and vice versa:

$$\partial z_f/\partial x_i = 0 \quad \text{and} \quad \partial x_f/\partial z_i = 0. \tag{3.28}$$

Combining the above equations gives the Jacobian determinant:

$$\frac{\partial(x_f, z_f)}{\partial(x_i, z_i)} = \cosh(\omega t)^2. \tag{3.29}$$

For our parameters, $\omega t_e < 1$, and therefore the Jacobian determinant is of order unity everywhere; if it is neglected, the final atom laser profile does not change substantially.

The number density on the outcoupling surface in the Thomas-Fermi limit (up to a normalisation factor, which is neglected) is given by Equation 3.6:

$$n(\mathbf{r}_i) = 1 - \frac{|\mathbf{r}_i|^2}{R^2} \tag{3.30}$$

Using all the above, the atom laser wavefunction and its gradient on the edge of the condensate (Equation 3.1) can be found. Explicitly, this is:

$$\psi(\mathbf{r}_f) = \cosh(\omega t_e)^2 \exp(i\phi) \exp(imv_{z_0} z_i/\hbar)\sqrt{1 - \frac{|\mathbf{r}_i|^2}{R^2}}, \tag{3.31}$$

where ϕ is given by Equation 3.21. The gradient of the wavefunction is:

$$\nabla\psi(\mathbf{r}_f) \approx i\frac{m}{\hbar}\mathbf{v}(\mathbf{r}_f)\psi(\mathbf{r}_f). \tag{3.32}$$

3.2 OUTSIDE THE CONDENSATE: KIRCHOFF-FRESNEL INTEGRAL

Outside the condensate, a Kirchoff-Fresnel integral is used to propagate the atom laser wavefunction, using the Green's function for the gravitational potential.

These integrals are a technique to solve a homogeneous differential equation of some function in a space, given values of the function and its gradient on the boundary of the space. The space we are solving for in this case is the entire region outside the condensate. The boundary of the space is the condensate itself (the previous section detailed how to find the boundary values there) and an imaginary surface at spatial infinity, where the atom laser wavefunction and its derivatives vanish.

The technique works in the following way. Let us imagine that there is some homogeneous equation that needs to be solved:

$$\hat{F}\phi = 0 \tag{3.33}$$

Where $\phi = \phi(\mathbf{x})$ is a complex scalar field and $\hat{F}$ is an operator that acts of ϕ. If a function (called a Green's function) $G = G(\mathbf{x}, \mathbf{x}')$ can be found such that:

$$\hat{F}G(\mathbf{x}, \mathbf{x}') = \delta(\mathbf{x} - \mathbf{x}'), \tag{3.34}$$

then by knowing both ϕ and $\nabla\phi$ on a surface S which encloses some volume V, ϕ may be found everywhere everywhere in V through the integral over the surface S:

$$\phi(\mathbf{x}) = \int_S d\mathbf{S}' \cdot (G\nabla'\phi - \phi\nabla' G) \tag{3.35}$$

Note that it may be possible to find a function G such that G or ∇G is zero on some region of the boundary. In that case it is sufficient to know *either* $\nabla\phi$ or ϕ on that region. However, if both ϕ and $\nabla\phi$ are known, then such a special G is unneccessary and any function satisfying Equation 3.34 is sufficient. In this case, the operator $\hat{F}$ is:

$$\hat{F} = \hat{H} - E \tag{3.36}$$

$$= -\frac{\hbar^2\nabla^2}{2m} - mgz - E, \tag{3.37}$$

where E is the total energy, $E = \mu + \frac{\hbar^2 k^2}{2m}$. The Green's function for this homogeneous equation is [62, 63]:

$$G(\mathbf{r}, \mathbf{r}') = \frac{m}{2\hbar}\frac{1}{R}\left(\mathrm{Ci}(-\rho^+)\,\mathrm{Ai}'(-\rho^-) - \mathrm{Ci}'(-\rho^+)\,\mathrm{Ai}(-\rho^-)\right), \tag{3.38}$$

where,

$$R = |\mathbf{r} - \mathbf{r}'|, \tag{3.39}$$

and

$$\mathrm{Ci}(x) = \mathrm{Ai}(x) + \mathrm{Bi}(x) \tag{3.40}$$

and

$$\rho^{\pm} = \frac{E}{mgl} + \frac{z + z'}{2l} \pm \frac{|\mathbf{r} - \mathbf{r}'|}{2l} \tag{3.41}$$

and

$$l = \left(\frac{\hbar^2}{2m^2 g}\right)^{1/3}. \tag{3.42}$$

$\mathrm{Ai}(x)$ and $\mathrm{Bi}(x)$ denote Airy functions of the first and second kind, and the prime marks $'$ denote differentiation. A surface integral over the vector field $\mathbf{v}$ is done:

$$\int_S \mathbf{v} \cdot d\mathbf{S} = \iint \mathbf{v}(\mathbf{x}(s,t)) \cdot \left(\frac{\partial \mathbf{x}}{\partial s} \times \frac{\partial \mathbf{x}}{\partial t} \right) ds\, dt, \tag{3.43}$$

where s and t parametrise the surface S. In this case, the surface S is technically an elipsoid. However, since we are making the approximation that there is no dependence along the weak trapping axis, we shall make it a cylinder, assumed to be infinitely long. The cylinder is parametrised by the variables y and θ, and is the locus of all points $\mathbf{x}$:

$$\mathbf{x} = (x, y, z) = (R\cos(\theta), y, R\sin(\theta)), \tag{3.44}$$

$$\theta \in [\theta_1, \theta_2] \quad \text{and} \quad y \in [-\infty, \infty], \tag{3.45}$$

where θ_1 and θ_2 are the angles to the intersection between the out-coupling surface and the condensate, $\theta_1 = \arctan(z_{\mathrm{int}}/x_{\mathrm{int}})$ and $\theta_2 = \arctan(-z_{\mathrm{int}}/x_{\mathrm{int}})$, with x_{int} and z_{int} given in Equation 3.14. Therefore the integral is:

$$\int_{-\infty}^{\infty} \int_{\theta_1}^{\theta_2} \mathbf{v}(\mathbf{x}(\theta, y)) \cdot (R\cos\theta, 0, R\sin\theta)\, d\theta\, dy, \tag{3.46}$$

where the integral over y is not done, since the integrand has no y dependence.

The gradient of the Green's function ∇G is:

$$\frac{\partial G}{\partial x} = G_0 \times (x - x'), \tag{3.47}$$

$$\frac{\partial G}{\partial z} = G_0 \times (z - z') - \left(\frac{1}{2l^2} \mathrm{Ci}(-\rho^+)\, \mathrm{Ai}(-\rho^-) \right), \tag{3.48}$$

where,

$$G_0 = \frac{1}{R^2} \left(G + \frac{1}{2l} \left(2\,\mathrm{Ci}'(-\rho^+)\, \mathrm{Ai}'(-\rho^-) + \left(\frac{z + z'}{l} + \frac{2E}{mgl} \right) \mathrm{Ci}(-\rho^+)\, \mathrm{Ai}(-\rho^-) \right) \right). \tag{3.49}$$

3.3 IN THE PARAXIAL REGIME

The third region is where the atom laser has accelerated under gravity sufficiently to have entered the *paraxial regime*. In this regime, the quantity M^2 (discussed in § 2.3) can be calculated as it becomes a constant of propagation. In this section, I derive the equations of motion for the atom laser in the paraxial regime, show how the transverse dynamics can be separated from the longitudinal dynamics and reduced to the time dependent 1D Schrödinger equation. I show how to calculate the M^2 value away from the waist of the atom laser beam. These derivations can be found in greater detail in many other places, for instance C. J. Bordé [64], the thesis of Yann Le Coq [65] or J.-F. Riou (which also considers parabolic potentials, not just the linear graviational potential considered here) [53].

We start with the time independent 3D Schrödinger equation:

$$\hat{H}\psi(\mathbf{r}) = E\psi(\mathbf{r})\,. \tag{3.50}$$

where

$$\hat{H} = -\frac{\hbar^2}{2m}\nabla^2 - mgz. \tag{3.51}$$

Since we are ignoring the dynamics along the weak trapping axis y, derivatives along this axes in the Hamiltonian are neglected:

$$\hat{H} = -\frac{\hbar^2}{2m}\left(\frac{\partial^2}{\partial x^2} + \frac{\partial^2}{\partial z^2}\right) - mgz. \tag{3.52}$$

We separate the wavefunction into a longitudinal part $\psi_{//}$ and a transverse part $\psi_{\perp}$:

$$\psi(\mathbf{x}) = \psi_{\perp}(\mathbf{x})\,\psi_{//}(z) \tag{3.53}$$

where $\psi_{//}$ satisfies the one dimensional equation

$$-\frac{\hbar^2}{2m}\frac{\partial^2\psi_{//}}{\partial z^2} + V\psi_{//} = E\psi_{//}\,, \tag{3.54}$$

When V is zero, the solutions to this are plane waves. In this case $V = -mgz$ and the equation has the solution:

$$\psi_{//} = c_1\,\mathrm{Ai}(-\frac{z}{l} - \frac{E}{mgl}) + c_2\,\mathrm{Bi}(-\frac{z}{l} - \frac{E}{mgl}), \tag{3.55}$$

where $l = (\hbar^2/2m^2g)^{1/3}$ and Ai and Bi are Airy functions of the first and second kind. The constants c_1 and c_2 need to be found in each case from

the boundary conditions. An alternative way to express $\psi_{//}$ is using the WKB method explicitly [66]:

$$\psi_{//}(z) = \sqrt{\frac{m}{p(z)}} \exp\left(\frac{i}{\hbar}\int_{z_0}^{z} p(z')\,dz'\right), \tag{3.56}$$

where $z_0 = -E/(mg)$ is the classical turning point. With $\psi_{//}$ written in this way, it is simpler to show that the derivative is:

$$\frac{\partial \psi_{//}}{\partial z} = \left(-\frac{1}{2p(z)}\frac{\partial p(z)}{\partial z} + \frac{i}{\hbar}p(z)\right)\psi_{//} \tag{3.57}$$

Using these expressions, and assuming an envelope $\psi_\perp = \psi_\perp(x,z)$ which is varies slowly along z, we obtain the paraxial equation of propagation for the transverse profile [56, 65]:

$$i\hbar\frac{p(z)}{m}\frac{\partial \psi_\perp}{\partial z} = -\frac{\hbar^2}{2m}\frac{\partial^2 \psi_\perp}{\partial x^2} + \frac{\hbar^2}{2m}\left(\frac{1}{p(z)}\frac{\partial p(z)}{\partial z}\frac{\partial \psi_\perp}{\partial z} - \frac{\partial^2 \psi_\perp}{\partial z^2}\right), \tag{3.58}$$

where $p(z)$ is the classical momentum:

$$p(z) = \sqrt{2m(E - V(z))}. \tag{3.59}$$

The paraxial approximation is made by neglecting the last two terms and reducing the equation to:

$$i\hbar\frac{p(z)}{m}\frac{\partial \psi_\perp}{\partial z} = -\frac{\hbar^2}{2m}\frac{\partial^2 \psi_\perp}{\partial x^2}. \tag{3.60}$$

To reduce this to the 1D Schrödinger equation, write z as a function of t, subject to the following constraint:

$$m\frac{d^2 z}{dt^2} = -\frac{dV}{dz} = mg, \tag{3.61}$$

and use this to rewrite:

$$\frac{\partial \psi_\perp}{\partial z} \longrightarrow \frac{\partial \psi_\perp}{\partial t}\frac{\partial t}{\partial z} = \frac{\partial \psi_\perp}{\partial t}\frac{m}{p(z)}. \tag{3.62}$$

Combining all of the above, it is possible to rewrite Equation 3.60 as the time dependent 1D Schrödinger equation:

$$i\hbar\frac{\partial \psi_\perp}{\partial t} = -\frac{\hbar^2}{2m}\frac{\partial^2 \psi_\perp}{\partial x^2}. \tag{3.63}$$

Such an equation can be expressed in the terms of Hermite-Gaussian polynomials, and so now we can make the connection to the gaussian optical beams discussed in §2.2. The lowest order Gaussian mode is:

$$\psi_\perp(x,t) = \left(\frac{2}{\pi w_0^2}\right)^{1/4} \exp\left(-\frac{x^2(1+i2\hbar t/(mw_0)}{w_0^2(1+4\hbar^2t^2/(m^2w_0^2)}\right). \tag{3.64}$$

The connection between optical laser beams and atom laser beams becomes particularly clear when expressed in this way:

$$\text{beam amplitude } (\psi \text{ or } E) \propto \exp\left(-\frac{x^2\,(1+i\alpha)}{w_0^2\,(1+\alpha^2)}\right), \tag{3.65}$$

where

$$\alpha = z/z_R, \quad z_R = w_0\sqrt{\pi/\lambda} \qquad \text{for light,} \tag{3.66}$$

$$\alpha = t/t_R, \quad t_R = w_0 m/(2\hbar) \qquad \text{for atoms.} \tag{3.67}$$

Therefore, all the analysis and calculations of the signal-to-noise ratio for optical laser beams in §2.2 apply equally to atom laser beams. For example, the visibility as a function of transverse displacement $V(d)$ is:

$$V(d) = \exp(-\tfrac{1}{2}d^2/w_0^2), \tag{3.68}$$

and is independent of propagation distance, the same as for optical gaussian laser beams.

3.4 ABCD MATRICES AND M^2

To map the position and width from t' to t, the ABCD matrices are used [53]:

$$\begin{pmatrix} x(t) \\ p(t)/\hbar \end{pmatrix} = \begin{pmatrix} A(\tau) & B(\tau) \\ C(\tau) & D(\tau) \end{pmatrix} \begin{pmatrix} x(t') \\ p(t')/\hbar \end{pmatrix}, \tag{3.69}$$

where $\tau = t - t'$. For free space, the ABCD matrix is:

$$\begin{pmatrix} A(\tau) & B(\tau) \\ C(\tau) & D(\tau) \end{pmatrix} = \begin{pmatrix} 1 & \hbar\tau/m \\ 0 & 1 \end{pmatrix} \tag{3.70}$$

These lead to a generalised second moment propagation law, which holds (in slightly different forms) for both light and atoms:

$$w(z)^2 = w_0^2 + M^4 \times \left(\frac{\lambda}{\pi w_0}\right)^2 (z - z_0)^2 \qquad \text{for light,} \tag{3.71}$$

$$w(t)^2 = w_0^2 + M^4 \times \left(\frac{\hbar}{2mw_0}\right)^2 (t - t_0)^2 \qquad \text{for atoms.} \tag{3.72}$$

The M^2 is calculated:

$$(M^2/2)^2 = (\Delta x(z))^2(\Delta k_x(z))^2 - C(z)^2, \tag{3.73}$$

where $\Delta x(z)$ is the beam width and $C(z)$ is the curvature-beam width product [53]:

$$C(z) = \frac{i}{2}\int_{-\infty}^{\infty} x\left(\psi\frac{\partial\psi^*}{\partial x} - \psi^*\frac{\partial\psi}{\partial x}\right)dx. \tag{3.74}$$

3.5 TRANSVERSE VELOCITY SPREAD

The classical trajectories model can be used to find the transverse velocity spread. This does not give the M^2 however, because after a diverging lens the waist is virtual and located above condensate. As above, we neglect divergence along the weak trapping axis, and so we consider the atom laser in cross section, in the plane of the two strong trapping axes. This model is valid in the regime where the velocity kick is large, specifically when $v_{z0} \gg \omega R$, where R is the Thomas-Fermi radius, and in the regime where the condensate sag is large, $z_{\text{sag}} \gg R$. The second condition allows us to approximate the outcoupling surface as a horizontal plane through the center of the condensate, (that is, the initial positions are $x_0 \in [-R, +R]$ and $z_0 = 0$).

Classically, an atom outcoupled at initial position x_0 has a transverse velocity after leaving the condensate:

$$v_x(x_0) = x_0\,\omega\sinh(\omega\,t_e) \approx x_0\omega^2 t_e, \tag{3.75}$$

where t_e is the time for an atom to leave the condensate (the escape time). For a large kick, atoms travel in almost straight lines along the kick direction, so the escape time is the vertical distance to the condensate

edge, divided by the kick magnitude, $t_e \approx \sqrt{(R^2 - x_0^2)}/v_{z0}$. The mean field transverse velocity is calculated:

$$(\Delta v_x)^2_{\mathrm{MF}} = \int_{-R}^{R} v_x(x_0)^2 n(x_0) dx_0, \tag{3.76}$$

where

$$n(x_0) = \frac{3}{4R}\left(1 - \frac{x_0^2}{R^2}\right) \tag{3.77}$$

is the linear number density across the out-coupling surface in the Thomas-Fermi regime. The transverse velocity spread due to the mean field is therefore:

$$(\Delta v_x)_{\mathrm{MF}} = \frac{2}{\sqrt{35}} \frac{\omega^2 R^2}{v_{z0}} \approx 0.3 \frac{\omega^2 R^2}{v_{z0}} = 0.6 \frac{\mu}{m} \frac{1}{v_{z0}}. \tag{3.78}$$

4

MEASUREMENT OF THE SPATIAL MODE

In this chapter, I describe a series of experiments on Raman atom lasers, which demonstrated their improved spatial mode compared to RF atom lasers. The results are compared to the theory of the previous chapter.

A list of experimental parameters is in Table 4.1, on page 72.

4.1 THE ANU BEC MACHINE (THIRD GENERATION)

The source of the atom laser is a Bose-Einstein condensate. This condensate is in ^{87}Rb, produced in a machine designed by Nick Robins and Cristina Figl, and built by Nick Robins, Cristina Figl, Julien Dugué and myself between July 2005 and January 2007. Pictures of the machine can be seen in Figures 4.1, 4.2, and 4.3. It is the third generation of experimental machine for producing BECs in our group. Details of the previous generations are contained in the PhD theses of Jessica Lye and Nick Robins [67, 68]. The design principles of this machine may be found in Nick Robins's thesis. I will briefly describe the operation of the machine here. It is based upon three different stages (see Figure 4.3):

1. A 2D MOT cools atoms from room temperature [69–72].
2. A 3D MOT in ultra high vacuum (UHV) is loaded from the 2D MOT by a near resonant laser beam which pushes cold atoms from one MOT to the other through a differential pumping stage.

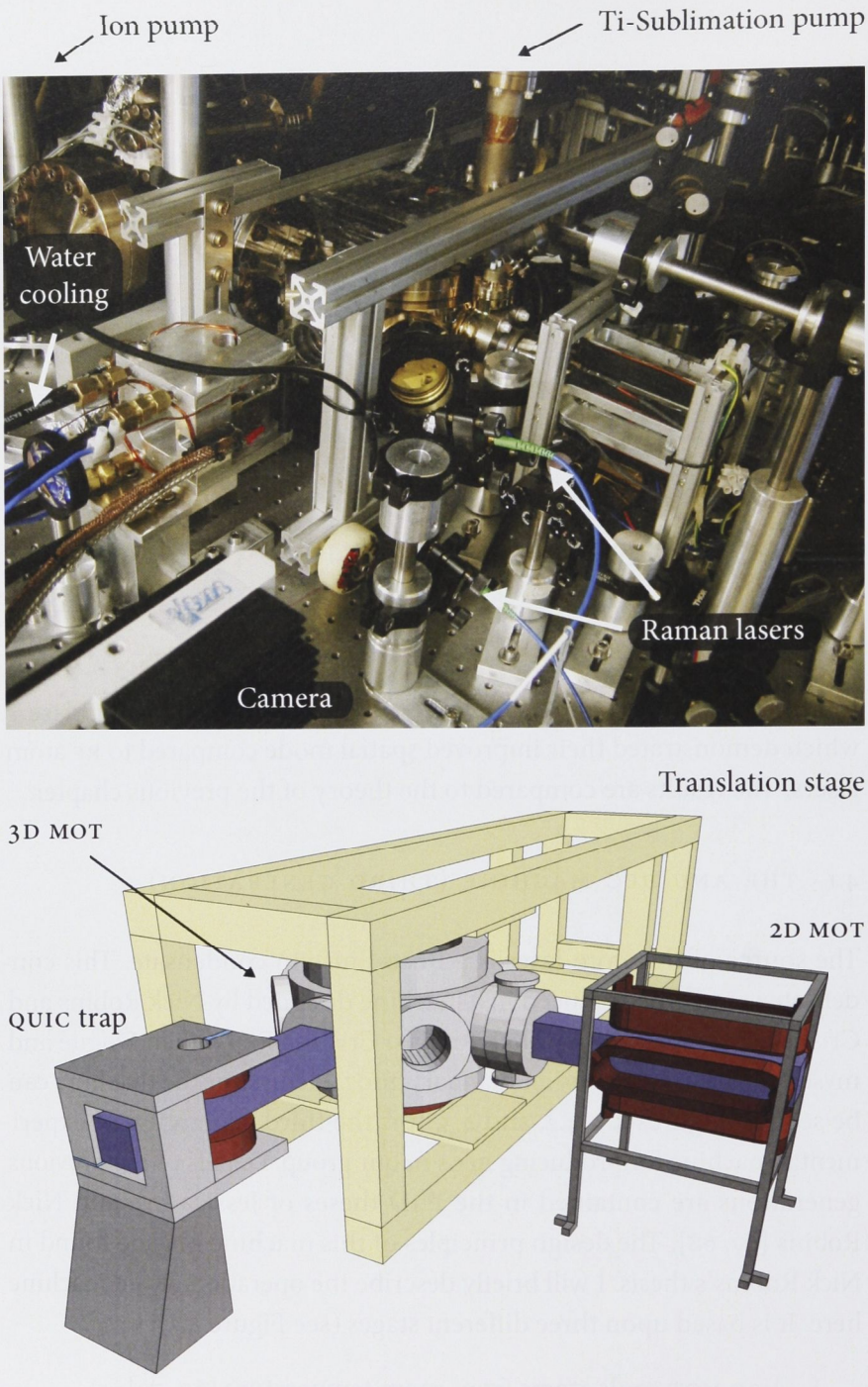

Figure 4.1: The experimental machine, designed by Nick Robins and Cristina Figl, and built by Nick Robins, Cristina Figl, Julien Dugué, and myself.

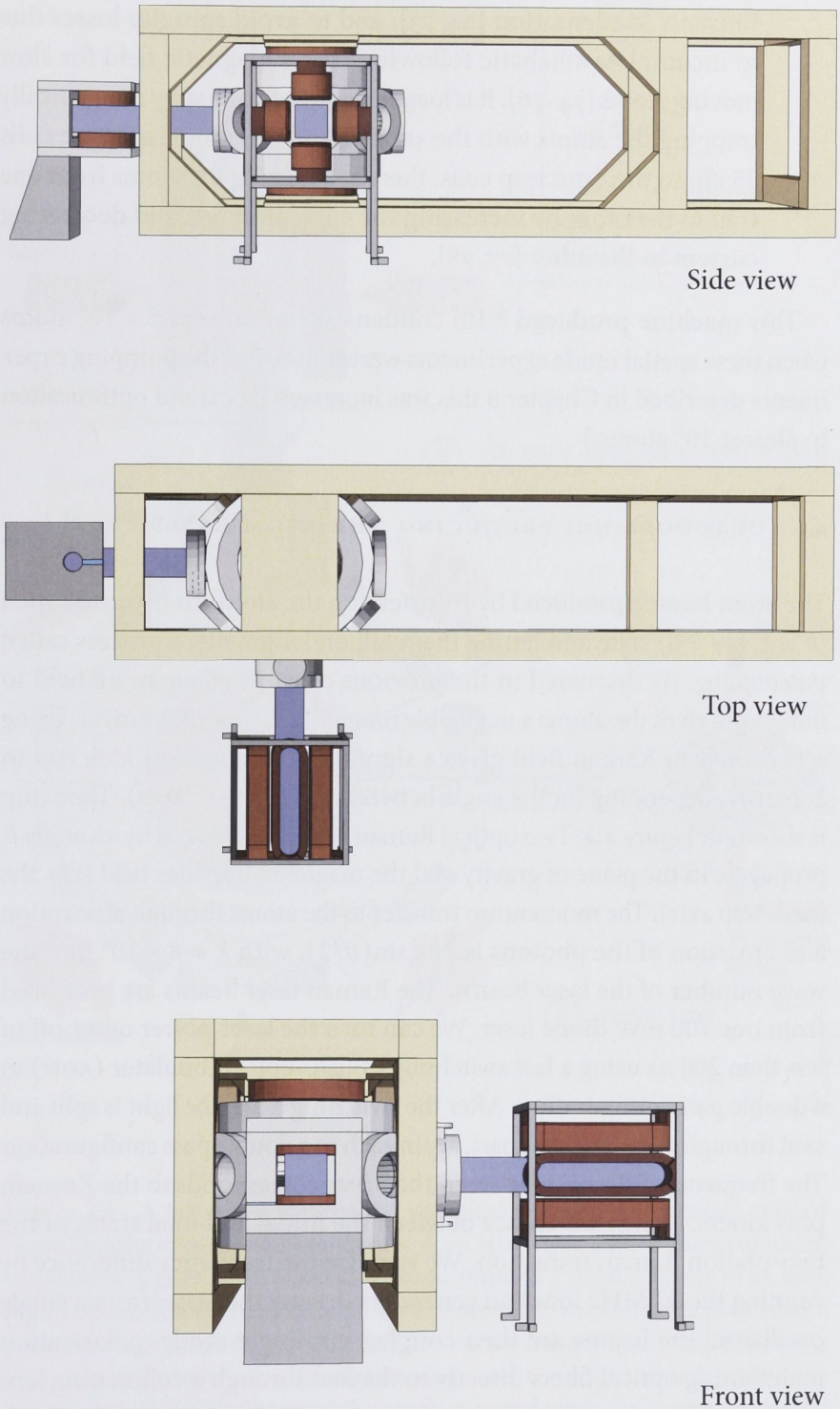

Figure 4.2: Side, top, and front view of the experimental machine.

3. A quadrupole Ioffe configuration (QUIC) magnetic trap creates a suitable harmonic potential for evaporating the atoms to Bose-Einstein condensation [24, 73], and to avoid spin flip losses due to incomplete adiabatic following of the magnetic field for slow moving atoms [74–76]. It is loaded from the 3D MOT by magnetically trapping the atoms with the 3D MOT coils and moving these coils 25 cm to the QUIC trap coils, then transferring the atoms from one trap to the other by increasing the current in one and decreasing current in the other [77, 78].

This machine produced ^{87}Rb condensates of around 5×10^5 atoms when these spatial mode experiments were done. (For the pumping experiments described in Chapter 8 this was increased by careful optimisation to almost 10^7 atoms.)

4.2 OUTCOUPLING: PRODUCING THE ATOM LASER

The atom laser is produced by transferring the atoms to the untrapped $|F = 1, m_F = 0\rangle$ state and letting them fall under gravity, a process called *outcoupling*. As discussed in the previous chapter, using an RF field to outcouple gives the atoms a negligible momentum kick (0.2 nm/s). Using a two-photon Raman field gives a significant momentum kick (up to 1.1 cm/s, depending on the angle between the Raman lasers). The setup is shown in Figure 4.4. Two optical Raman beams, separated by an angle θ, propagate in the plane of gravity and the magnetic trap bias field (i.e., the weak trap axis). The momentum transfer to the atoms through absorption and emission of the photons is $2\hbar k \sin(\theta/2)$, with $k = 8 \times 10^6$ m^{-1} the wave number of the laser beams. The Raman laser beams are produced from one 700 mW diode laser. We can turn the laser power on or off in less than 200 ns using a fast switching acousto-optic modulator (AOM) in a double pass configuration. After the switching AOM, the light is split and sent through two separate AOMs, again each in a double pass configuration. The frequency difference between the AOMs corresponds to the Zeeman plus kinetic energy difference between the initial and final states of the two-photon Raman transition. We stabilize the frequency difference by running the 80 MHz function generators driving the AOMs from a single oscillator. The beams are then coupled via single mode, polarization maintaining optical fibers directly to the BEC through a collimating lens and waveplate, providing a maximum intensity of 2500 mW/cm^2 per beam at the BEC. The polarization of the beams is optimized to achieve maximum outcoupling with a downward kick and corresponds to π

Raman laser beam setup

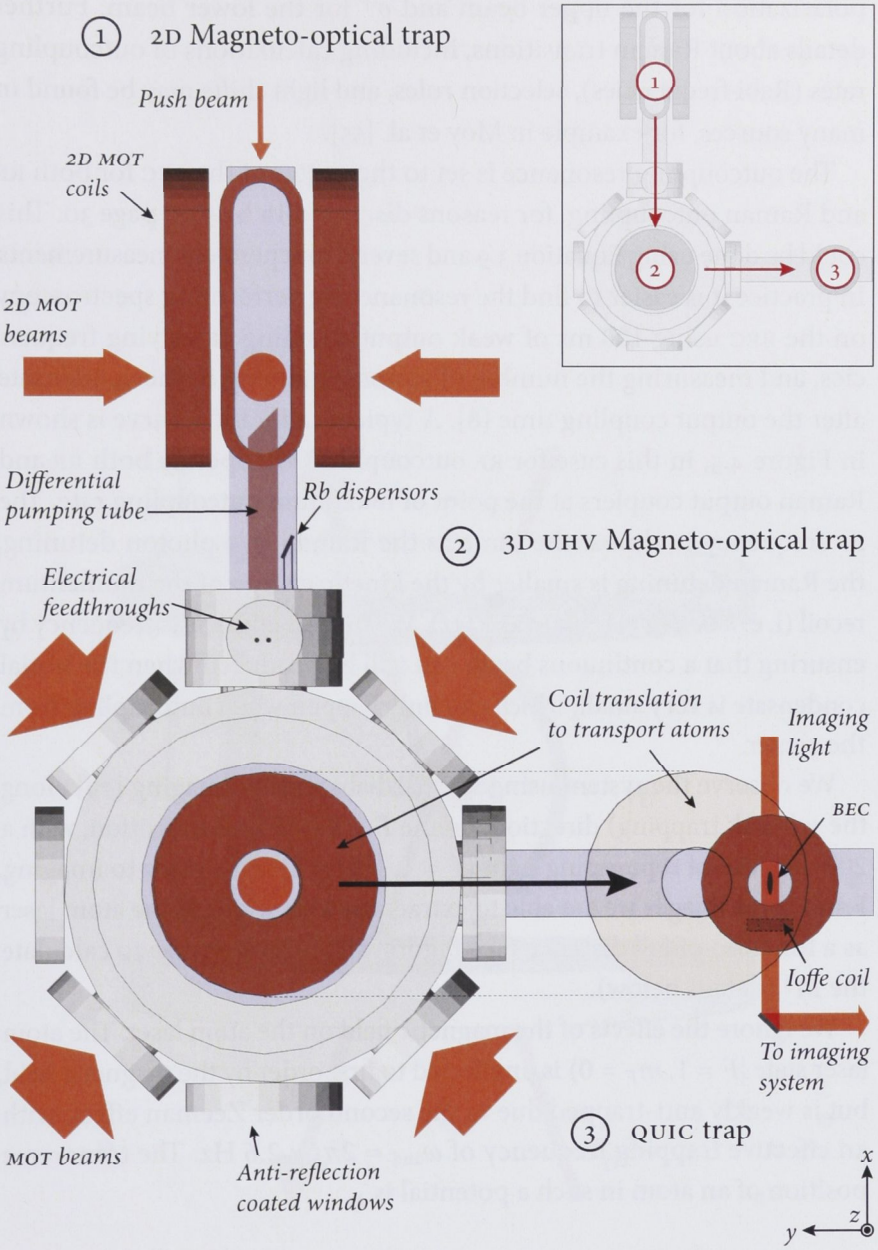

Figure 4.3: A top down view of the vaccuum system and magnetic coils, illustrating the experimental sequence. A 2D MOT (1) is loaded from rubidium dispensors. A laser beam pushes the atoms through a small aperture to an ultra high vacuum (UHV) chamber and into a 3D MOT (2). The atoms are polarisation gradient cooled, and the 3D MOT coils are used to magnetically trap the atoms. The coils are moved via a translation stage and the atoms transferred to the QUIC trap coils (3). In this trap the atoms are cooled via force RF evaporation to BEC. Vaccuum chamber is in grey, magnetic coils in maroon, glass cells in blue and lasers in red. *Inset:* minature showing progression of atoms through experimental cycle.

polarization for the upper beam and σ^+ for the lower beam. Further details about Raman transitions, including calculations of outcoupling rates (Rabi frequencies), selection rules, and light shifts may be found in many sources, for example in Moy et al. [55].

Outcoupling resonance

The outcoupling resonance is set to the center of the BEC for both RF and Raman outcoupling, for reasons discussed in §2.5 on page 30. This could be done using Equation 3.9 and several independent measurements. In practice it is easier to find the resonance by performing spectroscopy on the BEC using 100 ms of weak output coupling at varying frequencies, and measuring the number of atoms remaining in the condensate after the output coupling time [8]. A typical calibration curve is shown in Figure 4.5, in this case for RF outcoupling. We operate both RF and Raman output couplers at the point of maximum outcoupling rate. The RF frequency is almost the same as the Raman two photon detuning; the Raman detuning is smaller by the kinetic energy of the momentum recoil (i. e. $\hbar^2k^2/(2m) = h \times 13$ kHz). We further check this frequency by ensuring that a continuous beam can still be produced when the initial condensate is very small, which can only happen when outcoupling from the center.

We observe the system using standard absorption imaging [79] along the y (weak trapping) direction, on the $F = 2 \rightarrow F' = 3$ transition, with a 200 μs pulse of repumping light ($F = 1 \rightarrow F' = 2$) 1 ms prior to imaging. From these images we are able to extract the RMS width of the atom laser as a function of fall distance (see Figure 4.6), which we use to calculate the M^2 (details below).

Second order Zeeman effect

We ignore the effects of the magnetic field on the atom laser. The atom laser state $|F = 1, m_F = 0\rangle$ is unaffected to first order by the magnetic field, but is weakly anti-trapped due to the second order Zeeman effect, with an effective trapping frequency of $\omega_{2\text{nd}} = 2\pi i \times 2.6$ Hz. The transverse position of an atom in such a potential is

$$x(t) = x_0 \cosh(\omega_{2\text{nd}} t) \approx x_0(1 + \omega_{2\text{nd}}^2 t^2/2). \tag{4.1}$$

For the 1 mm (14 ms) propagation we consider here the transverse position is affected by less than 3%. We also ignore the AC Stark effect of the Raman beams on the atom laser, because the intensity of the beams does not change significantly over the 1 mm propagation.

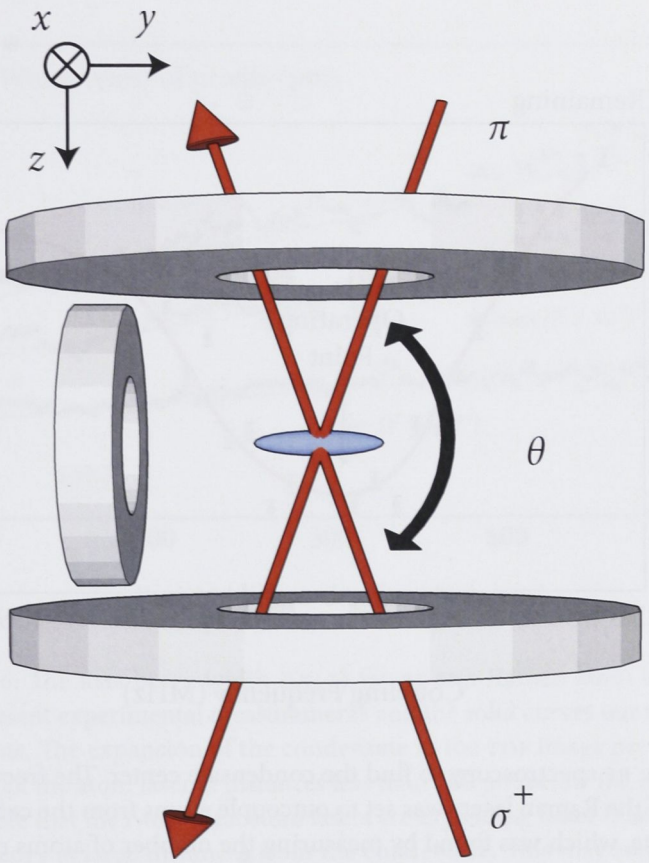

Figure 4.4: Experimental schematic (not to scale) showing the BEC, Raman lasers, and trapping coils.

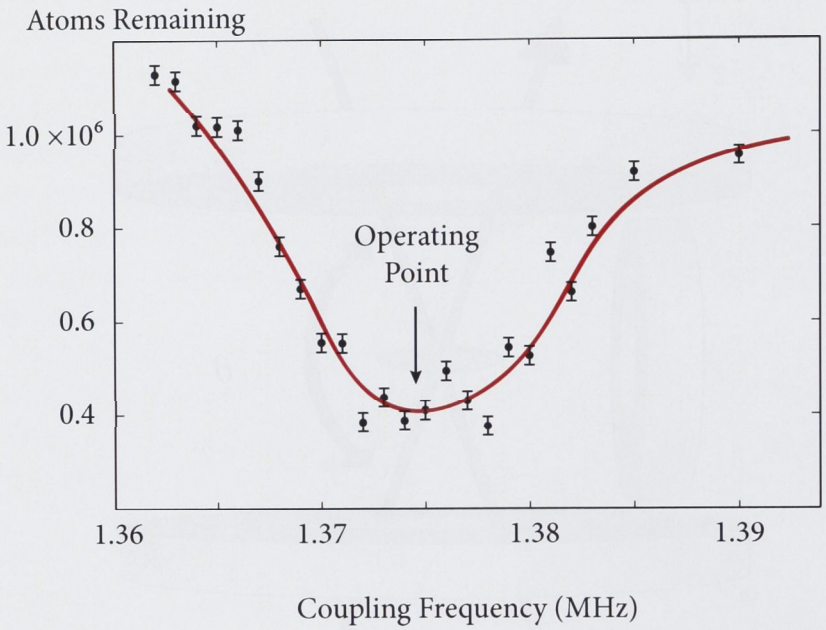

Figure 4.5: RF spectroscopy to find the condensate center. The frequency difference of the Raman lasers was set to outcouple atoms from the center of the condensate, which was found by measuring the number of atoms remaining after 100 ms of weak RF outcoupling. The operating frequency (or outcoupling frequency) of 1.374 MHz is indicated on the plot; the solid line is to guide the eye. Outcoupling from the center is equivalent (in the notation of the theory chapter §3) to setting the outcoupling radius r_{oc} equal to the gravitational sag z_c. The error bars are based upon the typical standard deviation; most frequencies were measured only once.

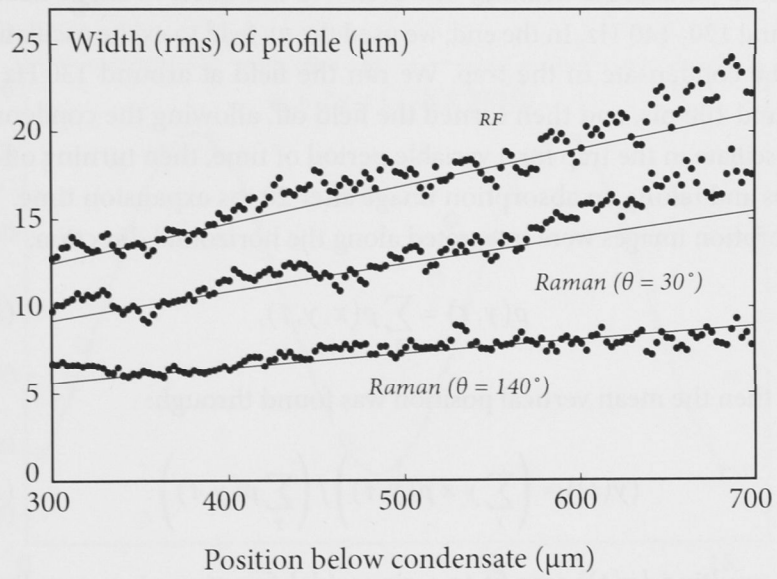

Figure 4.6: The RMS beam width $\Delta x(z)$ for RF and Raman atom lasers. The dots represent experimental measurements and the solid curves our theoretical predictions. The expansion of the condensate in the TOF image prevented observation of the atom laser at distances less than 300 μm below the condensate center. Note that the two widest atom lasers are expanding faster than predicted by the theory at large distances from the condensate. This may be due to the influence of the second order Zeeman effect: the wider the atom laser the greater its effect.

4.3 TRAP FREQUENCY

To measure the M^2 value requires measurement of the trap frequency ω. We initially tried to do this using a slowly oscillating electromagnetic field to induce parametric heating. In this process, the trap frequency is modulated at frequency $\Omega = 2\omega$, which causes the energy of the system to grow exponentially. We performed this with a simple coil outside the vacuum system and driving it at a frequency of 200–300 Hz, since modeling of the trap predicted a frequency of $\omega = 140$ Hz. We did not observe parametric heating, however. We did observe slight heating around 120–140 Hz. In the end, we used the RF field to excite oscillations of the condensate in the trap. We ran the field at around 130 Hz for around 100 ms, and then turned the field off, allowing the condensate to oscillate in the trap for a variable period of time, then turning off the traps and taking an absorption image after 20 ms expansion time. The absorption images were integrated along the horizontal direction:

$$\rho(y,t) = \sum_x \rho(x,y,t), \tag{4.2}$$

and then the mean vertical position was found through:

$$\langle y(t) \rangle = \left(\sum_y y \times \rho(y,t) \right) / \left(\sum_y \rho(y,t) \right). \tag{4.3}$$

The resulting $\langle y(t) \rangle$ was fit to a sinusoidal function via a non-linear recursive algorithm, to find the trap frequency $\omega = 2\pi \times (128 \pm 3)$ Hz. The data and the fit may be seen in Figure 4.7.

4.4 ANALYSIS OF RESULTS

Calculating the quality factor M^2 of the atom laser directly from Equation (2.27) requires measurement of the beam width at the waist Δx_0. Because the BEC acts as a diverging lens on the atom laser, the beam waist is *virtual* and located above the BEC, and so it is not possible to measure the beam quality M^2 using Equation 2.27 only. For our simulations, M^2 is calculated equivalently from the wavefunction $\psi(x,y,z)$ at some height z below the BEC in which the atom laser has reached the paraxial regime:

$$(M^2/2)^2 = (\Delta x(z))^2 (\Delta k_x(z))^2 - C(z)^2, \tag{4.4}$$

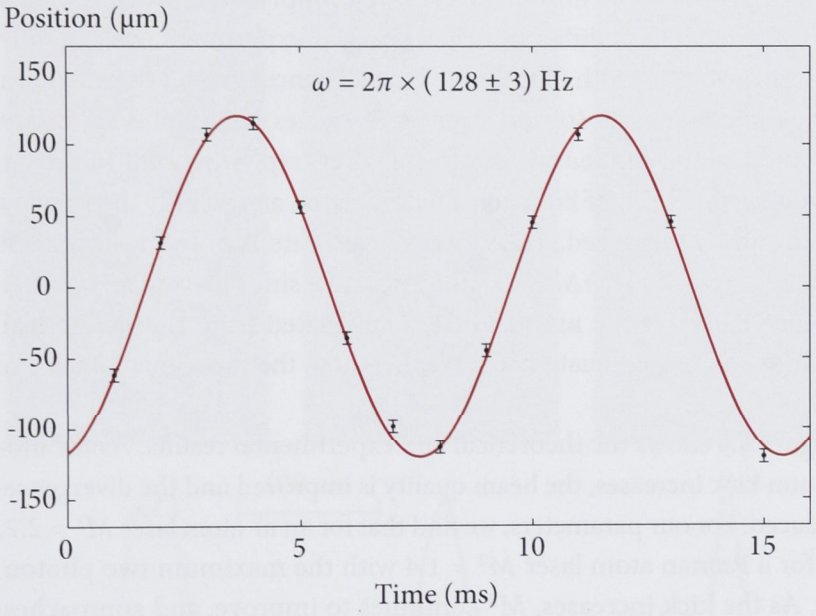

Figure 4.7: Trap frequency measurements. The fit to the data is in red, and gives the trap frequency as being $\omega = 2\pi \times (128 \pm 3)$ Hz. The weak trapping frequency $\omega_y = 2\pi \times 12$ Hz is derived from this frequency, from a previous measure of the aspect ratio when $F = 2$ atoms were used. The error bars are based upon the typical standard deviation for a measurement; most oscillation times were only measured once.

where $\Delta x(z)$ is beam width and $C(z)$ is the curvature-beam width product [53]:

$$C(z) = \frac{i}{2}\int_{-\infty}^{\infty} x\left(\psi\frac{\partial\psi^*}{\partial x} - \psi^*\frac{\partial\psi}{\partial x}\right)dx. \tag{4.5}$$

In practice it is difficult to measure the wavefunction phase, and hence $C(z)$. However, the beam width (in the paraxial regime) obeys:

$$\Delta(x(t))^2 = (\Delta x_0)^2 + (\Delta v_x)^2(t - t_w)^2, \tag{4.6}$$

where t_w is the time when the beam is at its waist, and Δx_0 is the beam waist. In principle M^2 may be determined simply from measurements of the beam width at different heights. In our experiment, we can only measure the beam width in the far field, at distances greater than 300 μm below the condensate (observation at distances less than 300 μm are prevented by the condensate expansion after trap switchoff.) In the far field the second term of Equation 4.6 dominates, and so only the velocity spread can be measured. Therefore we calculate Δx_0 and t_w from the model, $t_w = m\,C(z)/(\hbar\Delta k_x^2)$, with t_w negative since the waist is virtual and located above the BEC, and $C(z)$ calculated from the theoretical wavefunction using Equation 4.5. We then fit to the experimental data to find Δv_x.

Figure 4.9 shows the theoretical and experimental results. As the momentum kick increases, the beam quality is improved and the divergence is reduced. For our parameters, we find that for an RF atom laser $M^2 = 2.2$, and for a Raman atom laser $M^2 = 1.4$ with the maximum two photon kick. As the kick increases, M^2 continues to improve, and approaches but does not reach the Heisenberg limit of one. It asymptotes to a limit slightly above that, which for our parameters is equal to 1.3. In this regime of large kick, the interaction of the outcoupled atoms with the condensate becomes negligible, and the transverse atom laser wavefunction is approximately the free space evolution of the condensate wavefunction (along the outcoupling surface). It is therefore limited by the non-ideal (non-Gaussian) condensate wavefunction itself. We calculate the product $\Delta x\Delta p_x$ for the condensate wavefunction (taken through the central horizontal plane of the condensate) to be 1.3. We have therefore improved the beam quality M^2 by 40 percent from the RF outcoupled case, down to a factor of 1.4 above the Heisenberg limit.

Improvement in tightly confining traps

In addition, our simulations show that (using the same maximum two photon kick) it is possible to reach the condensate limit even for much tighter trapping potentials. In Figure 4.10, we show the results of simulations for increasing trap frequencies, up to $\omega = 2\pi \times 300$ Hz.

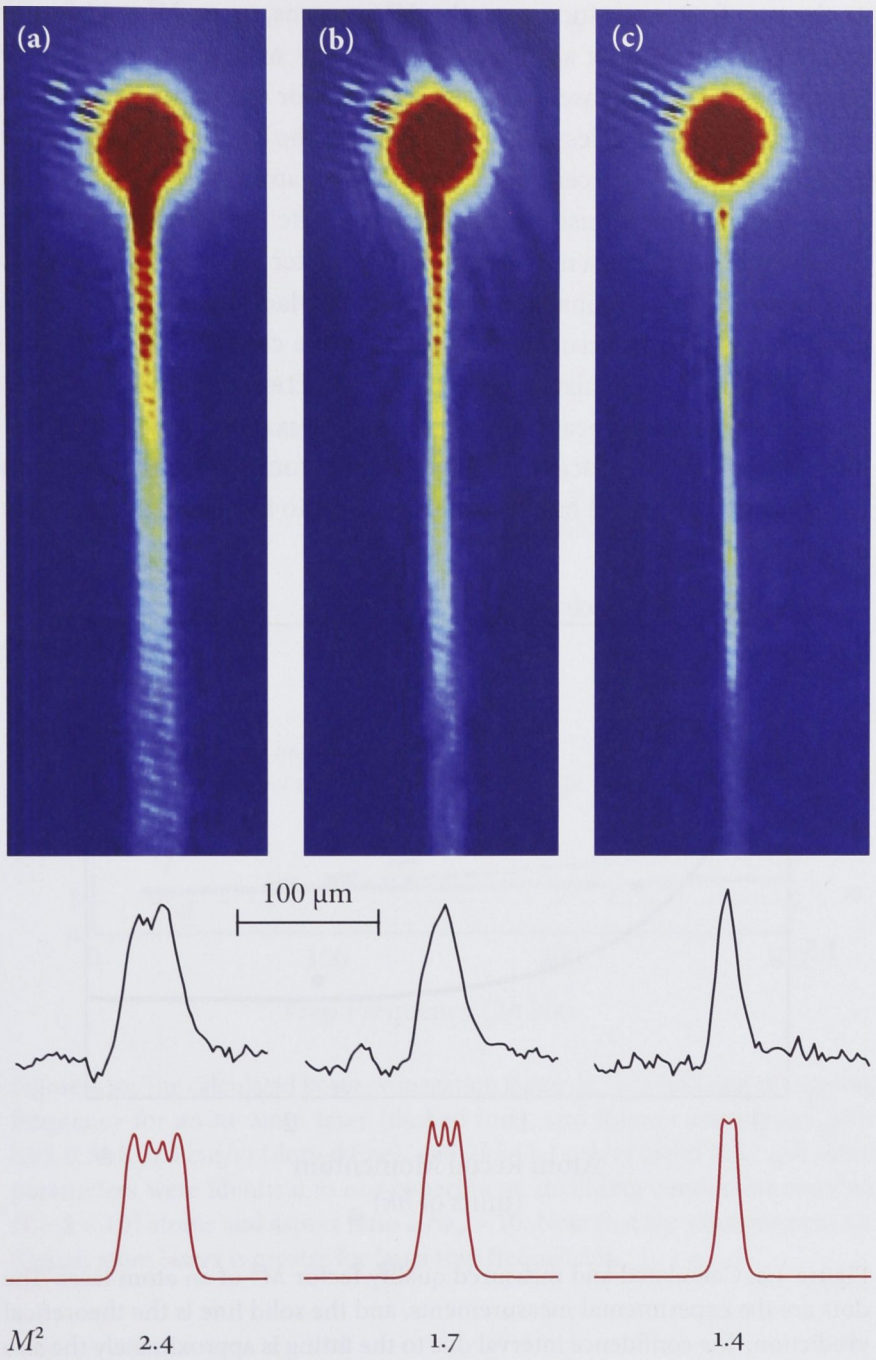

Figure 4.8: Top: Sequence of atom laser beams showing the improved beam profile of a Raman atom laser. The atom laser beams were produced using RF (a) and Raman (b and c) transitions. The angle between the Raman beams (see Figure 4.4) was $\theta = 30°$ in (b) and $\theta = 140°$ in (c), corresponding to a kick of $0.5\hbar k$ (0.3 cm/s and $1.9\hbar k$ (1.1 cm/s) respectively. The outcoupling rate differs between each atom laser. Below: Comparison of experimental (second row, in red) and theoretical (bottom row, in black) beam profiles 500 μm below the BEC. The theoretical profiles have been calculated using the method described in Chapter 3. The height of each profile is the only free parameter, and has been scaled to match the experimental data. The fringes that can be observed in the condensates are an imaging artifact (the CCD cover plate acts as an etalon for the coherent imaging light).

As the trap frequency increases, the M^2 worsens, up to $M^2 = 14$ for RF outcoupling from a $2\pi \times 300$ Hz trap. For the maximum Raman two photon kick, the increase is only to $M^2 = 1.7$ for the same $2\pi \times 300$ Hz trap. Only for traps of less than $2\pi \times 50$ Hz is the beam quality of an RF atom laser within 5 percent of that of a Raman atom laser.

Susceptability to transverse displacements

As discussed previously, it is difficult to relate the M^2 directly to the signal-to-noise ratio of a measurement. In Chapter 2, the specific example of a measurement dominated by transverse displacements was discussed. It was found that the crucial parameter in this case was $\partial^2 V/\partial d^2$. Figure 4.11 shows the calculated $\partial^2 V/\partial d^2$ as a function of momentum kick. In an interferometric measurement with high flux atom lasers (noise limited by transverse displacements), the Raman atom laser with maximum two photon kick would have a signal-noise-ratio five times greater than an RF atom laser.

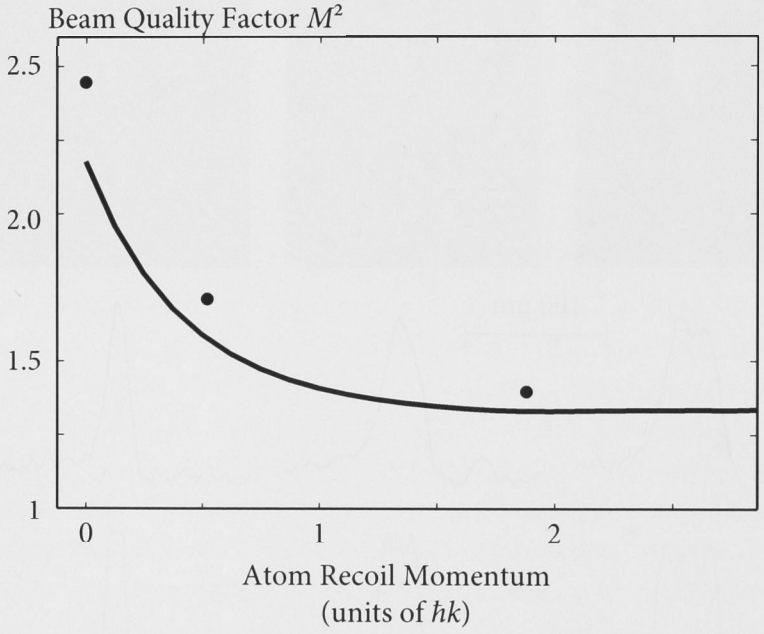

Figure 4.9: Calculated and measured quality factor M^2 of an atom laser. The dots are the experimental measurements, and the solid line is the theoretical prediction. The confidence interval due to the fitting is approximately the size of the dots; there may be systematic errors including the second order Zeeman effect affecting the results.

4.5 FUTURE WORK

This technique could be improved in several ways. Increasing the momentum kick only improves the spatial profile to the condensate limit;

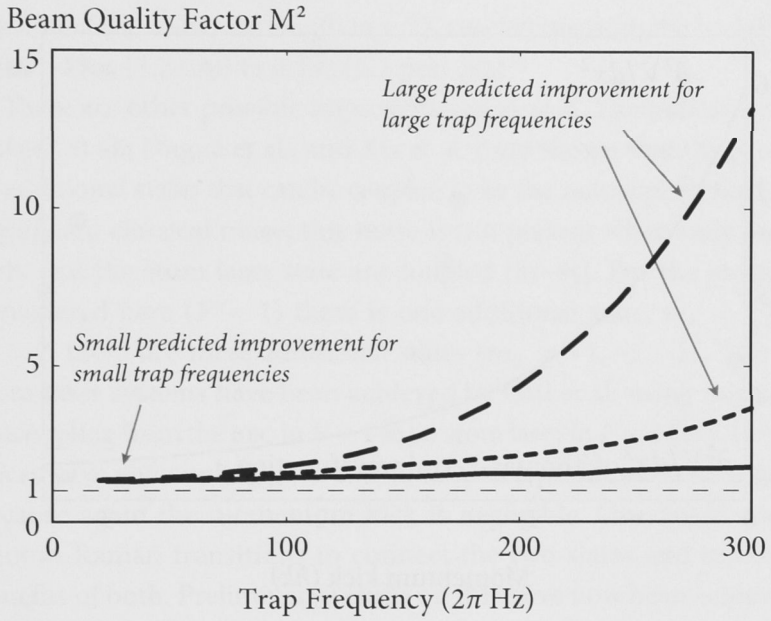

Figure 4.10: The calculated beam propagation factor M^2 as a function of trapping frequency for an RF atom laser (dashed line), and Raman atom lasers with kick $0.5\hbar k$ (0.3 cm/s) (dotted line), and $2\hbar k$ (1.1 cm/s) (solid line). All other parameters were identical to our experiment, including condensate number $N = 5 \times 10^5$ atoms and aspect ratio $\omega/\omega_y = 10$. Note that the improvement for Raman atom lasers is greater for large trap frequencies.

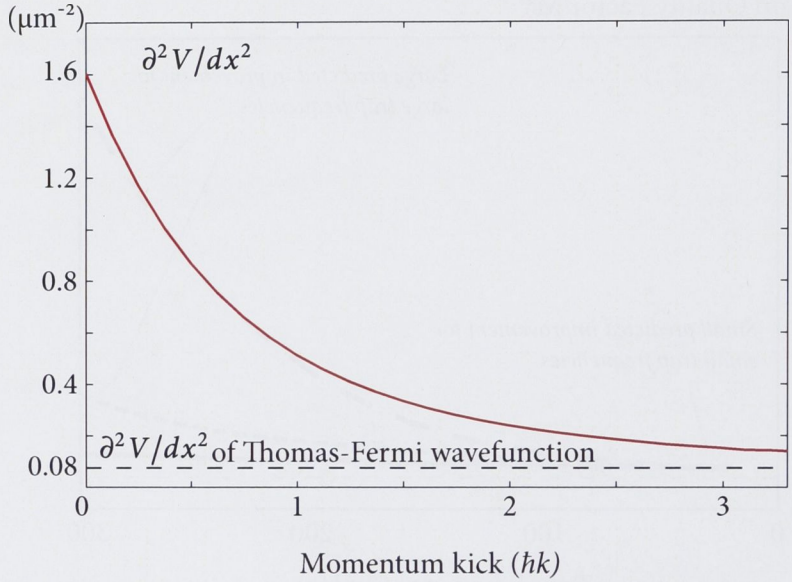

Figure 4.11: Calculated $\partial^2 V/\partial d^2$ (second partial derivative of fringe visibility V with respect to transverse misalignment x of interfering beams), as a function of momentum kick $\hbar k$ for the parameters of this experiment. (This directly influences the signal-to-noise ratio of a measurement, see §2.2 for details). The dotted line shows the calculated $\partial^2 V/\partial d^2$ of the Thomas-Fermi wavefunction (given by Equation 3.6 with our parameters R = 5 μm, ϵ = 10).

the maximum two photon is sufficient for our experiment (we measure $M^2 = 1.4$ compared to the infinite kick limit of $M^2 = 1.3$) but for tighter traps a larger momentum kick will be necessary. These could be done by combining Bragg and Raman transitions [80] or indeed any technique to selectively accelerate the atom laser out of the condensate: for example, one could outcouple to magnetically sensitive Zeeman states from an $m_F = 0$ condensate in an optical trap and using magnetic fields to accelerate the atom laser away. To go beyond the condensate limit will likely require removing the mean field interaction altogether with aid of a Feschbach resonance [81]. For example, Fattori et al. have reported reduction of the scattering length in a ^{39}K condensate from the background value $-33a_0$ (1.7 nm) to $0.1a_0$ (5.3 pm) [82].

Removing the mean field interaction

There are other possible improvements as well. Theoretical work by Robins et al., Dugué et al., and Xia et al. have shown that the presence of additional states that can be coupled to by the outcoupling field cause significant classical noise; this noise is not present when only the BEC state and the atom laser state are coupled [83–85]. For the atom laser considered here ($F = 1$) there is one additional state, $m_F = +1$. For $F = 2$, there are three additional states ($m_F = +1, -1, -2$). Two state atom laser systems have been achieved by Öttl et al. using microwave outcoupling from the BEC in $F = 1$ to an atom laser in $F = 2$ [86]. However, microwave outcoupling gives the same spatial profile as RF outcoupling because again the momentum kick is negligible. One could use two photon Raman transitions to connect the two states and receive the benefits of both. Preliminary results on this have now been achieved by J. Debs and D. Döring in our group (to be published).

Two state atom lasers

QUANTITY	VALUE	SYMBOL
Photon recoil atom velocity	5 mm/s	v_0
Photon recoil wavenumber	8×10^6 m^{-1}	k
Chemical potential	$h \times 1.8$ kHz	μ
Thomas-Fermi radius	5 μm	R
Gravitational sag	15 μm	z_c
Scattering length	5.77 nm	a
Raman beam intensity	2500 mW/cm^2	
Raman single photon detuning	300 GHz	Δ
Effective two photon Rabi frequency	100–1000 Hz	Ω_{eff}
Outcoupling frequency	1.374 MHz	
Outcoupling radius	15 μm	r_{oc}
Raman beam polarisation		
downward propagating	π	
upward propagating	σ^+	
Magnetic quadrupole trap gradient	200 G/cm	
Tight trapping frequency	$2\pi \times 128$ Hz	ω
Weak trapping frequency	$2\pi \times 12$ Hz	ω_y
Trap aspect ratio	10	ϵ
Second order Zeeman shift trapping frequency	$2\pi i \times 2.6$ Hz	ω_{2nd}
Magnetic bias field	2.0 G	B_0
Imaging detuning	- (resonance)	
Pixel size (at position of atoms)	2.8 μm	
Pixel size (on camera)	16 μm	
BEC atom number	5×10^5 atoms	N_c
BEC internal state	$\|F = 1, m_F = -1\rangle$	$\|1\rangle$
Atom laser internal state	$\|F = 1, m_F = 0\rangle$	$\|2\rangle$

Table 4.1: Selected parameters for Raman atom laser experiment.

Part II

GUIDED ATOM LASERS

5

ABOUT GUIDED ATOM LASERS

This chapter is about atom lasers propagating inside wave guides.

This work was done between October 2007 and April 2008 in the Laboratoire Kastler Brossel (LKB), located at the École Normale Supérieure (ÉNS) in Paris, in the group of David Guéry-Odelin. During this time we produced guided atom lasers with ^{87}Rb, and we produced the first *spinor* guided atom laser: that is, an atom laser which contains many different spin states in the same beam.

In the previous chapters, I have discussed atom lasers propagating in free space: their advantages, disadvantages, methods of production and techniques to improve them. In this chapter I do the same for atom lasers propagating in a guide. The waveguide used in these experiments was an *optical guide*. This is a beam of light that confines atoms along the intensity maximum, because its wavelength is longer than the wavelength of an atomic resonance. Most of the discussion, however, applies to any guide formed by any suitable potential.

Convention for this chapter: z is guide axis, y is down, x is fixed by the other two to be horizontal and perpendicular to the guide. The quantisation axis for angular momentum is always chosen relative to the magnetic field direction, so that $|F = 1, m_F = -1\rangle$ is the low field seeker.

5.1 THEORETICAL FORMALISM

By a *guided* atom laser, I mean that there is a potential field which confines the atom laser in two dimensions. This field is constant in value (or approximately so) along the propagation direction, so that the motion of

the atoms is unimpeded along the guide. An example of such a potential field would be a 2D harmonic potential:

$$V(\mathbf{x}) = \frac{1}{2} m \left(\omega_x^2 x^2 + \omega_y^2 y^2 \right) \tag{5.1}$$

Such a potential is separable, and admits solutions of the form:

$$\phi(\mathbf{x}) = \phi_x(x)\phi_y(y)\phi_z(z), \tag{5.2}$$

where ϕ_x and ϕ_y are solutions of the 1D harmonic oscillator potential,

$$\phi_x(x) = \sum_n c_n \frac{\exp(-\frac{x^2}{2}) H_n(x)}{\sqrt[4]{\pi}\sqrt{2^n n!}}, \tag{5.3}$$

and similarly for $\phi_y(y)$. The precise potential for our experiments was the intensity profile of a gaussian beam, which is well approximated by the harmonic potential above in a small region around the center of the beam (see §7.2 on page 92 for more details).

Advantages and disadvantages

Many advantages to a guide for an atom laser are similar to a guide for an optical laser: that stationary modes of propagation for the transverse modes may be found, which remove the problem of divergence and the changing of mode structure. For atom lasers, a guide also has the advantage that it can support the atoms in a gravitational field so that they do not fall. This is a significant technical problem for free space atom lasers, since the velocity increases linearly in time and the de Broglie wavelength (which is inversely proportional to the velocity) becomes smaller and smaller. This quickly becomes a problem: after 1 s of free fall the de Broglie wavelength is 0.5 nm (for Rubidium), which is already several orders of magnitude smaller than can be directly observed with absorption imaging. With a horizontal waveguide, acceleration of the atom laser can be reduced – to date, a reduction to 0.07 ± 0.06 m/s^2 has been reported [87].

There are disadvantages to using wave guides in a precision measurement. Fluctuations in the guide itself (position, size, shape, and so on) affect the atom laser, and create noise on any measurement performed. Atoms freely falling do not suffer from this problem, and act as a superb reference to make measurements against. For this reason, precision measurements with atoms (thermal beams) have so far been done in free space [88]. Of course, this is a technical problem, not an intrinsic problem, and it can in principle be solved.

In the previous chapter, I examined the importance of spatial mode for free space atom lasers. For guided atom lasers, this is also important

Spatial mode

and for precisely the same reason. The figure of merit for a *guided atom laser* is the mean excitation number $\langle n \rangle$. It is equivalent to the beam propagation factor M^2 for free space atom lasers, which was discussed in Chapter 2 of this thesis. The quantity $\langle n \rangle$ is defined in the usual way for the expectation value of a Hermitian operator:

$$\langle n \rangle \equiv \langle \psi | \hat{n} | \psi \rangle = \sum_j n_j |\langle j | \psi \rangle|^2, \qquad j = 0, 1, 2, \ldots, \tag{5.4}$$

where $|j\rangle$ are the energy eigenvalues of the guide potential. Figure 5.1 demonstrates the principle of $\langle n \rangle$, showing a hypothetical guided atom laser spectroscopy in one transverse dimension. Of course, in reality the guide has two transverse dimensions. In our experiment, we could only view the atom laser along one direction perpendicular to the guide (being the vertical direction). For simplicity, we therefore assumed rotational symmetry of the guide, since we measured the horizontal beam to be approximately circular, with an aspect ratio of typically 1.0–1.2. The variation occurred because of dust buildup on the optics, which imprinted a random, non-uniform and non-linear phase shift that was significant at the high powers used (see Figure 6.5 on page 86).

5.2 CONTEXT

Laboratoire Charles Fabry guided atom laser

The first experiment (and, to date, the only other experiment) to produce a guided atom laser was done by Guerin et al. in the group of Phillipe Bouyer and Alain Aspect at the Laboratoire Charles Fabry (LCF) in Orsay (now Palaiseau) [87, 89]. They first condensed magnetically trapped $m_F = -1$ atoms inside a hybrid optomagnetic trap, a superposition of Ioffe-Pritchard trap and horizontal optical waveguide, and then used a radio frequency (RF) transition to outcouple the atom laser into the guide. The second order Zeeman effect of their magnetic trap was used to cancel the curvature of the optical guide potential, so that the de Broglie wavelength of the atom laser remained roughly constant over the 1 mm propagation distance. Some differences between the experiments at Orsay and ÉNS are given in Table 5.1. The Orsay experiment has since measured the transmission of atoms through a partially reflecting mirror in the guide (formed by a separate blue detuned laser beam), with the goal of building a Fabry-Perot cavity for atoms [90]. Recently they have observed Anderson localisation inside the guide [91].

A laser needs a resonator a cavity, a gain medium, and an outcoupler. Inside the resonator is a large population inside one cavity mode. For an

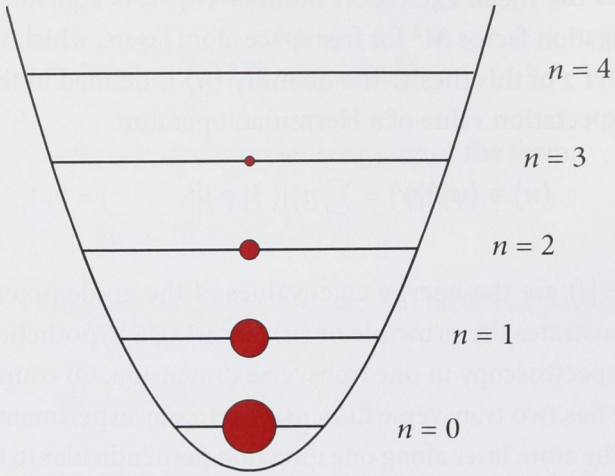

Figure 5.1: Hypothetical spectroscopy of a guided atom laser (along one transverse dimension), to illustrate the concept of mean excitation number $\langle n \rangle$. The area of each circle corresponds to the population in that state, being $|c_0|^2 = 0.6$, $|c_1|^2 = 0.3$, $|c_2|^2 = 0.08$, $|c_3|^2 = 0.02$, and giving $\langle n \rangle = 0.52$. The populations in each state are only shown for illustrative purposes, since in the experiment only $\langle n \rangle$ can be measured.

optical laser, this is a highly excited mode. For an atom laser, this mode is the ground state of the trap[1]. For an optical laser, the resonator is the cavity (e.g., partially reflecting mirrors or similar).

The first optical trapping of atoms was reported by Chu et al., in 1986 [92]. They used a single gaussian laser beam to trap around 500 atoms at around 1 mK. The first all-optical Bose-Einstein condensate (BEC) (that is, transferring atoms from a magneto-optical trap (MOT) to an optical trap with no intermediate magnetic trap stage) was reported by Barrett et al., in the group of Mark Chapman at the Georgia Institute of Technology. They used two intersecting beams from a CO_2 laser at 10.6 μm wavelength to produce a condensate of 3×10^4 atoms [93, 94]. The first optical atom laser (that is, outcoupling an atom laser by reducing the power in an optical trap) was reported by Anderson et al. in the group of Mark Kasevich at Yale (now Stanford) [95]. They held Bose-condensed

1 It is not essential that the mode be the ground state of the trap for an atom laser. The ground state is the only one that may be macroscopically populated by Bose-Einstein condensation, but after that process is complete the condensate could be transferred to an excited state of the trap and kept there.

PROPERTY	LCF	LKB
Mean excitation number $\langle n \rangle$	2.2 ± 0.1	0.65 ± 0.05
Flux (atom/s)	5×10^5	4×10^5
Guide frequency (Hz)	$2\pi \times 360$	$2\pi \times 245$
Propagation distance (mm)	1.5	4
Propagation time (s)	0.1	0.5
Longitudinal velocity spread	Small ($\sim t$)	Large ($\sim t^2$)
Uses state-changing outcoupling	Yes (RF)	No
Zeeman states of atom laser	$m_F = 0$	All

Table 5.1: Comparison of the guided atom lasers produced at the Laboratoire Charles Fabry (LCF) in Orsay and the Laboratoire Kastler Brossel (LKB) at ÉNS.

atoms at multiple anti-nodes of a vertical optical standing wave, with the atoms tunnelling through to form a coherent pulsed beam.

The first quasicontinuous optical atom laser was reported by Cennini et al., in the group of Martin Weitz at Tübingen. Their experiment used a single trapping beam: with a small waist of 27 μm and the small Raleigh length from the CO_2 laser, they had longitudinal confinement sufficient to condense in a single beam trap. The beam profile of their atom laser was very high quality (essentially equal to the Thomas-Fermi profile of the condensate) for the same reason as was the LKB guided atom laser: the non-state changing outcoupling extracts atoms from the edge of the condensate, avoiding the effect of the mean field divergence [51, 96].

Magnetic outcoupling of an optical BEC has been reported by Lundblad et al. in the group of Lute Maleki at the Jet Propulsion Laboratory (JPL) in CalTech [97, 98]. They prepared an all optical condensate in $m_F = 0$ using the spin distillation technique, and used magnetic outcoupling to produce free space beams that were not guided.

Other experiments on guided atomic beams include :

- Evaporative cooling of atoms in a magnetic guide has been reported by the group of David Guéry-Odelin at ÉNS, using several techniques: microwave transitions, a material surface, and a train of moving magnetic traps [99–101]. The quantum degenerate regime has not yet been reached.

- A BEC inside a blue detuned Laguerre-Gaussian donut laser beam has been reported by Bongs et al., in the group of Wolfgang Ertmer at Hannover [102]. This is arguably another guided atom laser, in the same sense that a releasing a BEC from a trap creates a single

pulse atom laser, analogous to cavity dumping in a photon laser [6, 79].

- On atom chips, magnetic guiding of cold atoms has been reported by Key et al. in the group of Ed Hinds at Imperial College London, by Leanhardt et al. in the group of David Pritchard at MIT, and by Dekker et al. in the group of Mara Prentiss at Harvard [103–105].
- Guiding of atoms in hollow-core optical fibers has been reported by Renn et al., in the group of Eric Cornell at JILA [106].

These experiments are all in the proof-of-principle stage, but they show the increasing degree of control built in many different geometries and with many different confining potentials, each suited to a particular task.

6

CONDENSATES IN AN OPTICAL TRAP

6.1 THE EXPERIMENT

The source of the atom laser for these experiments was a Bose-Einstein condensate (BEC), as in the previous section. The condensate was produced in a trap formed by the crossing of two laser beams, as shown in Figure 6.1, with wavelength of $\lambda_{tr} = 1.072$ μm. This is larger than the wavelength of the strongest atomic resonance (780 nm) and so the atoms are trapped at the intensity maximum. The two beams did not interfere to form an optical grating, because the laser had a linewidth of 1 nm, and hence a tiny 1 mm coherence length, much smaller than the (roughly) 30 cm difference in beam path lengths. Also, the frequency difference between them was set at 80 MHz by an acousto-optic modulator (AOM), and so any interference pattern would be moving with velocity $\frac{1}{2}\Delta f\,\lambda \approx$ 40 m/s [107].

A summary of experimental parameters is at the end of the section, in Table 7.1 on page 103

I will briefly give the details of condensate production here. The source of cold atoms for the experiment is a Zeeman slower, which loads a 2D MOT to 10^9 atoms in 1 s, with the long axis of the 2D MOT along the horizontal beam. The MOT position is optimised by adjusting the current in the four independent coils. The power in each MOT beam was actively stabilised by using a polarising beam splitter to divert a small part of the power to a photodiode, after the single-mode polarisation maintaining optical fiber. The photodiode signal was fed back to an AOM before the fiber. This reduced the sensitivity to power fluctuations, and also to

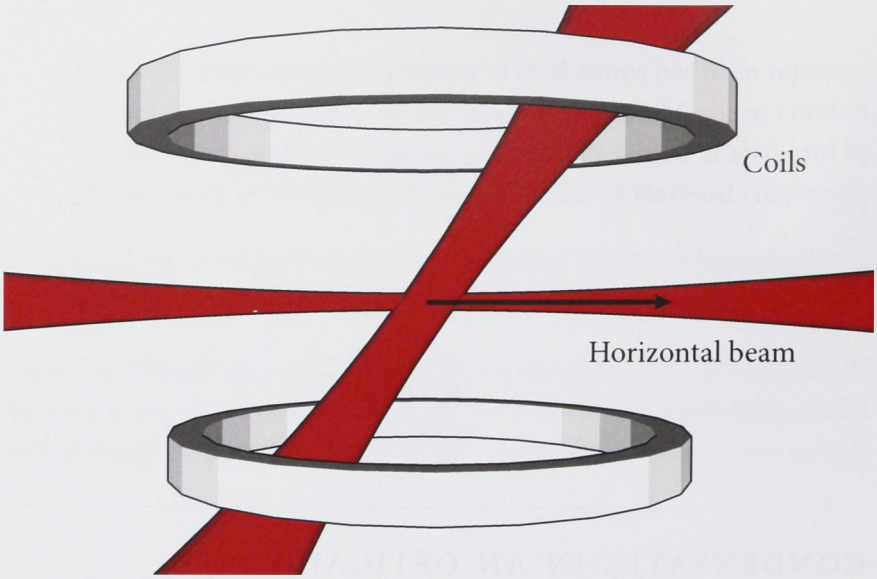

(a) Experimental schematic, showing optical trap laser beams and magnetic coils (not to scale). The horizontal coils, used to outcouple the atom laser, are not shown.

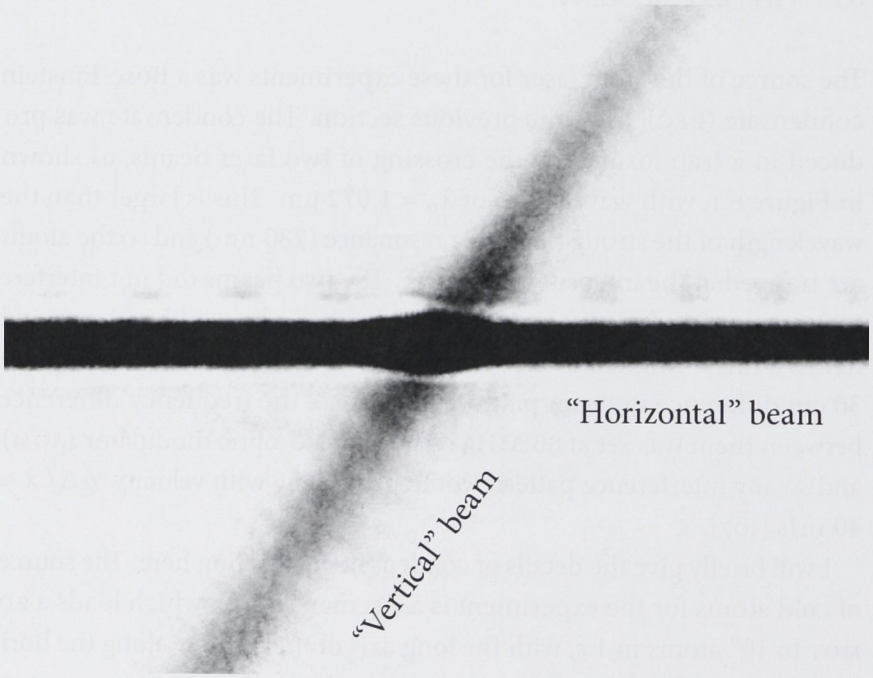

(b) Absorption image of atoms released from the trap, after 1 ms free expansion. The field of view is 3 mm across.

Figure 6.1: The cross dipole optical trap.

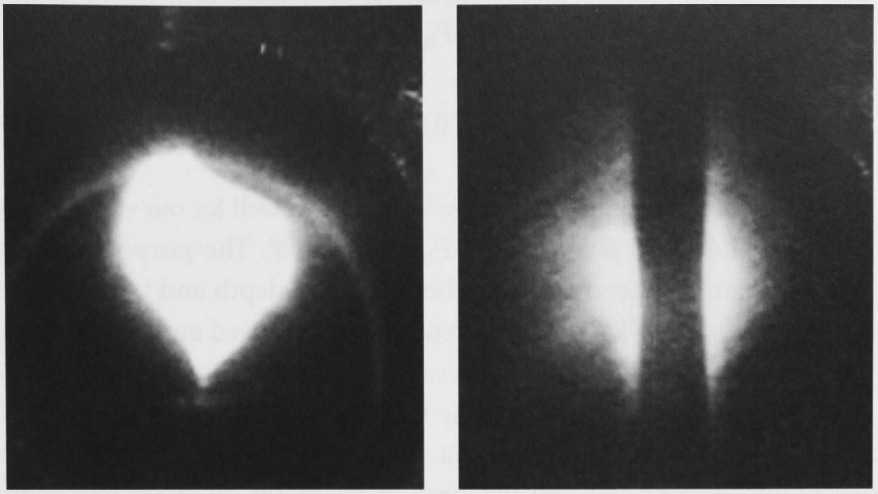

(a) Conventional MOT (b) Dark line MOT

Figure 6.2: Gaining atoms with a dark line MOT. Fluorescence images of the MOT (a) and dark line MOT (b) (expanding molasses shown). The dark vertical band in (b) contains a high density of atoms in the $F = 1$ ground state which does not absorb the cooling lasers. It is caused by a 2 mm wide object which partially masks the (vertically propagating) repump beam, which would otherwise return them to the $F = 2$ state. This technique more than doubled the number of atoms loaded into the optical trap. The large faint circle in the background is a reflection from the vacuum chamber.

fluctuations of the input polarisation to the fiber, which became power fluctuations after a polarising beam splitter before the chamber.

Dark line magneto-optical trap

A dark line MOT stage was run for 200 ms (see Figure 6.2), in which a long opaque object 2 mm wide partially masked the center of the (vertically propagating) repump beam [108, 109]; this object was imaged to the optical trap using a standard $4f$ imaging system. The lack of repump light produced a high density of atoms in the $F = 1$ ground state, which is *dark* (i.e. non-absorbing) because it is 6.8 GHz detuned from the cooling lasers. These atoms did not scatter MOT cooling light and hence did not contribute to the radiation pressure, which is what limits the density of a MOT in the high atom number regime. Using this technique we were able to more than double the number of atoms loaded into the optical trap. We experimented between having the optical trap turned on *throughout* the MOT loading, and turing the it on *after* the loading, but it made no difference which method was used.

Evaporative cooling

To evaporatively cool, we reduced the power in the trapping laser,

following the model of O'Hara et al. (2001) [110]. According to this model, the power in the horizontal beam P_h is reduced as:

$$P_h(t) = P_h(0)\left(1 + \frac{t}{\alpha}\right)^{-\beta}. \tag{6.1}$$

The values of the scaling constants which worked well for our experiment were $\alpha = 1.6$ s and $\beta = 4.2$ and $P_h(0) = 20$ W. The purpose of this ramp is maintain a constant ratio between trap depth and temperature (a constant $\eta = U/(kT)$), which determines the speed and efficiency of the evaporative cooling. (Efficient evaporative cooling is when few atoms are lost for the same gain in phase space density.) High η is slow and efficient, low η is fast and inefficient. Of course, other causes of loss may exist and compete with the evaporation processes. In our experiment, using $\eta \approx 5$ gave the greatest atom number. It was possible to condense using a sequence of five linear evaporation stages, but with about half the final atom number compared to the above method. A plot of the power during the evaporation is shown in Figure 6.3. For the vertical beam, the evaporation was similar, although higher in initial power and with an offset to maintain a high trap frequency during the evaporation. It followed:

$$P_v(t) = 10 \times P_h(t) + 2 \text{ W}. \tag{6.2}$$

After 3–4 seconds of evaporation, we produced a condensate of around one hundred thousand atoms. Figure 6.4 shows a typical absorption image and profile of the BEC. From start to end, the entire duty cycle was less than 6 seconds. It was necessary to adjust the parameters of the evaporation daily, as the shape and size of the beams would change due to the accumulation of dust on the optics (see Figure 6.5).

Imaging technique

To make quantitative measurements of the atomic column density, standard absorption imaging (also known as "shadow" imaging) was used. The details on this technique can be found in (for example) Ketterle et al. (1999) [79, page 34].

6.2 PRODUCING CONDENSATES IN ANY SPIN STATE

Ordinarily, evaporative cooling produced a *spinor* condensate, with equal mixtures of all three Zeeman state. All are equally well confined in the optical trap and equal numbers of each are initially loaded (see Figure 6.10). We used such condensates to make spinor atom lasers (that is, atom lasers which contain all three spin states—see §7.4).

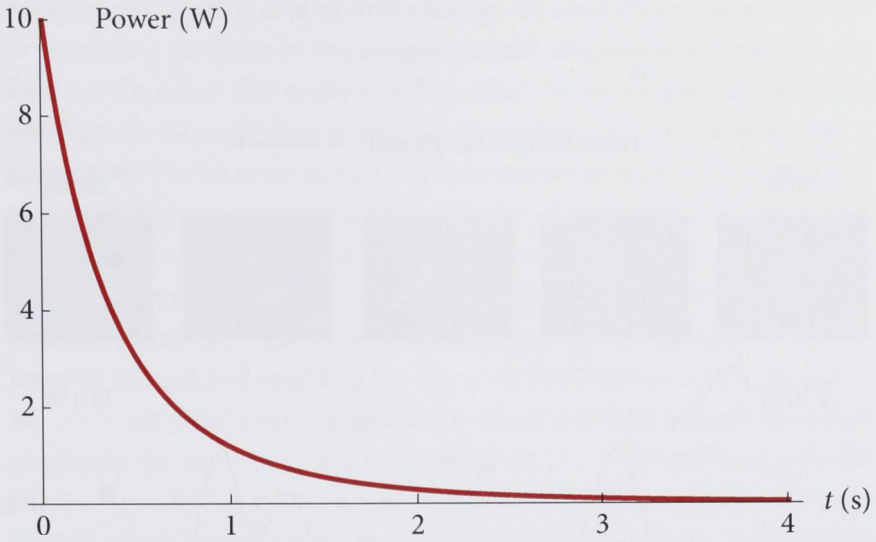

Figure 6.3: Evaporation ramp of laser power.

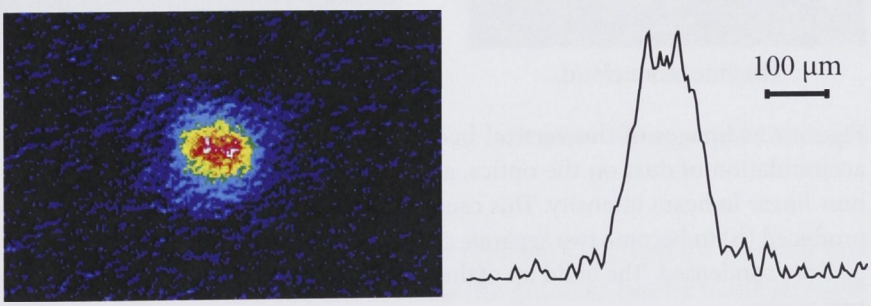

Figure 6.4: All optically produced Bose-Einstein condensate of 2×10^5 atoms, after 20 ms free expansion.

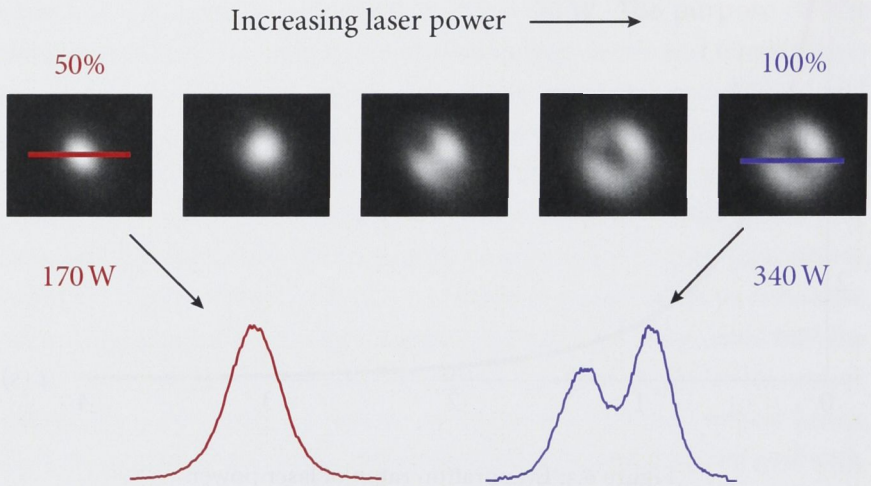

(a) Vertical laser beam profiles.

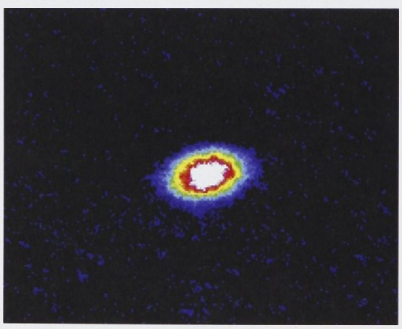

(b) One atom cloud.

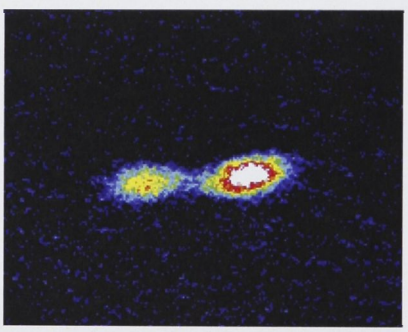

(c) Two atom clouds.

Figure 6.5: Images of the vertical beam intensity profile (a) affected by the accumulation of dust on the optics, and the resulting phase shifts which are non-linear in beam intensity. This caused the usual single cloud of cold atoms produced (b) to become two separate clouds of cold atoms (c), which could not be Bose condensed. The build up of dust required cleaning approximately every two weeks.

We also used a technique to produce condensates in any one *pure* spin state. This technique we called spin distillation, in analogy to the distillation of spirits, which purifies a mixture by removing unwanted components. During evaporative cooling, we used a single magnetic coil to produce a gradient in the magnetic field amplitude $|\mathbf{B}|$, and hence a force on the atoms due to the Zeeman effect. At the location of the atoms, this force is directed almost entirely along the axis of whichever coil is being used. Purification to one m_F state occurs because, when the force is applied during evaporation, the trap is less deep for the other m_F states, and they are evaporated first [19, 20]. For example, to purify $m_F = 0$, we use a gradient which is horizontal and perpendicular to the guide. This gradient forces the other m_F states out of the trap, attracting the $m_F = -1$ towards the coil and repelling the $m_F = +1$ (see Figure 6.6 (a)). To purify $m_F = -1$, we used a vertical gradient, which partially cancels the effect of gravity for $m_F = -1$, has little effect on $m_F = 0$, and increases the effect of gravity for $m_F = +1$ (see Figure 6.6 (b)). To purify $m_F = +1$, we used the same technique as $m_F = -1$ but with a coil above the chamber rather than below. This method is simple and robust: simple, because it

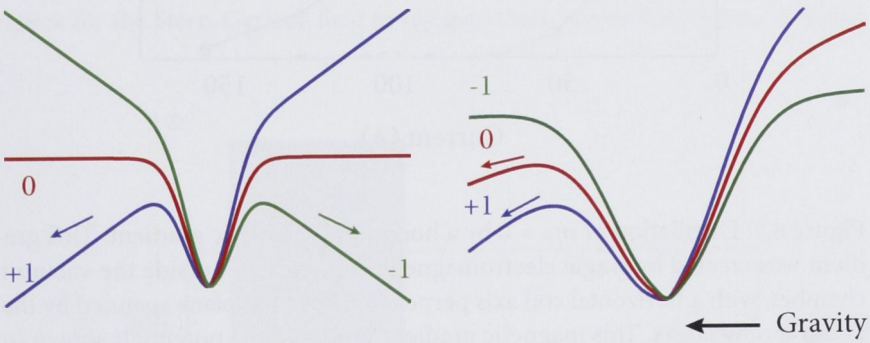

(a) Horizontal gradient. (b) Vertical gradient.

Figure 6.6: Potentials for the three different spin states during a spin distillation process.

requires only one external coil, which in our case was an existing coil used for the MOT; and robust, because the gradient can be made stronger than strictly necessary, so that unwanted spins are removed well before evaporation is finished, and in this case fluctuations are minimised. Such a distillation scheme was also used by Cennini et al., in the group of Martin Weitz at Tübingen and Chang et al., in the group of Mark Chapman at Georgia [51, 96, 111, 112]. The results are shown in figures 6.7, 6.9 .

Crossing the beams

An extension of this method was used to optimise the crossing of the two beams. The procedure for $m_F = 0$ distillation was used (perpendicular

horizontal gradient) but by stopping the evaporation early and using the Stern-Gerlach field during the time of flight (TOF) expansion. When we saw two small clouds of equal size for $m_F = -1$ and $+1$, and one larger cloud of $m_F = 0$, then we knew the beams were well crossed. When the largest cloud was either $m_F = -1$ or $+1$, then the crossing needed to be optimised. The fine adjustment for this was done with a mirror mounted on two piezo-electric crystals, and by adjusting the voltage across either one.

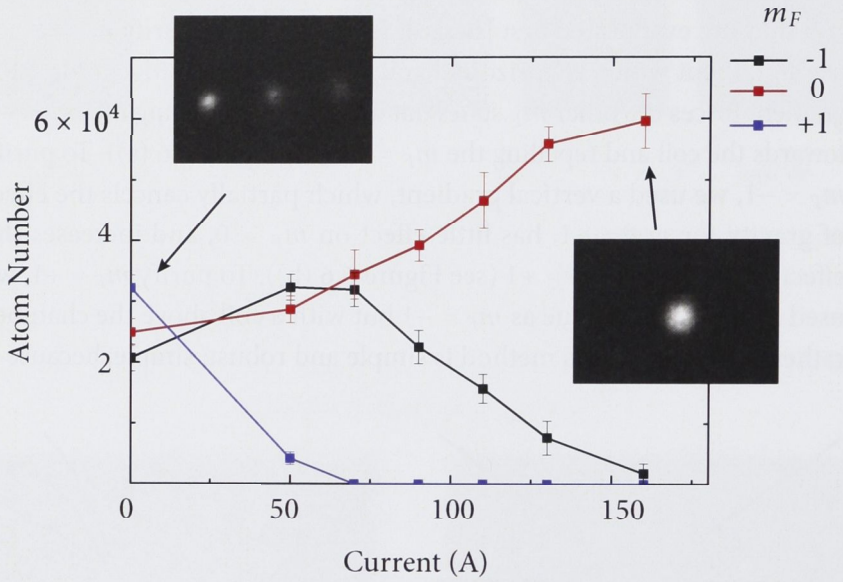

Figure 6.7: Distillation of $m_F = 0$ by a horizontal magnetic gradient. This gradient was created by single electromagnetic coil, located outside the vacuum chamber, with a horizontal coil axis perpendicular to the plane spanned by the two trapping lasers. This magnetic gradient produces the potentials shown in Figure 6.6 (a). This trap depth for $m_F = -1$ and $m_F = +1$ are reduced, and are preferentially evaporated, leaving $m_F = 0$.

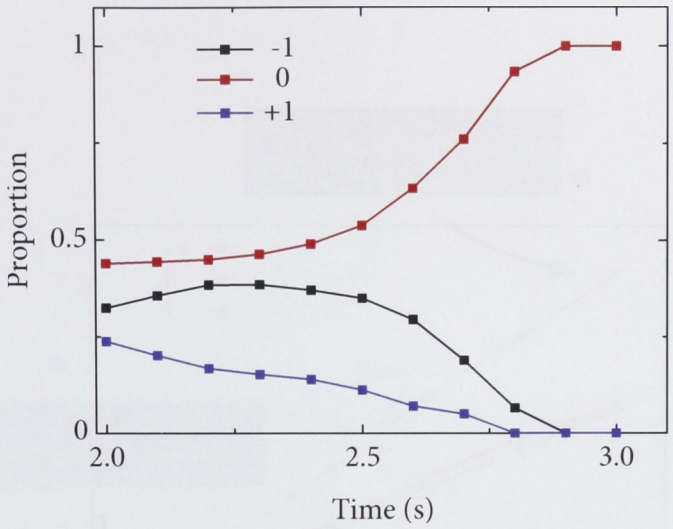

Figure 6.8: Dynamics of $m_F = 0$ distillation with a 160 G/cm horizontal gradient (corresponding to the data points at 160 G/cm in Figure 6.7). Note how only at the end of the evaporation (when the trap frequencies are sufficiently low) are the unwanted spins removed. It was not possible to observe the evaporation at times less than 2 s, as the expansion of the three (hot) thermal clouds was too quick for the Stern-Gerlach field to separate them before they fell out of view.

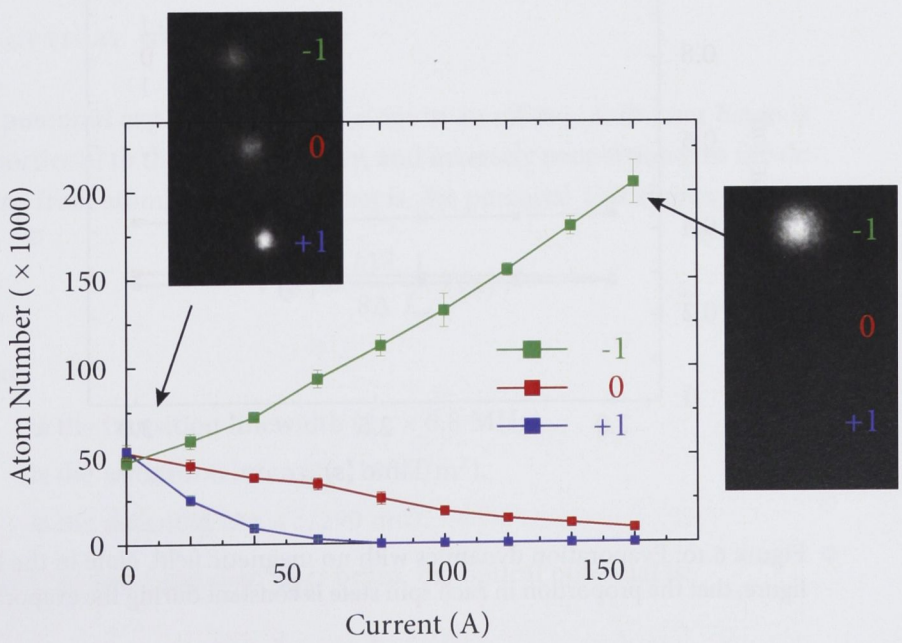

Figure 6.9: Distillation of $m_F = -1$ by a vertical magnetic gradient.

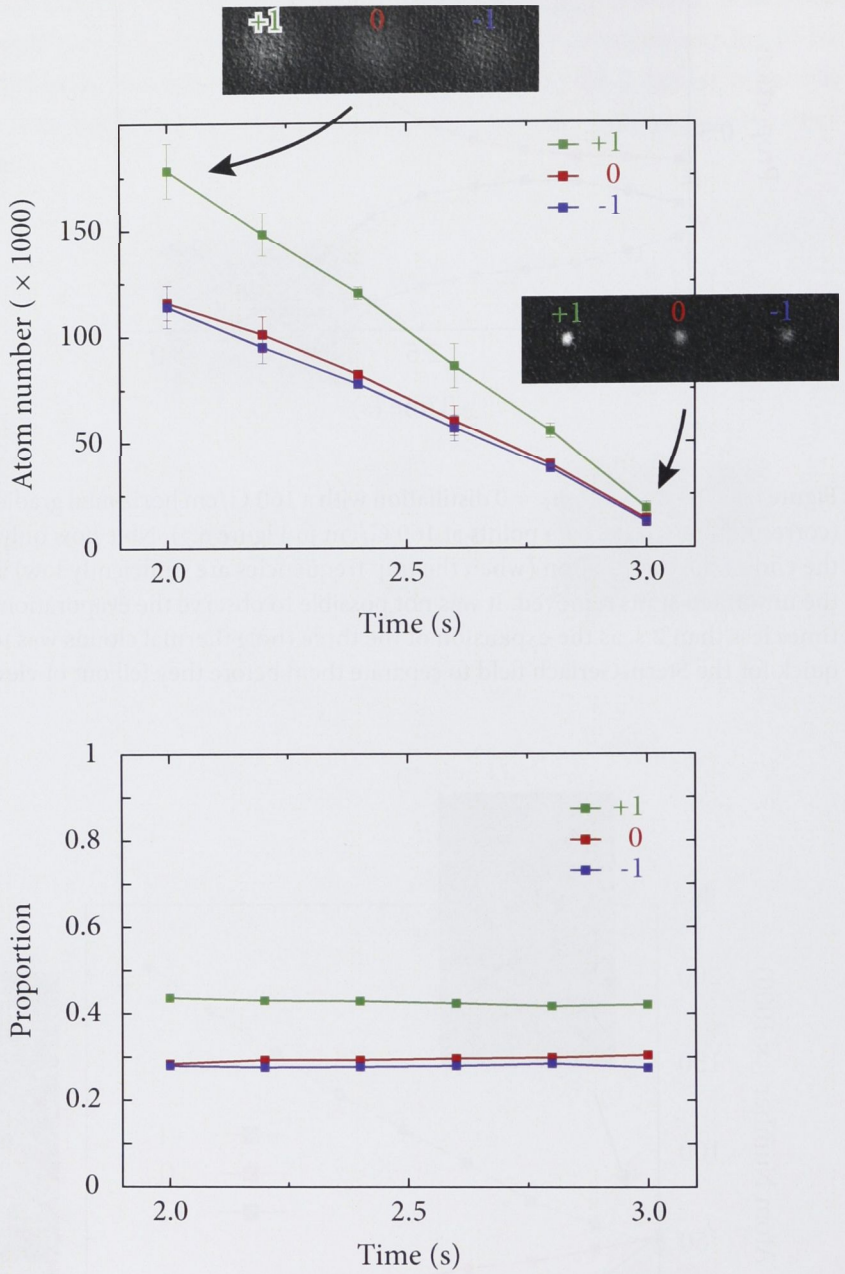

Figure 6.10: Evaporation dynamics with no magnetic field. Note in the lower figure, that the proportion in each spin state is constant during the evaporation.

7

EXPERIMENTS WITH GUIDED ATOM LASERS

In this chapter, I describe the experiments on the atom laser in the optical waveguide, quantifying the spatial mode by measurement of the mean excitation number $\langle n \rangle$.

7.1 OPTICAL GUIDES

The potential experienced by an atom in an off-resonant laser beam is proportional to the beam intensity, and inversely proportional to the detuning from atomic resonance. That is, the potential V is approximately:

$$V(\mathbf{x}) \approx \frac{\hbar\Gamma^2}{8\Delta}\frac{1}{I_{\text{sat}}} I(\mathbf{x}), \tag{7.1}$$

where,

- Γ is the transition linewidth ($2\pi \times 6.8$ MHz)
- I_{sat} is the saturation intensity (16 W/m^2),
- Δ is the detuning ($2\pi \times c/290$ nm).

Since we use a gaussian laser beam, the optical potential is:

$$U(\mathbf{x}) = \frac{\hbar\Gamma^2}{8\Delta}\left(\frac{1}{1+\frac{z^2}{z_R^2}}\right)\exp\left(-\frac{2\,(x^2+y^2)}{w_0^2\left(1+\frac{z^2}{z_R^2}\right)}\right), \tag{7.2}$$

where w_0 is the beam waist (40 μm). The trap frequencies for each direc-

(a) $m_F = 0$

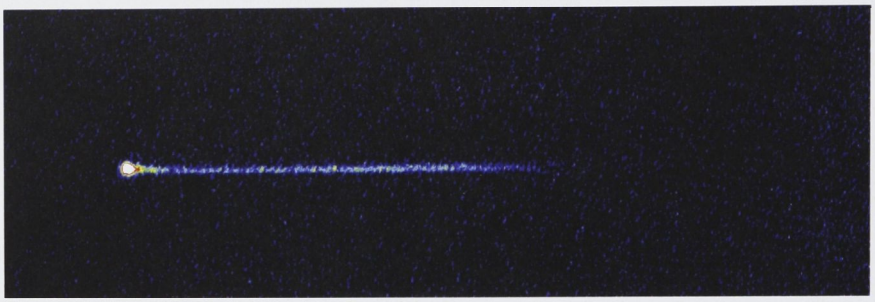

(b) $m_F = -1$

Figure 7.1: Guided atom laser images after 15 ms free expansion. In both images atoms remaining in the condensate are visible on the left, with the atom laser propagating to the right. The field of view in each image is 5 mm across.

tion are:

$$\omega_\rho = \frac{1}{w_0}\sqrt{\frac{4U_0}{m}} \quad \text{and} \quad \omega_z = \frac{1}{z_0}\sqrt{\frac{2U_0}{m}}, \tag{7.3}$$

where $U_0 = \hbar\Gamma^2/(8\Delta)$. Therefore the guide frequency ω_ρ (or simply ω) is proportional to:

$$\omega_\rho \propto \begin{cases} 1/w_0^2 & \text{for constant } \textit{power}, \text{ and} \\ 1/w_0 & \text{for constant } \textit{depth}. \end{cases} \tag{7.4}$$

7.2 PRODUCING THE ATOM LASER

The outcoupling is done by lowering the power in the vertical beam, so that the depth of the trap becomes insufficient and atoms in the condensate leave and form an atom laser [113]. This is done in the following way: after the evaporation is complete, there is a 200 ms preparation stage prior to outcoupling, in which simultaneously:

- P_h is increased from 50 to 200 mW;

- P_v is decreased from 3 to 1 W;
- the magnetic field gradient is increased from 0 to 18 G/cm.

This preparation is done so the maximum magnetic field gradient (22 G/cm) will be sufficient. For the outcoupling itself, we hold the power in each beam constant and increase the magnetic gradient from 18 G/cm to 22 G/cm over a further 200 ms to produce the beam. To image the beam, we switch off all fields and lasers, and allow a short expansion time (5–25 ms) before taking an absorption image (see Figure 7.1 on the preceding page).

Measuring $\langle n \rangle$

How is $\langle n \rangle$ measured? Using the Hamiltonian for the transverse modes:

$$\mathcal{H} = \tfrac{1}{2}mv^2 + \tfrac{1}{2}m\omega^2 x^2, \tag{7.5}$$

and noting that:

$$\langle \mathcal{H} \rangle \equiv \mathrm{E} = \hbar\omega\left(\langle n \rangle + \tfrac{1}{2}\right), \tag{7.6}$$

then by using the virial theorem:

$$\langle \mathcal{H} \rangle = \tfrac{1}{2}\langle T \rangle + \tfrac{1}{2}\langle V \rangle, \tag{7.7}$$

where the operator T is for kinetic energy and V is for potential energy, one can rearrange the above equations to find:

$$\langle n \rangle = \frac{m}{\hbar}\frac{(\Delta v)^2}{\omega} - \frac{1}{2}. \tag{7.8}$$

Therefore to know $\langle n \rangle$ requires measurement of Δv and ω.

Measuring Δv

To measure the transverse velocity spread, Δv, we make TOF measurements of the expansion of the atom laser beam. The corresponding absorption images are integrated along the atom laser propagation direction z, (excluding the region of the BEC), and the resulting one dimensional profiles are fitted with a Gaussian function to find the width $\Delta x(t)$. We then find Δv through the relation:

$$[\Delta x(t)]^2 = [\Delta x(0)]^2 + [\Delta v]^2 t^2. \tag{7.9}$$

Measuring ω

We measure the trap frequency ω of the guide by observing the oscillation of the cloud center of mass in TOF images, after giving a momentum kick to the cloud from the fast switch off (less than 1 ms) of the magnetic gradient used for distillation. The maximum time we can observe these oscillations is limited by the expansion of the cloud inside the waveguide, because there is almost no confinement along the guide axis. After 100 ms (or ~ 20 oscillations), the cloud has expanded to a length of 1 mm, or to

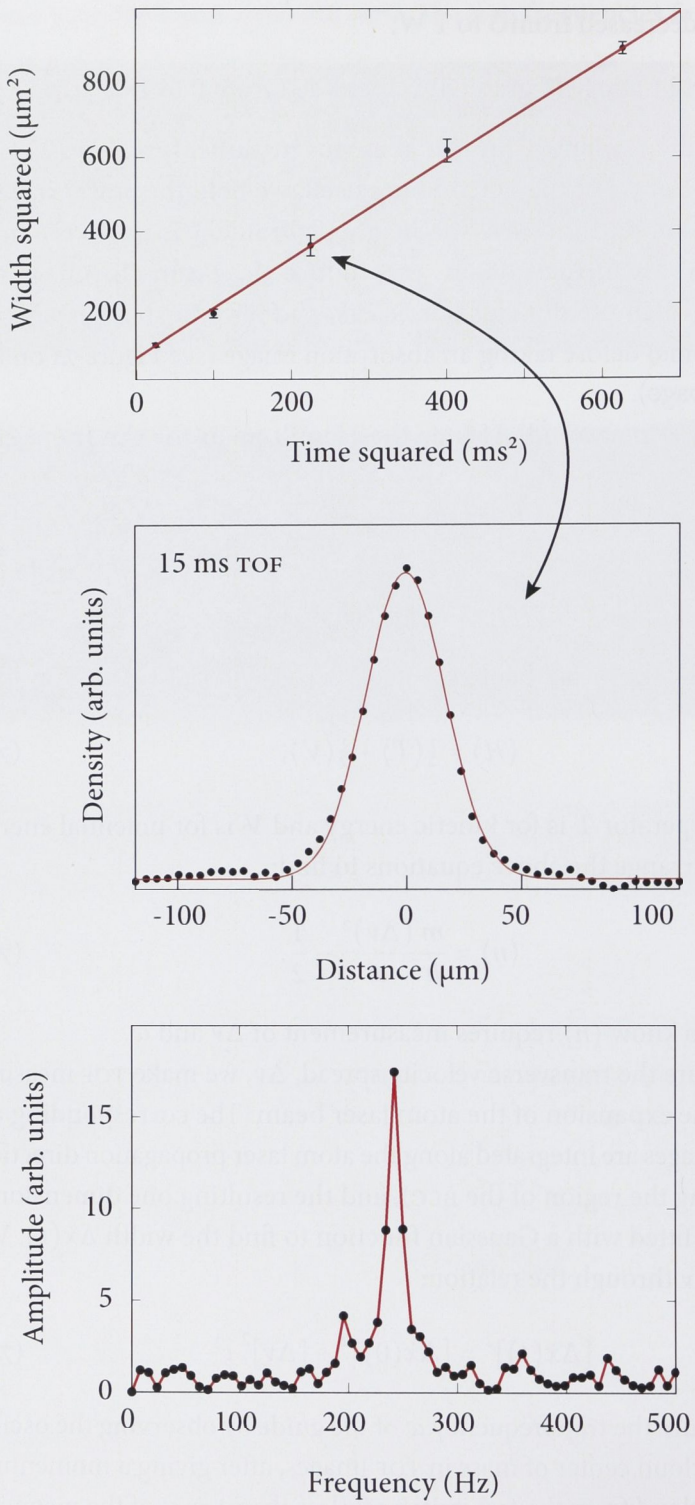

Figure 7.2: Measuring $\langle n \rangle$, in this case for an $m_F = 0$ atom laser. The top plot shows the free expansion measurements and the fit to them. The middle plot shows one particular fit at 15 ms expansion time to find the width (in total 20 measurements for each expansion time were done). The bottom plot shows the Fourier transform of vertical oscillations of the atom cloud in the waveguide, to measure the guide frequency. For the $m_F = \pm 1$ atom lasers, the data and analysis were similar. The error bars are the standard deviation of repeated measurements.

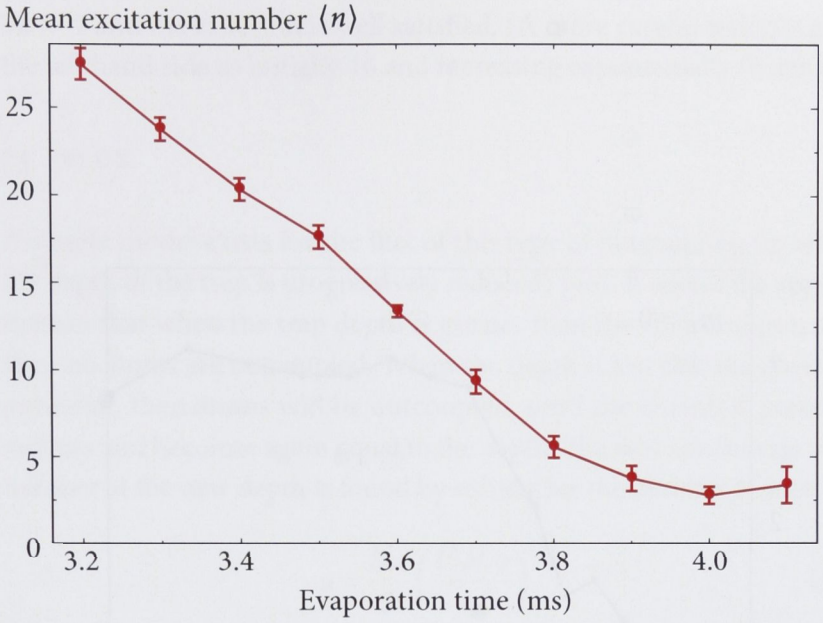

Figure 7.3: Effect of incomplete evaporation on $\langle n \rangle$. The value for $\langle n \rangle$ quoted here is actually an upper bound, since they are all based on measurements with TOF being 25 ms, with the assumption of neglible starting width, not on fits to measurements with a many different expansion times as in Figure 7.2 on the preceding page.

one fifth of the Raleigh length. Then the change in the trap frequency over the cloud length (10 Hz) is of the same order as the fourier width of the observation time, so further observation is not useful. A typical fit and TOF measurement can be seen in Figure 7.2 on the facing page, for the case of $m_F = 0$ and giving $\langle n \rangle = 0.65 \pm 0.05$.

Trap switchoff

It is important that the horizontal guide switch off suddenly. That is, as the power in the horizontal beam is reduced and the trap frequency drops, it is important that the wavefunction does not adiabatically follow the changing potential. It could then "adjust" to some new potential with a lower trap frequency, expand more slowly and *underestimate* Δv and hence also underestimate $\langle n \rangle$. The criterion for *non*-adiabaticity is [79, page 16]:

$$\frac{1}{\omega^2}\frac{d\omega}{dt} \gg 1 \tag{7.10}$$

We measured the switchoff of the light through the AOM with a fast photodiode. The intensity decayed exponentially with time constant $\tau =$ 25 μs. For a simple calculation, let us assume that the trap frequency goes from linearly 200 Hz to 0 Hz in 25 μs, then equation 7.10 becomes

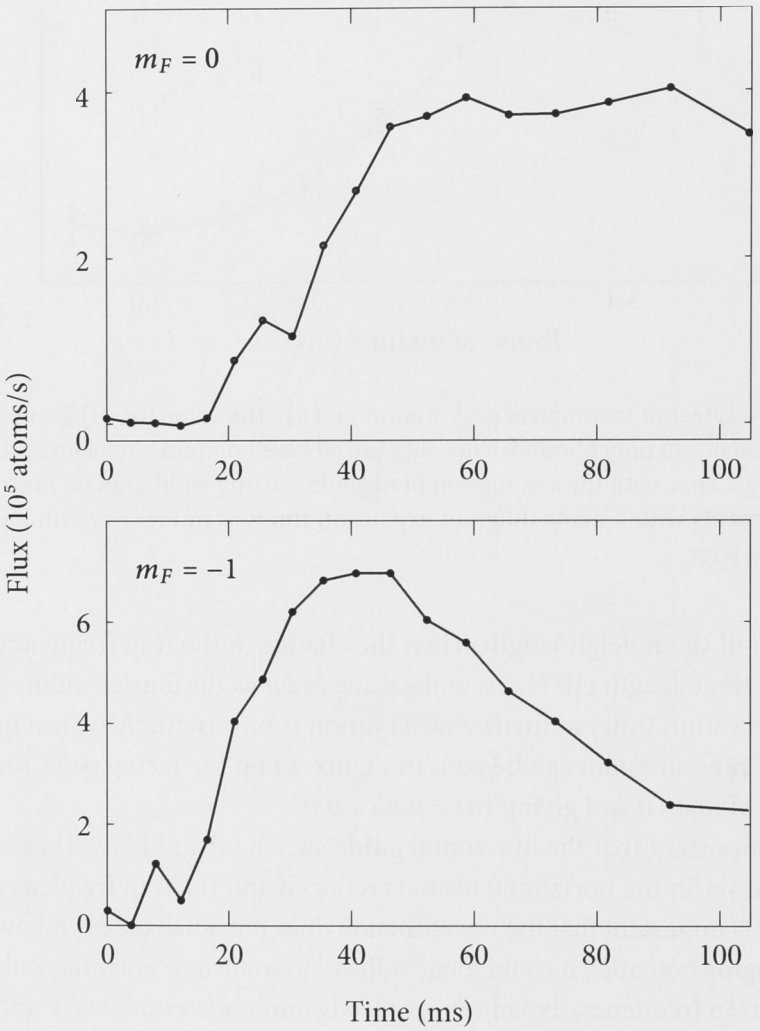

Figure 7.4: Flux. Each data point has been averaged over 30 pixels (140 μm) to remove high spatial frequency imaging noise

$32 \gg 1$ and the criterion is well satisfied. (A more careful analysis gives the left hand side as initially 16 and increasing exponentially thereafter.)

7.3 FLUX

Model for outcoupling

A simple model exists for the flux of this type of outcoupling (in which the depth of the trap is progressively reduced) [96]. It makes the approximation that when the trap depth is greater than the chemical potential, then no atoms are outcoupled. When the depth is less that the chemical potential, then atoms will be outcoupled, until the chemical potential reduces and becomes again equal to the depth. The new condensate atom number at the new depth is found by solving for the number of atoms in:

$$\mu = \frac{\hbar\omega}{2}\left(\frac{15N_c a}{a_{\mathrm{h}}}\right)^{2/5} \tag{7.11}$$

where μ is set equal to the trap depth and $a_{\mathrm{h}} = \sqrt{\hbar/(m\omega)}$ is the harmonic oscillator length. To find the flux using this model would require finding the depth of the trap numerically as a function of time.

Extracting the flux from an absorption image

We have not made this numerical study in this work, but we have measured the flux as a function of time from the absorption images. The absorption image gives the atomic column density $\sigma(y,z)$, such that the number of atoms in the pixel at location (y,z) is $\sigma(y,z)\Delta y\,\Delta z$, where Δy and Δz are the pixel dimensions (each is 4.7 μm at the location of the atoms). Integrating along the transverse (vertical) direction y gives the linear atomic density $\sigma(z)$ along the propagation direction z:

$$\sigma(z) = \sum_y \sigma(y,z)\Delta y \tag{7.12}$$

The flux $\phi(t)$ may be found by taking:

$$\phi(t)\Delta t = \sigma(z)\Delta z, \tag{7.13}$$

and then by using $\Delta z = (dz/dt)\Delta t$, the flux may be written:

$$\phi(t) = \sigma(z)\frac{dz}{dt} \tag{7.14}$$

We therefore need a mapping from position to time, which we shall take from the classical trajectories of the atoms. The atoms accelerate continuously from the time they are outcoupled. The acceleration α is due to the magnetic field gradient, and is $\alpha = 6\ \mathrm{m/s^2}$ for $m_F = -1$

and $\alpha = 0.3$ m/s^2 for $m_F = 0$ (due to the second order Zeeman effect). Note that we have made the approximation that the acceleration does not change between when outcoupling begin and ends. (In reality, it increases linearly by at most 10%.) During the time of flight t_{TOF}, the magnetic fields are switched off, so acceleration stops, but the atoms of course continue to move with the velocity $v = at$ that they have acquired. Their position, z as a function of time, is therefore:

$$z(t) = \tfrac{1}{2}\alpha t^2 + (\alpha\, t)\; t_{\mathrm{TOF}}, \tag{7.15}$$

where t is the time since the beginning of coupling, and t_{TOF} is the time of flight (the time for free expansion between the end of outcoupling and the image being taken).

Unlike the Ramam atom lasers in Chapter 2, no atoms overtake any other atoms, and so the mapping from position to time is one-to-one and can be easily inverted:

$$t(z) = -t_{\mathrm{TOF}} + \sqrt{t_{\mathrm{TOF}}^2 + \frac{2z}{\alpha}}. \tag{7.16}$$

Finally, then, the flux is:

$$\phi(t) = \sigma\Big(z(t)\Big)\, \alpha\, (t + t_{\mathrm{TOF}}). \tag{7.17}$$

Figure 7.4 shows the measured flux for both the $m_F = 0$ and $m_F = -1$ atom lasers showed in Figure 7.1 (averaged over 30 pixels to remove high spatial frequency imaging noise).

7.4 SPINOR GUIDED ATOM LASERS

All the atom lasers that I have discussed so far in this thesis have been atom lasers of one spin state only. However, we were also able to use the Paris machine to produce atom lasers which contain all three Zeeman states $m_F = -1, 0,$ and $+1$. This was done by evaporating with no external magnetic fields applied, and then linearly reducing the power in the vertical beam. Absorption images of these spinor atom laser can be seen in Figure 7.5 on the facing page.

Vengalattore et al., the group of Dan Stamper-Kurn at Berkeley, has reported using a spinor ^{87}Rb BEC to measure the magnetic fields with sensitivity of 8.3 pT/Hz$^{1/2}$ [37]. This proof of principle spinor atom laser could one day be part of a magnetic field measurement. The advantage of such a measurement would be that every aspect of the guide (including

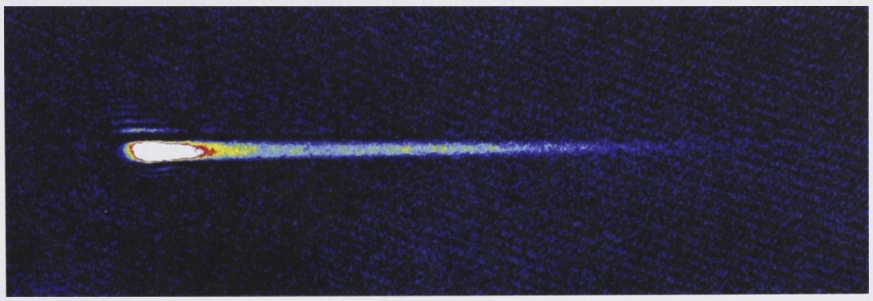

(a) Different spin states superimposed.

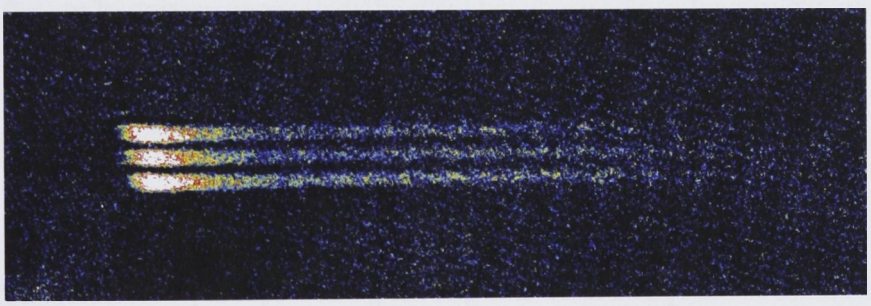

(b) Different spin states separated.

Figure 7.5: Guided spinor atom laser, with equal population of all three spin components of the $F = 1$ manifold, propagating in the horizontal waveguide. The upper image shows all three spin states superimposed; the lower image shows the spins separated by a magnetic field gradient during the free expansion. In both images atoms remaining in the condensate are visible on the left, with the atom laser propagating to the right. The field of view in each image is 5 mm across.

imperfections) would affect each spin state equally, that is it would be "common-mode" noise and therefore would not affect a measurement. To a good approximation, only the magnetic field would affect the phase of each spin differently.

7.5 ADDITIONAL EXPERIMENTS

The system of a spinor $F = 1$ condensate in a crossed dipole trap is extremely versatile, and we were able to do a number of proof-of-principle experiments.

Using a longitudinal magnetic field gradient and a condensate with all three spin states, we were able to produce an atom laser beam in which $m_F = -1$ propagates in one direction along the guide and $m_F = +1$ propagates in the other direction (see Figure 7.6 on the next page). Such outcoupling was first done by Lundblad et al. in the group of Lute Maleki at the Jet Propulsion Laboratory (JPL) in CalTech [97, 98], but into free space rather than in a guide. The $m_F = -1$ and $+1$ atoms needed for such an experiment can be produced from adiabatic compression of $m_F = 0$ atoms, which produce pairs of $m_F = +1$ and -1 atoms through angular momentum changing collisions. In that case, the two atom laser beams would be number correlated, and so represent an oppurtunity to study entanglement and squeezing in a BEC [97].

Atom laser waterfall

We also were able to extract the atoms from the guide and let them propagate in free space, forming an "atom laser waterfall". This occurs because as the optical laser diverges, the guide frequency decreases, and the gravitational sag increases until the atoms fall out (see Figure 7.7 on page 102). This could become a crude method to outcouple an atom laser from the guide into free space.

7.6 FURTHER WORK

Further work will improve the atom laser spatial mode, and add coherent coupling between the spin states so interferometery becomes possible.

One improvement would be to improve the position locking of the laser guide. The current mirror-piezo system has a bandwidth of around 20 Hz, and is only really useful for long term stability. A feedback system with an AOM to change the laser pointing could have a bandwidth of several megahertz. Such systems have been successfully implemented by several groups [114, 115].

Measurements of magnetic fields and other interferometry experiments would require initial state preparation, and the ability to coherently couple the three spin states. The metal vacuum chamber with the small (5 cm) windows located at a distance from the atoms prevents RF from being used. Therefore future work on the experiment will include $F = 1 \longrightarrow 2$ microwave transitions at 6.8 GHz to prepare the spinor BEC in a particular superposition of the three spin states, and to perform coherent coupling of states in $\pi/2$ and π pulses.

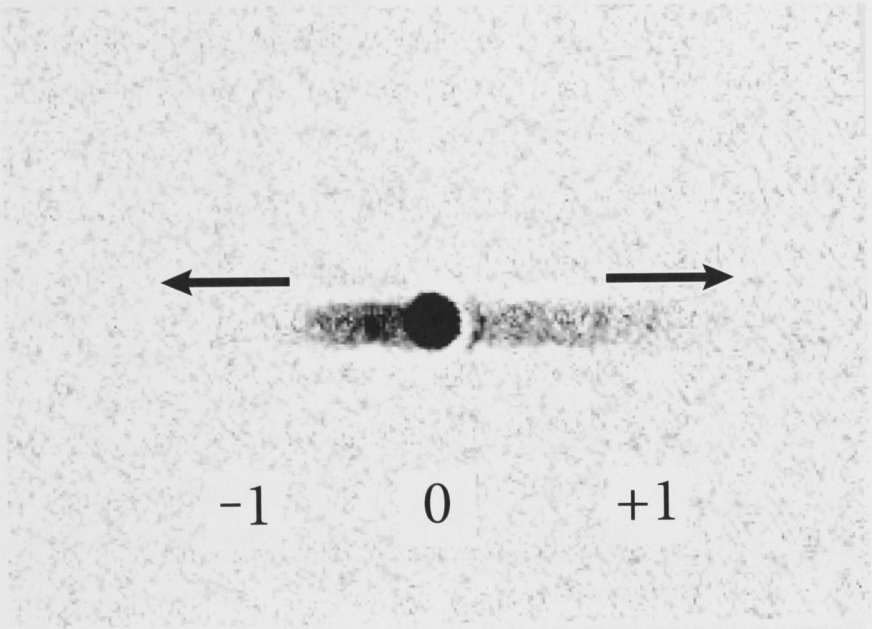

Figure 7.6: Multi-spin component guided atom lasers propagating in different directions. The field of view is 1.2 mm across.

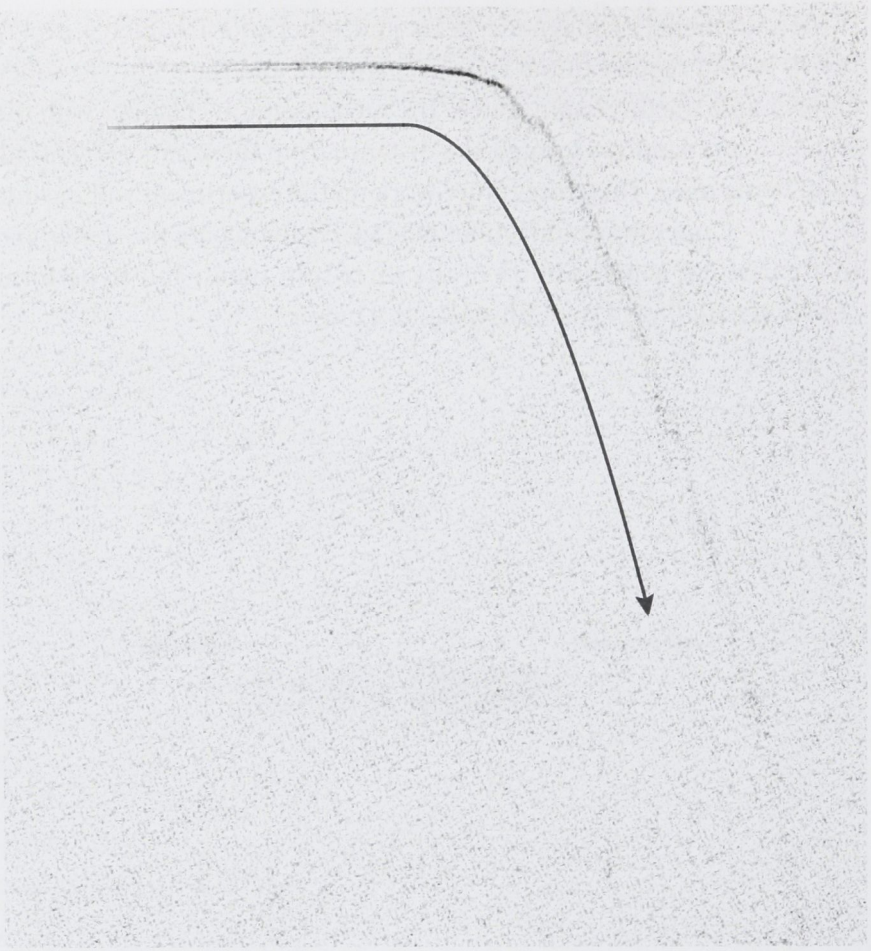

Figure 7.7: An atom laser waterfall: gravity eventually overcomes the guiding potential, and the atom laser beam falls out. The field of view is 4 mm across.

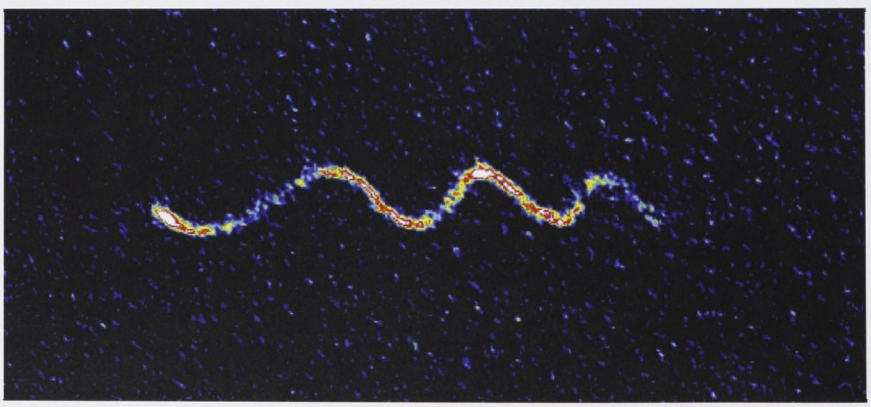

Figure 7.8: Transverse oscillations in the guide. These are due to excitations that occurred when the preparation for outcoupling was not adiabatic (for example, when the laser power was changed too quickly). They could be suppressed by careful optimisation. The field of view is 2.6 mm across.

QUANTITY	VALUE	SYMBOL
Coil spec bias field	0.35 G/A	
Coil spec gradient	0.1 G cm^{-1} A^{-1}	
Distillation magnetic bias field	70 G	B_0
Distillation magnetic gradient	20 G/cm	b
Optical trap laser wavelength	1072 nm	λ_{tr}
Optical trap laser linewidth	1 nm	
Horizontal beam		
waist	40 μm	w_h
Rayleigh length	5 mm	
power (initial)	20 W	P_h
power (final)	100 mW	
Vertical beam		
waist	110 μm	w_v
Rayleigh length	35 mm	
power (initial)	100 W	P_v
power (final)	10 W	
Frequency difference	80 MHz	
Imaging detuning	- (resonance)	
Pixel size (at position of atoms)	4.7 μm	
Pixel size (on camera)	6.45 μm	
MOT loading time	1 s	
Dark MOT time	200 ms	
Compression	20 ms	
Polarisation cooling	10 ms	
Evaporation	3–5 s	
Time of flight	0–30 ms	
Imaging pulse duration	5 ms	
MOT atom number	10^9 atoms	
Crossed trap atom number	5×10^7 atoms	
BEC atom number	10^5 atoms	N_c

Table 7.1: Selected parameters for the guided atom laser experiment.

Part III

CONTINUOUS ATOM LASERS

8

CONTINUOUS ATOM LASERS

Every atom laser produced so far has drawn upon a fixed source of atoms. This source (typically 10^6) could not be refilled, so when it was emptied the atom laser flux stopped. The source of atoms used has always been a Bose-Einstein condensate (BEC), and there is a good reason for this. An atom laser needs many atoms in one quantum mode. Conveniently, this is created inside a BEC when it condenses. (For a condensate, the mode is the ground state of a trap.) The process of producing an atom laser (known as *outcoupling*) transfers atoms from the trapped mode to a freely propagating mode. The outcoupling process only needs to preserve this concentration of atoms in one mode, it does not need to create it.

To make an atom laser truly continuous requires a mechanism to add atoms to the condensate mode *whilst* outcoupling an atom laser, a process known as *pumping*. In this chapter I will discuss different approaches that have been used to try and create a pumped atom laser; I will discuss what is means to pump an atom laser; and I will discuss the pumping experiments done here at ANU.

8.1 DIFFERENT APPROACHES TO THE PROBLEM

Two approaches to the attempts to produce a continuous atom laser

There are two main approaches taken by the groups attempting to produce a continuous atom laser (see Figure 8.1). The first approach is to extend the operation of a conventional atom laser, by replenishing the BEC while

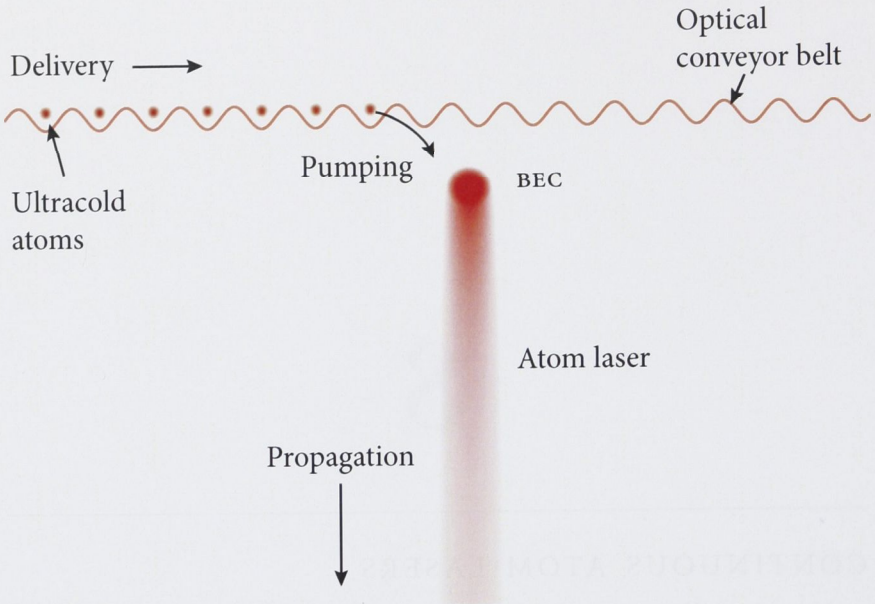

(a) Replenishment of a condensate (delivery and pumping) with simultaneous outcoupling

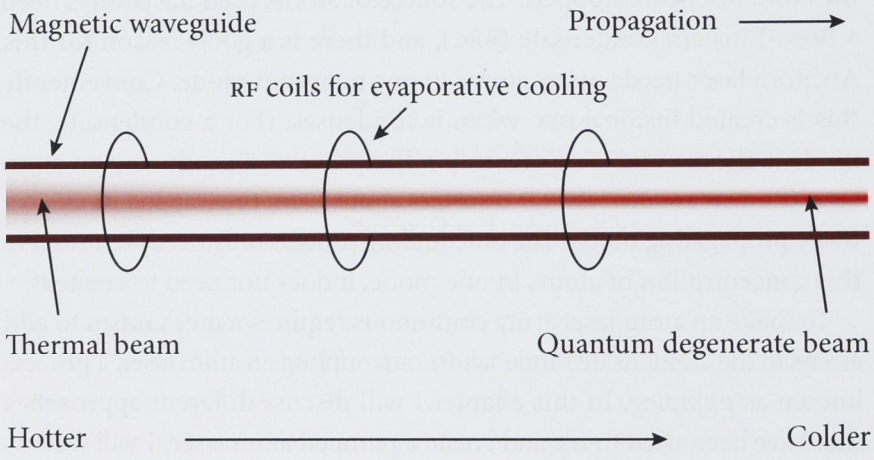

(b) Cooling of a continuous thermal beam

Figure 8.1: Two approaches to the goal of producing a continuous atom laser. The first approach (a) involves replenishing a conventional trapped BEC whilst simultaneously outcoupling an atom laser. Replenishment has two aspects, *delivery* of ultracold atoms to the condensate and *pumping* them into it. An optical conveyor belt represents the delivery aspect, but several techniques (magnetic fields, electric fields) could be used. The second approach (b) is to evaporatively cool a continuous thermal atomic beam. The RF coils represent the evaporation method (microwave and surface evaporation techniques have also been used [99, 100, 116].)

at the same time outcoupling an atom laser from it. This is the approach that our group at ANU has taken. The second approach is to produce a conventional continuous thermal atomic beam, and to cool it to quantum degeneracy as it travels. Because of the need to cool via evaporation, it is important the density of the beam remain high as it travels, and so it is confined to propagate inside a magnetic guide. This second approach is being pursued by many groups around the world, including the group of David Guéry-Odelin at ÉNS Paris (the group with whom I worked on the guided atom laser experiments discussed in Chapter 5).

Longitudinal coherence

Both approaches have the potential to produce continuous atom lasers, but the atom laser that each experiment may produce will have different properties. An atom laser produced from a Bose-Einstein condensate has excellent longitudinal (or temporal) coherence; a thermal beam evaporated in a waveguide has such coherence only over a limited region. The longitudinal coherence of atom lasers outcoupled from a BEC was demonstrated by Köhl et al. [27]. In this experiment, an atom laser was outcoupled by an RF field from a magnetic trap and allowed to propagate 400 μm under gravity. Then the atoms passed through two Raman lasers which transfered them into the magnetically trapped $|F = 2, m_F = 1\rangle$ state. At this position below the condensate, the magnetic field gradient is large (200 G/cm) and the atoms were reflected upward. An RF spectroscopy technique allowed the inteference pattern between the start and end of the atom laser to be measured, showing excellent longitudinal (temporal) coherence, and limited by the finite outcoupling time (Fourier limit) and condensate phase fluctuations.

Evaporation of a continuous thermal beam

The evaporation of a guided atomic beam was considered in an article by Castin et al. [117]. They modelled the system as an ideal quantum Bose gas in a 2D harmonic waveguide of length L and guide frequency $\omega_\perp$. The natural choice of basis to describe such a system is for the two transverse dimensions to use harmonic oscillator states (labelled l_x and l_y) and for the longitudinal dimension to use particle-in-a-box states (labelled l_z). In thermodynamic equilibrium, the number density in each state is given by:

$$n(l_x, l_y, l_z, \mu) = \frac{1}{\exp\left(\frac{1}{k_B T}\left(\frac{\hbar^2 k_z^2}{2m} + (l_x + l_y)\hbar\omega_\perp - \mu\right)\right) - 1} \tag{8.1}$$

where,

- μ is the chemical potenial,
- k_z is the wavenumber of the l_z transverse eigenstate $(2\pi l_z/L)$,
- k_B is Boltzmann's constant,
- T is the absolute temperature.

In the thermodynamic limit, in which $L \to \infty$ and $N \to \infty$ but $N/L =$

ρ_{lin} = constant, they found that there is no Bose-Einstein condensation to the absolute ground state ($l_x = l_y = l_z = 0$). (This is related to the fact that there is no Bose-Einstein condensation in one dimension.) There is, however, a phase transition to the *transverse* ground state ($l_x = l_y = 0$) that occurs when the linear density is greater than a certain critical density $\rho_{\text{lin}}^{(c)}$, given by:

$$\rho_{\text{lin}}^{(c)} = \frac{1}{\lambda}\left(\frac{k_B T}{\hbar\omega_\perp}\right)^2 \zeta(5/2), \tag{8.2}$$

where,

λ is the thermal de Broglie wavelength ($h/\sqrt{2\pi m k_B T}$),

$\zeta(5/2)$ is the Riemann Zeta function of 5/2 (approximately 1.341).

Any density above this critical value will accumulate in the transverse ground state. In this case, the atom laser has a longitudinal coherence length l_c given by:

$$l_c = \frac{\lambda^2}{2\pi}(\rho_{\text{lin}} - \rho_{\text{lin}}^{(c)}). \tag{8.3}$$

Practically, this means that an interferometer produced with this type of atom laser will need to be a zero path length difference interferometer (sometimes called a *white light interferometer*), or at least would need to operate with a path length difference smaller than the coherence length. Phase fluctuations of an elongated condensate in a 1D geometry were observed by Dettmer et al. [118].

8.2 WHAT DOES IT MEAN TO REPLENISH A CONDENSATE?

As mentioned above, our approach is to extend the operation of a conventional atom laser, by replenishing the condensate while at the same time outcoupling an atom laser from it. Replenishment may be separated into two processes:

1. *Delivery* of cold atoms to the location of the condensate.
2. *Pumping* the cold atoms into the condensate mode.

Delivery of ultracold atoms to a condensate

Delivery is a challenging process, because of the strict and incompatible requirements of the different techniques used to cool atoms to the condensation threshold, and the fragility of atoms cooled to such temperatures. One example given by Howard Wiseman is that [4]:

- to laser cool atoms from room temperature, each atom must scatter *at least* 10^4 photons; but

- to evaporatively cool atoms in a trap, the atoms must scatter *no more than* one photon every 10 seconds.

Since the scattered photons are emitted in all directions, the atoms undergoing laser cooling must be physically shielded from the evaporatively cooled atoms and then transported to them, all in ultra high vacuum[1]. To produce the level of shielding needed whilst transportation the atoms in vacuum is of course difficult to achieve.

Despite these difficulties, delivery has already been demonstrated with several techniques. Chikkatur et al. repeatedly delivered 2×10^6 Bose condensed atoms to another condensate every 18 seconds with a moving optical trap, and successfully merged the two condensates together [119]. Ultracold atoms have been transported more than 20 cm using moving optical lattices by Schmid et al. using Bessel beams and Lattimore et al. using near-resonant lasers and fast transit times [120, 121]. The magnetic guide experiment at ÉNS described above (§8.1) transported ultracold atoms over 5 m [99].

But delivery of additional ultracold atoms (or even Bose condensed atoms) to a BEC is not sufficient to produce a continuous atom laser. If very cold (but not Bose condensed) atoms are simply added to a condensate, they will likely heat and destroy it. When adding one condensate to another, such as in the experiment by Chikkatur et al. described above, each condensate can be regarded as a coherent state with its own (effectively random) phase; mixing the two condensates will result in one new condensate but with a new phase somewhere between the two original phases [119].

Therefore, to replenish a condensate requires an extra process: adding atoms into the condensate mode or *pumping*. The pumping process should satisfy four requirements:

Four requirements of pumping

1. It should *coherently* add atoms to the laser mode, giving them the same phase as the lasing mode. This done by Bosonic stimulation (the fact that the rate of transitions to a mode containing N bosons is is proportional to $N + 1$.

2. It should *irreversibly* add atoms to the lasing mode. This requires coupling to a reservoir. Two reservoirs are available: the empty modes of the electromagnetic field accessible by transitions from

1 Technically, the laser cooling stage may be done at a pressure which is less than UHV, and often happens at Rb vapour pressure (10^{-7} torr for room temperature). Then the transport process would move the atoms into a UHV region through an aperture which preserves the pressure difference between the two regions.

excited atomic states, and the empty modes of the atomic field accessible by collisions.

3. It should operate *continuously*.

4. It should do all the above, while *at the same time* an atom laser is outcoupled.

The pumping scheme in the experiment described below satisfies all these conditions.

8.3 PUMPING

The pumping experiment used the same basic experimental machine (vacuum system, lasers and optics, computer control, imaging system) as was used for the spatial mode experiments described in §4.1, with some modifications.

The pumping experiment used two clouds of atoms: each cloud in a different internal state, both clouds Bose condensed, both held in a magnetic trap, with one cloud a few microns distance above the other. The upper cloud was a condensate in $|F = 2, m_F = +2\rangle$, which was the reservoir of ultracold atoms. The lower cloud was a condensate in $|F = 1, m_F = -1\rangle$, which was the lasing mode into which atoms were pumped. Figure 8.2 shows an absorption image of the both condensates and atom laser all together. Figure 8.3 shows RF spectroscopy of the density of each condensate.

Production of the two condensates by sympathetic cooling

The two condensates were produced by optical pumping and sympathetic cooling [122]. After the polarisation gradient cooling stage of the experiment, there was an optical pumping stage to transfer the atoms from $F = 2$ to $F = 1$. This was how the $F = 1$ condensates were produced for the spatial mode experiments described in Chapter 4. This optical pumping was achieved by a 20 μs pulse of σ^- light at the $|F = 2\rangle \rightarrow |F' = 2\rangle$ which pumps most of the atoms into the $|F = 1, m_F = -1\rangle$ state. A small fraction remain in $F = 2$. The $F = 2$ atoms have twice the magnetic moment as the $F = 1$ atoms and therefore the gravitational sag is half as much. Therefore, although they remain in thermal contact with the $F = 1$ atoms during the evaporation, the $F = 1$ atoms are preferentially evaporated as they sit physically below the $F = 2$ atoms. At the end of the evaportion, there are two condensates, one in each hyperfine state, and each contains approximately the same size (5×10^5 atoms). By changing the length and power of this pulse, and the length of the evaporation stage, the relative number of atoms in each condensate can be varied.

The pumping process

The pumping process is illustrated in Figures 8.4 and 8.5. Atoms are outcoupled from the source condensate in $F = 2$ by an RF field which transers the atoms from $m_F = 2$ to 1 and to 0. (The small expected population in the intermediate state of $m_F = +1$ could not be directly observed in the absorption images to be above the noise level.) These atoms fall under gravity and enter the lasing mode condensate which is in $F = 1$. The size of each condensate is around 5 μm, and the distance between them around 8 μm, so they slightly overlap (see Figure 8.3). During this time, a weak upward propagating laser with π polarisation and resonant to the $F = 2 \rightarrow F' = 1$ transition is incident upon the atoms. The atoms absorb this light and are stimulated to enter the condensate mode in $|1, -1\rangle$ by the presence of the atoms already in that mode. Figures 8.4 and 8.5 illustrate how the pumping scheme works.

This pumping experiment is not the first experiment to have coherently added atoms to a condensate, but it is the first to do so in manner compatible with building a continuous atom laser. The first phase coherent amplification of matter wave experiments used a source condensate to coherently add atoms to an input atomic pulse [18, 19]. Superradiant Raman scattering (which is related to our experiment) extended this technique by transferring the atoms to a different hyperfine state [123, 124]. Ginsberg et al. coherently transfered atoms between two falling condensates, using an EIT technique to cause the input pulse to adiabatically enter the second condensate mode [125]. All these experiments, however, have "pumped" travelling atomic pulses, which subsequently moved away from their source condensate, or they have added atoms to a condensate in free-fall. Our experiment pumps atoms into stationary condensate in a conventional trap, which is the key step to producing a continuous atom laser.

Momentum conservation

It is important to ensure that the momentum of the incoming atoms can be matched to the lasing mode. This means that the atomic momentum after the absorption and emission of the photons has to lie within the momentum spread of the lasing mode condensate (around 0.3 mm/s). The magnetic trapping frequencies used place the clould near each other, without a significant spatial overlap, but also ensure that the velocity acquired by a $|2, 0\rangle$ atom in falling from the centre of the $|2, 2\rangle$ cloud to the centre of the $|1, -1\rangle$ laser mode (12 mm/s) can be cancelled by the absorption of an upward propagating π-photon and the emission of an appropriately directed and phased σ^- photon; a single-photon recoil corresponds to 6 mm/s. The velocity at the lasing mode centre can be tuned by around ±2 mm/s by moving the coupling surface within the source cloud up or down. While the pump atoms are falling through the

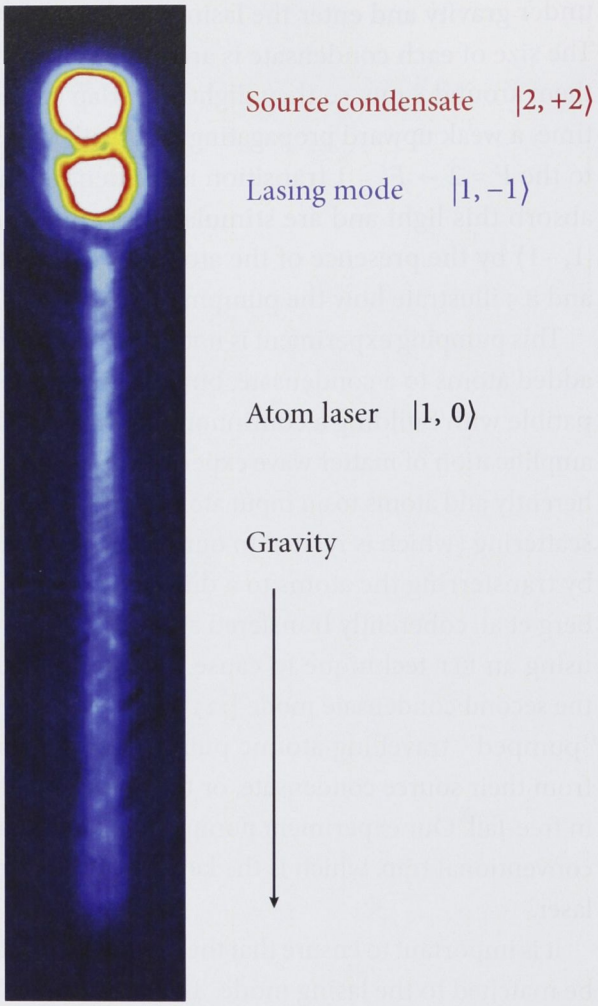

Figure 8.2: Absorption image showing source condensate, laser mode condensate and atom laser (outcoupled from the laser mode condensate). The image is for illustrative purposes. In reality, the outcoupling rate used for the atom laser in this image was orders of magnitude greater than that used for the pumping experiments. The field of view is 0.5 mm across.

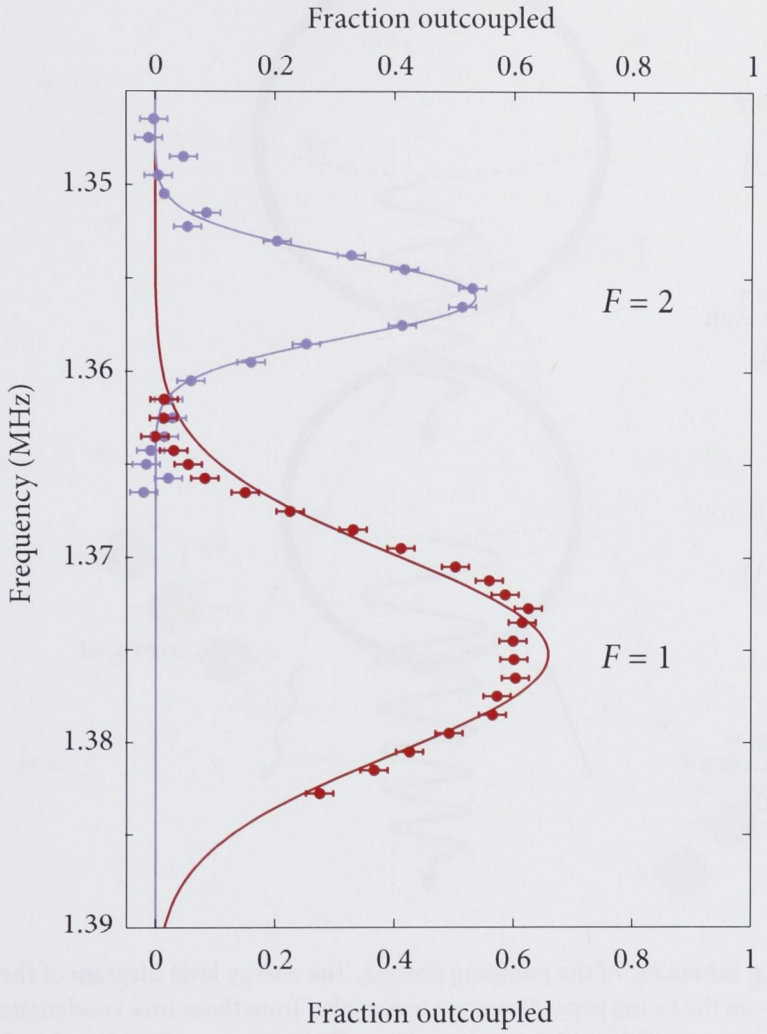

Figure 8.3: RF spectroscopy of the two condensates. The spin states are physically separated by a magnetic field gradient during the a period of free expansion. Solid curve to guide the eye. The independent variable is on the vertical axis (contrary to normal use), to resemble the experiment more closely. The error bars are based upon the typical standard deviation for repeated measurements (3 %). This was found by measuring four particular RF frequencies multiple times; most frequencies were only measured once.

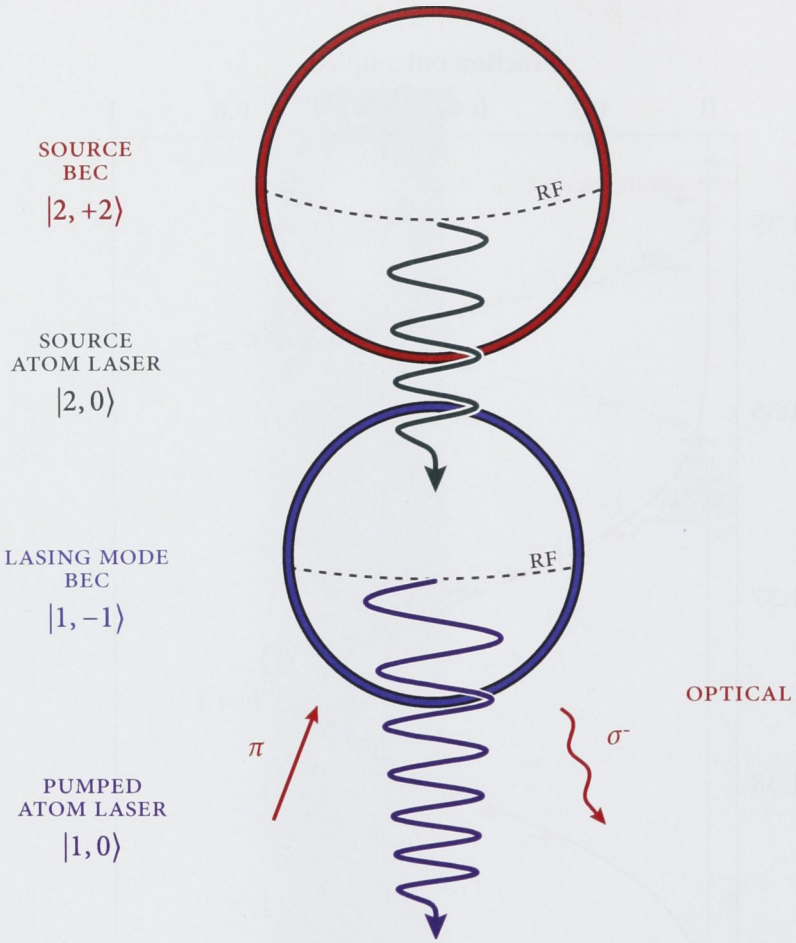

Figure 8.4: Schematic of the pumping process. The energy level diagram of the process is on the facing page. Atoms are outcoupled from the source condensate in $F = 2$ by an RF field which transers the atoms from $m_F = 2$ to 1 and to 0. These atoms fall under gravity and enter the lasing mode condensate which is in $F = 1$. The size of each condensate is around 5 μm, and the distance between them around 8 μm, so they slightly overlap at the beginning of the experiment (see Figure 8.3). During this time, a weak upward propagating laser with π polarisation and resonant to the $F = 2 \rightarrow F' = 1$ transition is incident upon the atoms. The atoms absorb this light and are stimulated to enter the condensate mode in $|1, -1\rangle$ by the presence of the atoms already in that mode. Whilst all the above is occuring, an atom laser is outcoupled from the $F = 1$ lasing mode condensate.

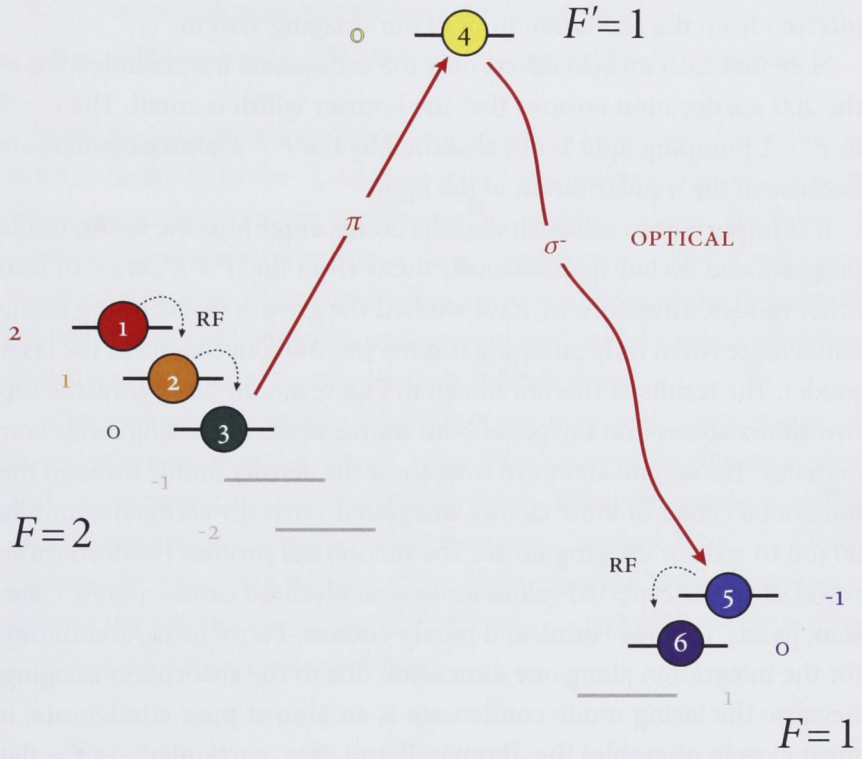

Figure 8.5: Energy level diagram of the pumping process. The description and and a schematic of the process is in the caption on the facing page.

laser mode, the velocity changes by 3 mm/s owing to gravity, and the time for which the pumping atoms satisfy momentum resonance with the laser mode is much shorter (100 μs) than the traversal time across the laser mode (1 ms). The velocity spread of the laser mode is of the order of 0.3 mm/s; thus, cancelling the atomic momentum of the $|2,0\rangle$ state requires an extreme level of control over the pumping parameters. We did not observe collective motion, such as sloshing or breathing of either the source or laser mode condensates. This implies that if the pumping does indeed drive excitations, they occur with an amplitude of less than 5% of the full-width at half-maximum of the laser-mode condensate, which is inferred from the resolution limit of our imaging system.

Note that each RF field affects only the condensate it is intended for, as the 200 ms duration ensures that the Fourier width is small. The $F = 2$ to $F' = 1$ pumping light is not absorbed by the $F = 2$ source condensate because of the π polarisation of the light.

Isolating the pumping process

It is important to establish that the atoms enter into the lasing mode properly, and do not spontaneously decay from the $|F = 1', m_F = 0\rangle$ into other modes. Therefore we have studied the growth in the lasing mode condensate when only pumping is done (no outcoupling from the laser mode). The results of this are shown in Figure 8.6. In this figure, the top row shows absorption images of both source mode and lasing mode condensates. The second and third rows show the density profile through the horizontal center of those clouds, integrated vertically across the middle 30 μm to reduce imaging noise. The theoretical profiles (bottom three rows) show the expected values for several idealised cases—purely Gaussian, purely Thomas-Fermi, and purely Thomas-Fermi in 3D, accounting for the integration along one dimension due to the absorption imaging. Because the lasing mode condensate is an almost pure condensate, it most closely resembles the Thomas-Fermi case, particularly in the flat top in the center of the profile. The slight asymmetry in the profile is likely due to imaging noise.

Rate equation study

It is not possible to measure the atom laser directly whilst it is being pumped: the outcoupling rate is low and hence the atom laser optical density is also low. Therefore we have made a rate equation study of the pumping process, by studing the atom number dynamics in the the lasing mode and source mode for three cases: (1) pumping only, (2) outcoupling only, (3) both. We compared this measurements to a simple rate equation model, to establish the independence of the pumping and outcoupling.

The model used was:

$$\dot{N}_2 = -\gamma_P N_2 \tag{8.4}$$

$$\dot{N}_1 = +\gamma_P N_2 \alpha N_1 - \gamma_0 N_1, \tag{8.5}$$

where,

N_1 is the lasing mode BEC atom number (initially $(6.7 \pm 0.5) \times 10^5$),

N_2 is the source BEC atom number (initially $(5 \pm 0.4) \times 10^5$),

γ_P is the outcoupling rate from the source condensate (9/s),

γ_0 is the outcoupling rate from the lasing mode condensate (1.4/s),

αN_1 is the pumping efficiency into the lasing mode condensate.

Both measurements and the comparison to theory are found in Figure 8.7. In the fit to the "pumping only" experiment, the reduction in the source condensate was used to find γ_P, and the increase in the lasing mode condensate used to find α. The "outcoupling only" experiment was used to find γ_0. Therefore no free parameters exist to the fit to the experiment with both pumping and outcoupling, and the good agreement shows that the two process are largely independent.

Although a Bose-Einstein condensate was used as a source, this is not an essential feature of the system. What is necessary is that the absorption and emission of two photons is sufficient to bring the atoms to within the momentum width of the lasing mode BEC (around 10^5 m^{-1}). Consequently, the source of atoms for replenishing needs to have a temperature around the photon recoil limit ($\hbar^2 k^2/(mk_B) \approx 400$ nK for Rb); but the source need not be Bose condensed.

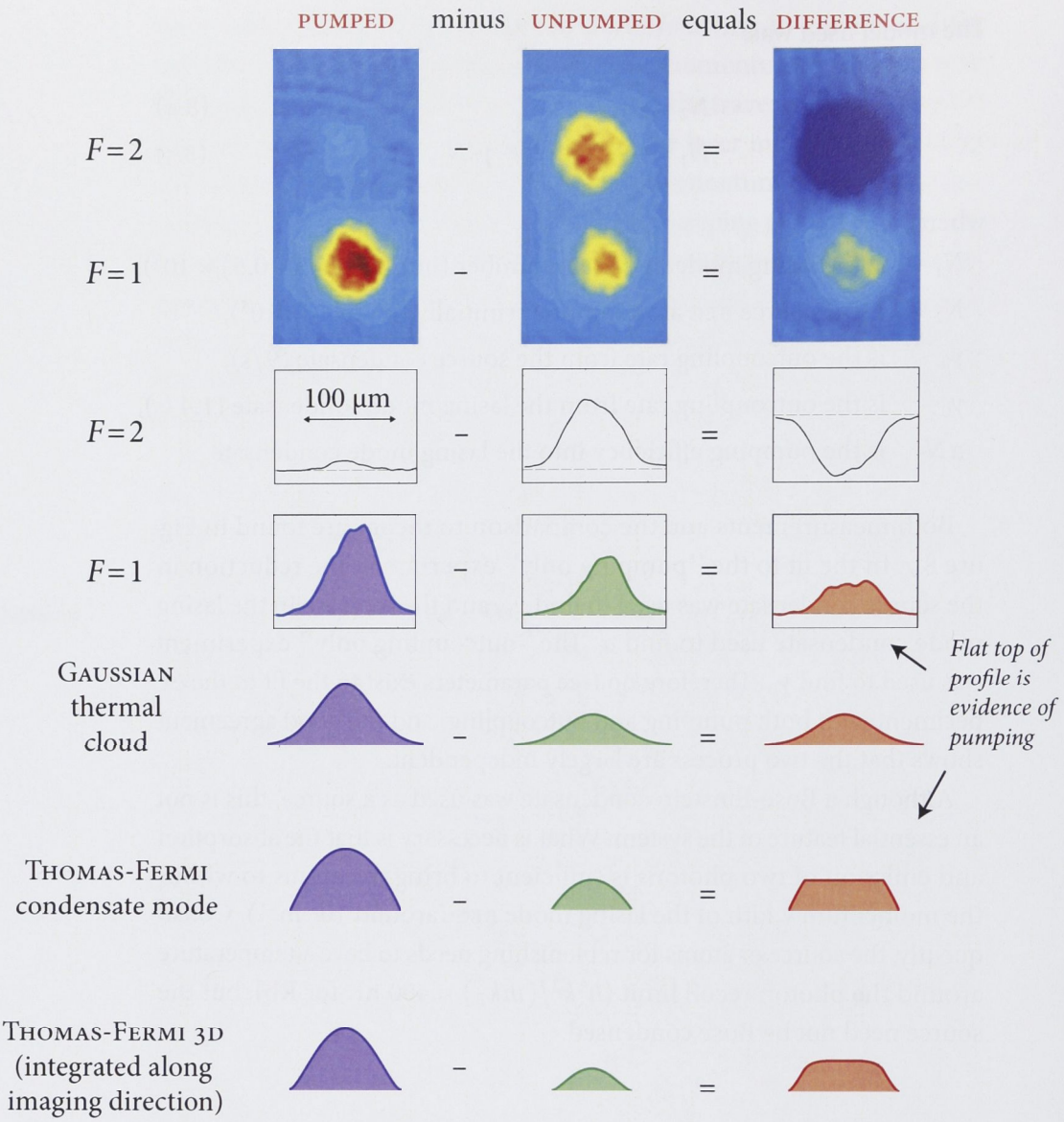

Figure 8.6: Isolating the pumping mechanism: results from pumping the lasing mode condensate (with no outcoupling from it). The three columns show the pumped cased, the unpumped case (i. e. initial conditions), and the results of subtracting one from another.

The top row shows absorption images of both source mode and lasing mode condensates. The second and third rows show the density profile through the center of those clouds, integrated across the central 30 μm. The theoretical profiles (bottom three rows) show the expected values for several idealised cases—purely Gaussian, purely Thomas-Fermi, and purely Thomas-Fermi in 3D, accounting for the integration along one dimension due to the absorption imaging. Because the lasing mode condensate is an almost pure condensate, it most closely resembles the Thomas-Fermi case, particularly in the flat top in the center of the profile. The slight asymmetry in the profile is likely due to imaging noise.

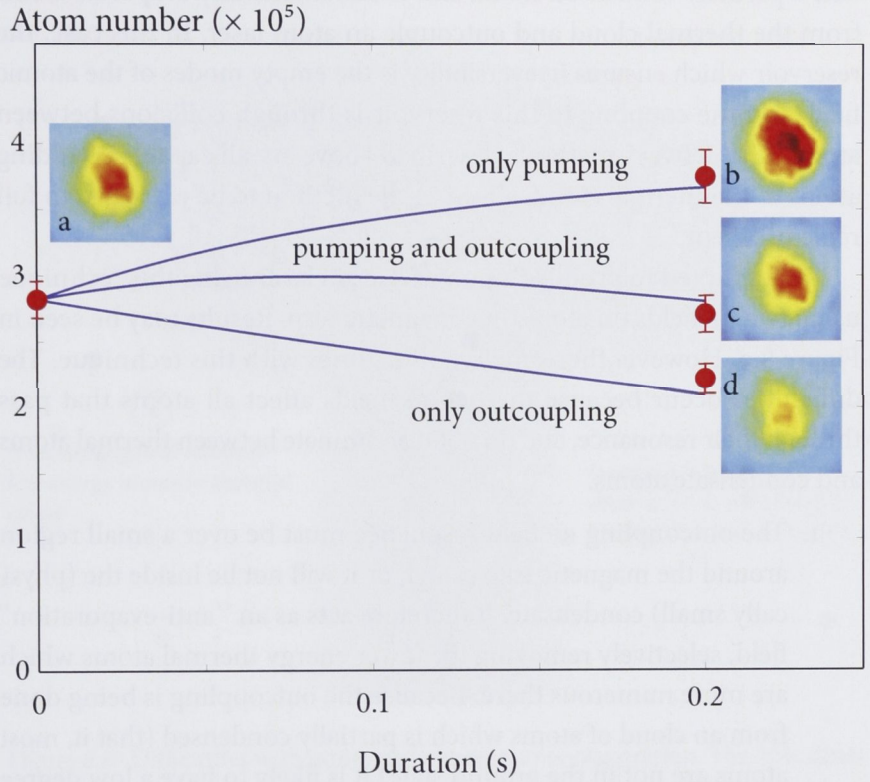

Figure 8.7: Results of a rate equation study of a pumped atom laser. The error bars are the standard error, or standard deviation divided by $\sqrt{n}$ where $n = 20$ is the number of independent measurements made. The solid lines are the best fit of the solution to Equation 8.5, done in this manner: in the pumping only experiment, the reduction in the source condensate was used to find γ_P, and the increase in the lasing mode condensate used to find α. The outcoupling only experiment was used to find γ_0. Therefore no free parameters exist to the fit to the experiment with both pumping and outcoupling. The detailed dynamics of the pumping will be explored in an article by D. Döring et al. (to be published).

8.4 PUMPING VIA CONTINUOUS EVAPORATION

All cooling to BEC by evaporation can be considered pumping. Of the four requirements discussed above, the first three are clearly satisfied by evaporative cooling, which uses Bose stimulation to populate the condensate mode [20]. An obvious pumping method to try, therefore, is to take a partially condensed cloud, and to simultaneously evaporate atoms from the thermal cloud and outcouple an atom laser. In this case, the reservoir which ensures irreversibility is the empty modes of the atomic field, and the coupling to this reservoir is through collisions between atoms. The delivery methods described above are all capable of adding atoms to the thermal cloud, allowing the method to be extended to full replenishment.

We attempted to produce a pumped atom laser using this technique, using two RF fields on atoms in a magnetic trap. Results may be seen in Figure 8.9. However,there are two difficulties with this technique. The difficulties occur because the two RF fields affect all atoms that pass through their resonance, and do not discriminate between thermal atoms and condensate atoms.

1. The outcoupling RF field resonance must be over a small region around the magnetic trap center, or it will not be inside the (physically small) condensate. It therefore acts as an "anti-evaporation" field, selectively removing the lower energy thermal atoms which are more numerous there. Because the outcoupling is being done from an cloud of atoms which is partially condensed (that it, most atoms are not in the ground state) it is likely to have a low degree of coherence ($g^{(2)} > 1$) [26].

2. The atom laser falls through the pumping RF field resonance (which must be near the edge of the thermal cloud to remove the higher energy atoms) and transfers atoms to other m_F states, creating noise on the beam. In fact atoms transferred in to magnetically trapped states will reenter and heat the condensate.

These problems are illustrated in Figure 8.8. Because of them, we abandoned this technique; it could be possible to achieve with a different experimental arrangement.

8.5 FUTURE DIRECTIONS

As discussed in §8.2, producing a continuous atom laser has two components: delivery of ultracold atoms to a condensate, and pumping the atoms

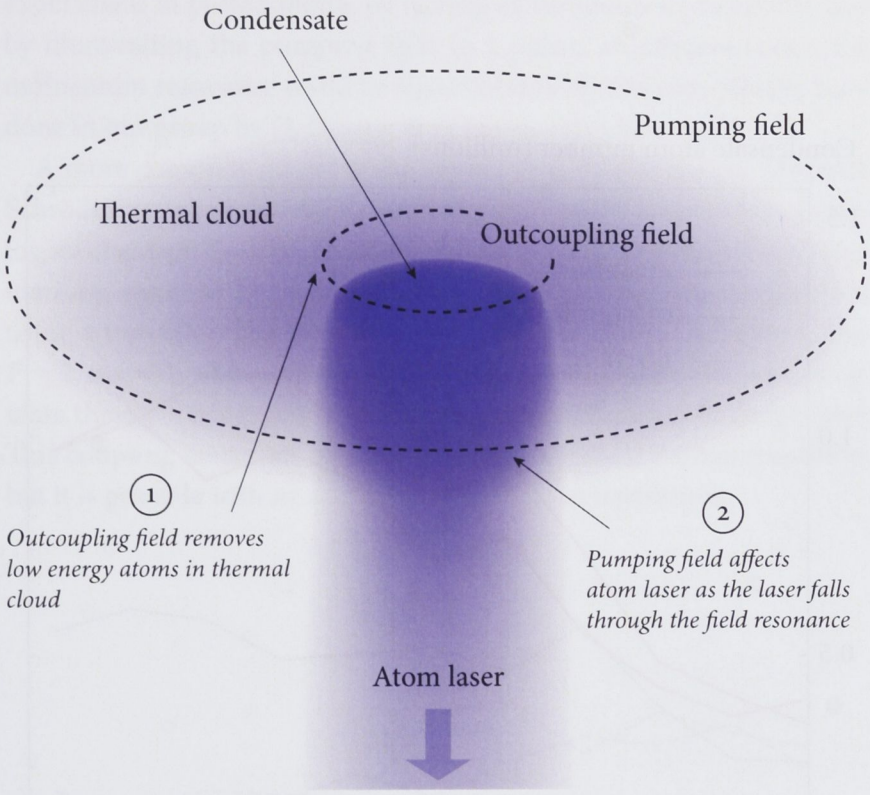

Figure 8.8: Difficulties with pumping by continuous evaporation. The difficulties occur because the two RF fields affect all atoms that pass through their resonance, and do not discriminate between thermal atoms and condensate atoms. (1) The outcoupling RF field resonance must be over a small region around the magnetic trap center, or it will not be inside the (physically small) condensate. It therefore acts as an "anti-evaporation" field, selectively removing the lower energy thermal atoms which are more numerous there. (2) The atom laser falls through the pumping RF field resonance (which must be near the edge of the thermal cloud to remove the higher energy atoms) and transfers atoms to other m_F states, creating noise on the beam. In fact, atoms transferred in to magnetically trapped states will reenter and heat the condensate. The direction of view is along the strong axis of the trap, the atomic density is in blue and the resonant surface of the RF fields is shown with a dotted line. Further detail on why the atom clouds and RF fields have this geometry may be found in §3.1.

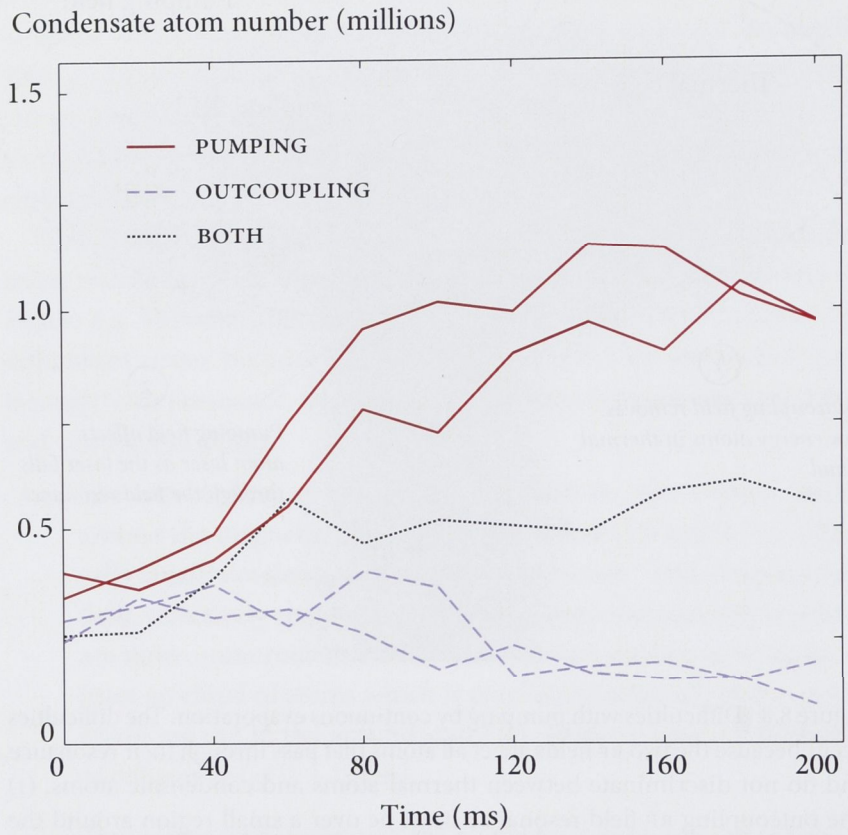

Figure 8.9: Tentative results indicating RF pumping from the thermal cloud into the condensate. There are two difficulties with this method (see Figure 8.8 on the preceding page), and so we did not pursue the method any further than this. The two condensate pumping scheme discussed in §8.3 does not suffer these difficulties

into the condensate. Delivery has previously been done [119]. Pumping has now been done. To produce a continuous atom laser, the two processes need to be combined.

The pumping process could be investigated further by running the experiment in pulsed mode. By having all the atoms in one pulse, and by illuminating the pumping light in a pulses at different times, the momentum resonance could be observed directly. This has already been done in our group by D. Döring et al. (to be published soon).

A more complete model of the system would be to use the Maxwell-Schrödinger equation, which would also aid understanding of the pumping mechanism. Graham Dennis has done detailed versions of such simulations, again to be published soon. These simulations suggest that using a transition that directly couples the $F = 2, m_F = +2$ state to the $F = 2, m_F = 0$, with no intermediate state, would more efficiently populate the $m_F = 0$ state and increase the overall efficiency of the process. This coupling many not be done through an optical Raman transition, but it is possible with RF and microwave Raman transitions.

QUANTITY	VALUE	SYMBOL
Tight trapping frequency ($F = 1$)	$2\pi \times 128$ Hz	ω_ρ
Weak trapping frequency ($F = 1$)	$2\pi \times 13$ Hz	ω_y
Trapping frequency ratio $F = 2 : F = 1$	$\sqrt{2} : 1$	
Magnetic bias field	2.0 G	B_0
Thomas Fermi radius ($F = 1$)	5.1 μm	R_1
Thomas Fermi radius ($F = 2$)	4.4 μm	R_2
Gravitational sag ($F = 1$)	15 μm	
Gravitational sag ($F = 2$)	7.5 μm	
Pumping light resonance	$F = 2 \rightarrow F' = 1$	
power	10 pW	
polarisation	π	
duration	200 ms	
Time to cross lasing mode condensate	1 ms	
Time in momentum resonance	0.1 ms	
Pumping efficiency	20 %	
Source outcoupling rate	9/s	γ_P
Lasing mode outcoupling rate	1.4/s	γ_0
Imaging detuning	- (resonance)	
Pixel size (on camera)	9 μm	
Pixel size (at position of atoms)	5 μm	
Source BEC internal state	$\lvert F = 2, m_F = +2\rangle$	
Source BEC atom number	$(6.7 \pm 0.5) \times 10^5$	N_2
Source atom laser internal state	$\lvert F = 2, m_F = 0\rangle$	
Lasing mode BEC internal state	$\lvert F = 1, m_F = -1\rangle$	
Lasing mode BEC atom number	$(5 \pm 0.4) \times 10^5$	N_1
Pumped atom laser internal state	$\lvert F = 1, m_F = 0\rangle$	

Table 8.1: Selected parameters for the pumped atom laser experiment.

CONCLUSION

9

CONCLUSION

This thesis has described improvements to the spatial mode of guided and free space atom lasers, and the production of the first pumped atom laser. At the end of each section so far, I have described ideas to further develop each technique. In this chapter, I would like to discuss the possible development of atom lasers in general, particularly as it applies to precision measurement.

The important consideration in precision measurement is, of course, the signal-to-noise ratio. The signal is proportional to the flux, N. The noise is proportional to the square root of the flux, $\sqrt{N}$, when all significant technical noise is eliminated and shot noise is dominant.

The obvious direction for atom lasers is to increase the flux, by building better BEC sources, and to decrease the noise, by introducing quantum squeezing techniques.

9.1 INCREASING THE FLUX

The key to increasing the flux of atom lasers is to improve their source, BECs: to produce larger condensates more quickly. Current atom laser techniques can use all the atoms in a condensate with low noise two orders of magnitude faster than a condensate can be produced, so it is clear that the emphasis needs to be on improving BEC sources. It should be possible to design BEC machines to increase flux by two orders of magnitude,

without needing radically new techniques but simply by incorporating several new ones into one experiment. Currently, our machine at ANU produces a condensate of around 10^6 atoms in slightly less than a minute, or a flux of around 2×10^4 atoms per second. For atom chip experiments and optical traps, the production time is shorter yet the condensate number is smaller, yielding a comparable flux. For example, the optical trap experiment at ÉNS produced a condensate of around 10^5 atoms in 6 s.

The largest pure condensate to date contained 1.2×10^8 atoms (in sodium), reported by van der Stam et al. at Utrecht [126]. The magnetic trap was decompressed near the end of the evaporation to reduce the density and prevent three body loss. Their experiment produced a condensate every 50 s, with a flux of 2×10^6 atoms per second, the current state of the art. The Utrecht experiment used a Zeeman slower which loaded the MOT at a rate of 3×10^9 atoms per second. Loading rates of 2×10^{10} atoms per second (in Rb) have been reported by Lahaye et al., using an optimised Zeeman slower design [99]. Similarly, using large diameter (3 cm) laser beams should produce similar loading times using a 2D MOT.

Further increases in flux could come from advanced cooling techniques which have already been demonstrated successfully, but which have not yet been incorporated into large condensate machines. These include Raman cooling [127], and Doppler cooling of atoms inside a magnetic trap to the Doppler limit [127]. Finally, the realisation of pumping and the possibility of making a continuous atom laser would make it possible to run each stage of BEC production (MOT loading, cooling, evaporation, delivery and pumping) in parallel rather than sequentially, further improving the production rate.

9.2 DECREASING THE NOISE

Once atom lasers have ideal gaussian modes, with perfectly stable BEC sources and outcoupling fields (or decent approximations thereof), conventional quantum number fluctuations will be the remaining noise source. For a shot noise limited measurement, the sensitivity is $N^{-1/2}/\sqrt{\text{Hz}}$. If the quantum fluctuations can be suppressed (perfect squeezing) then the sensitivity is N^{-1}/Hz (the Heisenberg limit). For the current best BEC source (10^6 atoms per second), this is a potential three orders of magnitude improvement. As the flux increases, so does the potential improvement.

There have been several experimental proposals to squeeze an atom laser. Haine et al. have suggested using a squeezed optical laser as a Ra-

man outcoupler, showing theoretically that the squeezing is efficiently transferred to the atoms [128]. Squeezing in optical lasers is already highly developed, at the correct wavelengths for BEC experiments, at high degrees of squeezing, over many frequency bands [129]. By operating in the regime where the Raman outcoupling beam is partially absorbed, the atom laser would be entangled with the outcoupling, allowing studies of massive particle entanglement [130]. Another proposal is to use the inherent non-linearity of the atoms in the condensate, which can produce Kerr-type squeezing [131, 132].

For atom laser experiments able to reach the quantum noise limit, when they have high flux and that limit is low, the potential is great. Atom lasers, which were only invented a little over a decade years ago, are quickly maturing into an exciting and powerful technology.

BIBLIOGRAPHY

[1] I.A. Getting. The Global Positioning System. *Spectrum, IEEE*, 30 (12):36–38, 43–47, Dec 1993. ISSN 0018-9235. doi: 10.1109/6.272176. (Cited on pages 2 and 8.)

[2] P. C. Lauterbur. Image Formation by Induced Local Interactions: Examples Employing Nuclear Magnetic Resonance. *Nature*, 242: 190–191, March 1973. doi: 10.1038/242190a0. (Cited on page 2.)

[3] Falcon Project. BHP Billiton Airborne Gravity Gradiometer. URL `http://falcon.bhpbilliton.com/falcon`. (Cited on page 2.)

[4] H. M. Wiseman. Defining the (atom) laser. *Physical Review A*, 56(3):2068–2084, 1997. URL `http://prola.aps.org/pdf/PRA/v56/i3/p2068_1?qid=987b6a2fafb47ef0&qseq=40&show=10`. (Cited on pages 3 and 110.)

[5] E. W. Hagley, L. Deng, W. D. Phillips, K. Burnett, and C. W. Clark. The atom laser. *Optics & Photonics News*, 12:22–26, May 2001. (Cited on page 4.)

[6] M.-O. Mewes, M. R. Andrews, D. M. Kurn, D. S. Durfee, C. G. Townsend, and W. Ketterle. Output Coupler for Bose-Einstein Condensed Atoms. *Physical Review Letters*, 78(4):582–585, 1997. (Cited on pages 5, 6, 29, and 80.)

[7] Dallin Durfee and Wolfgang Ketterle. Experimental studies of bose-einstein condensation. *Opt. Express*, 2(8):299–313, 1998. URL `http://www.opticsexpress.org/abstract.cfm?URI=oe-2-8-299`. (Cited on page 6.)

[8] I. Bloch, T. W. Hänsch, and T. Esslinger. Atom Laser with a cw Output Coupler. *Physical Review Letters*, 82(15):3008, 1999. (Cited on pages 5, 6, 29, 40, and 60.)

[9] E. W. Hagley, L. Deng, M. Kozuma, J. Wren, K.Helmerson, S. L. Rolston, and W. D. Phillips. A Well-Collimated Quasi-Continuous Atom Laser. *Science*, 283:1706–1708, 1999. URL `http:`

//www.sciencemag.org/cgi/reprint/283/5408/1706.pdf. (Cited on pages 5, 7, 29, and 32.)

[10] N. P. Robins, C. Figl, S. A. Haine, A. K. Morrison, M. Jeppesen, J. J. Hope, and J. D. Close. Achieving Peak Brightness in an Atom Laser. *Physical Review Letters*, 96(14):140403, 2006. doi: 10.1103/PhysRevLett.96.140403. (Cited on pages 5, 7, and 32.)

[11] M. H. Anderson, J. R. Ensher, M. R. Matthews, C. E. Wieman, and E. A. Cornell. Observation of Bose-Einstein Condensation in a Dilute Atomic Vapor. *Science*, 269(5221):198–201, 1995. doi: 10.1126/science.269.5221.198. URL http://www.sciencemag.org/cgi/content/abstract/269/5221/198. (Cited on page 4.)

[12] C. C. Bradley, C. A. Sackett, J. J. Tollett, and R. G. Hulet. Evidence of bose-einstein condensation in an atomic gas with attractive interactions. *Phys. Rev. Lett.*, 75(9):1687–1690, Aug 1995. doi: 10.1103/PhysRevLett.75.1687. (Cited on page 4.)

[13] C. C. Bradley, C. A. Sackett, J. J. Tollett, and R. G. Hulet. Evidence of bose-einstein condensation in an atomic gas with attractive interactions [phys. rev. lett. 75, 1687 (1995)]. *Phys. Rev. Lett.*, 79(6): 1170, Aug 1997. doi: 10.1103/PhysRevLett.79.1170. (Cited on page 4.)

[14] K. B. Davis, M. O. Mewes, M. R. Andrews, N. J. van Druten, D. S. Durfee, D. M. Kurn, and W. Ketterle. Bose-Einstein Condensation in a Gas of Sodium Atoms. *Phys. Rev. Lett.*, 75(22):3969–3973, Nov 1995. doi: 10.1103/PhysRevLett.75.3969. (Cited on page 4.)

[15] E. A. Cornell and C. E. Wieman. Nobel Lecture: Bose-Einstein condensation in a dilute gas, the first 70 years and some recent experiments. *Rev. Mod. Phys.*, 74(3):875–893, Aug 2002. doi: 10.1103/RevModPhys.74.875. URL http://prola.aps.org/abstract/RMP/v74/i3/p875_1. (Cited on page 4.)

[16] Wolfgang Ketterle. Nobel lecture: When atoms behave as waves: Bose-Einstein condensation and the atom laser. *Rev. Mod. Phys.*, 74(4):1131–1151, Nov 2002. doi: 10.1103/RevModPhys.74.1131. URL http://prola.aps.org/abstract/RMP/v74/i4/p1131_1. (Cited on page 4.)

[17] M. R. Andrews, C. G. Townsend, H.-J. Miesner, D. S. Durfee, D. M. Kurn, and W. Ketterle. Observation of interference between two bose condensates. *Science*, 275:637–641, 1997. (Cited on page 4.)

[18] M. Kozuma, Y. Suzuki, Y. Torii, T. Kuga, E. W. Hagley, and L. Deng. Phase-Coherent Amplification of Matter Waves. *Science*, 286(5448):2309, 1999. URL http://www.sciencemag.org/cgi/content/abstract/286/5448/2309. (Cited on pages 5 and 113.)

[19] S. Inouye, T. Pfau, S. Gupta, A. P. Chikkatur, A. Görlitz, D. E. Pritchard, and W. Ketterle. Phase-coherent amplification of atomic matter waves. *Nature*, pages 641–, 1999. (Cited on pages 5 and 113.)

[20] H.-J. Miesner, D. M. Stamper-Kurn, M. R. Andrews, D. S. Durfee, S. Inouye, and W. Ketterle. Bosonic Stimulation in the Formation of a Bose-Einstein Condensate. *Science*, 279:1005–1007, 1998. (Cited on pages 5 and 122.)

[21] L. Deng, E. W. Hagley, J. Wen, M. Trippenbach, Y. Band, P. S. Julienne, J. E. Simsarian, K. Helmerson, S. L. Rolston, and W. D. Phillips. Four-wave mixing with matter waves. *Nature*, 398(6724):218–220, 1999. URL http://dx.doi.org/10.1038/18395. (Cited on page 5.)

[22] J. R. Abo-Shaeer, C. Raman, J. M. Vogels, and W. Ketterle. Observation of Vortex Lattices in Bose-Einstein Condensates. *Science*, 292:476–479, April 2001. doi: 10.1126/science.1060182. (Cited on page 5.)

[23] M. Greiner, O. Mandel, T. Rom, A. Altmeyer, A. Widera, T. W. Hänsch, and I. Bloch. Quantum phase transition from a superfluid to a mott insulator in an ultracold gas of atoms. *Physica B: Condensed Matter*, 329-333(Part 1):11 – 12, 2003. ISSN 0921-4526. doi: 10.1016/S0921-4526(02)01872-0. URL http://www.sciencedirect.com/science/article/B6TVH-483BX36-3/2/af9d15933ca19c1e5ca32d98cde2e10e. Proceedings of the 23rd International Conference on Low Temperature Physics. (Cited on page 5.)

[24] Tilman Esslinger, Immanuel Bloch, and Theodor W. Hänsch. Bose-Einstein condensation in a quadrupole-Ioffe-configuration trap. *Phys. Rev. A*, 58(4):R2664–R2667, Oct 1998. doi: 10.1103/PhysRevA.58.R2664. URL http://prola.aps.org/abstract/PRA/v58/i4/pR2664_1. (Cited on pages 5 and 58.)

[25] I. Bloch, T. W. Hänsch, and T. Esslinger. Measurement of the spatial coherence of a trapped Bose gas at the phase transition. *Nature*, pages 166–170, 2000. URL http://www.nature.com/nature/journal/v403/n6766/abs/403166a0.html. (Cited on page 8.)

[26] Anton Öttl, Stephan Ritter, Michael Köhl, and Tilman Esslinger. Correlations and Counting Statistics of an Atom Laser. *Phys. Rev. Lett.*, 95(9):090404, Aug 2005. doi: 10.1103/PhysRevLett.95.090404. URL http://link.aps.org/doi/10.1103/PhysRevLett.95.090404. (Cited on pages 8 and 122.)

[27] M. Köhl, T. W. Hänsch, and T. Esslinger. Measuring the Temporal Coherence of an Atom Laser Beam. *Physical Review Letters*, 87 (16):160404–(1–4), 2001. URL http://link.aps.org/doi/10.1103/PhysRevLett.87.160404. (Cited on pages 8 and 109.)

[28] A. D. Cronin, J. Schmiedmayer, and D. E. Pritchard. Atom Interferometers. *ArXiv e-prints*, December 2007. (Cited on pages 8 and 10.)

[29] Norman F. Ramsey. A Molecular Beam Resonance Method with Separated Oscillating Fields. *Phys. Rev.*, 78(6):695–699, Jun 1950. doi: 10.1103/PhysRev.78.695. (Cited on page 8.)

[30] Norman F. Ramsey. A New Molecular Beam Resonance Method. *Phys. Rev.*, 76(7):996, Oct 1949. doi: 10.1103/PhysRev.76.996. (Cited on page 8.)

[31] W. H. Oskay, S. A. Diddams, E. A. Donley, T. M. Fortier, T. P. Heavner, L. Hollberg, W. M. Itano, S. R. Jefferts, M. J. Delaney, K. Kim, F. Levi, T. E. Parker, and J. C. Bergquist. Single-atom optical clock with high accuracy. *Physical Review Letters*, 97(2): 020801, 2006. doi: 10.1103/PhysRevLett.97.020801. URL http://link.aps.org/abstract/PRL/v97/e020801. (Cited on page 8.)

[32] Alan Lenef, Troy D. Hammond, Edward T. Smith, Michael S. Chapman, Richard A. Rubenstein, and David E. Pritchard. Rotation sensing with an atom interferometer. *Phys. Rev. Lett.*, 78(5):760–763, Feb 1997. doi: 10.1103/PhysRevLett.78.760. (Cited on page 8.)

[33] A. Peters, K. Y. Chung, and S. Chu. High-precision gravity measurements using atom interferometry. *Metrologia*, 38:25–61(37), 1 February 2001. URL http://www.ingentaconnect.com/content/bipm/met/2001/00000038/00000001/art00004. (Cited on page 10.)

[34] A. Peters, K. Y. Chung, and S. Chu. Measurement of gravitational acceleration by dropping atoms. *Nature*, 400:849–852, August 1999. doi: 10.1038/23655. (Cited on page 10.)

[35] M. J. Snadden, J. M. McGuirk, P. Bouyer, K. G. Haritos, and M. A. Kasevich. Measurement of the Earth's Gravity Gradient with an Atom Interferometer-Based Gravity Gradiometer. *Phys. Rev. Lett.*, 81(5):971–974, Aug 1998. doi: 10.1103/PhysRevLett.81.971. (Cited on page 10.)

[36] J. M. McGuirk, G. T. Foster, J. B. Fixler, M. J. Snadden, and M. A. Kasevich. Sensitive absolute-gravity gradiometry using atom interferometry. *Phys. Rev. A*, 65(3):033608, Feb 2002. doi: 10.1103/PhysRevA.65.033608. (Cited on page 10.)

[37] M. Vengalattore, J. M. Higbie, S. R. Leslie, J. Guzman, L. E. Sadler, and D. M. Stamper-Kurn. High-resolution magnetometry with a spinor bose-einstein condensate. *Physical Review Letters*, 98(20): 200801, 2007. doi: 10.1103/PhysRevLett.98.200801. URL `http://link.aps.org/abstract/PRL/v98/e200801`. (Cited on pages 10 and 98.)

[38] Savas Dimopoulos, Peter W. Graham, Jason M. Hogan, Mark A. Kasevich, and Surjeet Rajendran. Atomic gravitational wave interferometric sensor. *Physical Review D (Particles, Fields, Gravitation, and Cosmology)*, 78(12):122002, 2008. doi: 10.1103/PhysRevD.78.122002. URL `http://link.aps.org/abstract/PRD/v78/e122002`. (Cited on page 10.)

[39] Holger Müller, Sheng wey Chiow, Quan Long, Sven Herrmann, and Steven Chu. Atom interferometry with up to 24-photon-momentum-transfer beam splitters. *Physical Review Letters*, 100 (18):180405, 2008. doi: 10.1103/PhysRevLett.100.180405. URL `http://link.aps.org/abstract/PRL/v100/e180405`. (Cited on page 10.)

[40] Born and Wolf. *Principles of Optics*. Cambridge University Press, 1999. (Cited on page 22.)

[41] A. A. Michelson. On the Application of Inteference Methods to Astronomical Measurements. *Philosophical Magazine*, 5:1, 1891. (Cited on page 23.)

[42] A. E. Siegman. Defining the effective radius of curvature for a non-ideal optical beam. *IEEE Journal of Quantum Electronics*, 27:1146–1148, May 1991. URL `http://ieeexplore.ieee.org/xpls/abs_all.jsp?isnumber=2717&arnumber=83370&count=23&index=9`. (Cited on page 27.)

[43] J.-F. Riou, W. Guerin, Y. Le Coq, M. Fauquembergue, V. Josse, P. Bouyer, and A. Aspect. Beam quality of a non-ideal atom laser. *Physical Review Letters*, 96:070404, 2006. (Cited on pages 27, 29, 30, and 35.)

[44] A. E. Siegman, G. Nemes, and J. Serna. How to (Maybe) Measure Laser Beam Quality. In *DPSS (Diode Pumped Solid State) Lasers: Applications and Issues*, page MQ1. Optical Society of America, 1998. URL http://www.opticsinfobase.org/abstract.cfm?URI=URI=DLAI-1998-MQ1. (Cited on page 28.)

[45] URL http://www.toptica.com/. (Cited on page 29.)

[46] URL http://www.innolight.de/. (Cited on page 29.)

[47] URL http://www.ipgphotonics.com/. (Cited on page 29.)

[48] D. Wright, P. Greve, J. Fleischer, and L. Austin. Laser beam width, divergence and beam propagation factor —an international standardization approach. *Optical and Quantum Electronics*, 24(9): S993–S1000, 1992. URL http://dx.doi.org/10.1007/BF01588600. (Cited on page 29.)

[49] International Organisation for Standardization. Lasers and laser-related equipment – Test methods for laser beam widths, divergence angles and beam propagation ratios. *ISO 11146-1:2005*, 2005. URL http://www.iso.org/iso/iso_catalogue/catalogue_tc/catalogue_detail.htm?csnumber=33625. (Cited on page 29.)

[50] Y. Le Coq, J. H. Thywissen, S. A. Rangwala, F. Gerbier, S. Richard, G. Delannoy, P. Bouyer, and A. Aspect. Atom laser divergence. *Physical Review Letters*, 87(17):170403, 2001. URL http://link.aps.org/doi/10.1103/PhysRevLett.87.170403. (Cited on pages 29 and 30.)

[51] G. Cennini, G. Ritt, C. Geckeler, and M. Weitz. All-Optical Realization of an Atom Laser. *Physical Review Letters*, 91(24):240408–+, December 2003. doi: 10.1103/PhysRevLett.91.240408. URL http://prola.aps.org/abstract/PRL/v91/i24/e240408. (Cited on pages 29, 79, and 87.)

[52] M. Köhl, T. Busch, K. Mølmer, T. W. Hänsch, and T. Esslinger. Observing the profile of an atom laser beam. *Phys. Rev. A*, 72 (6):063618–+, December 2005. doi: 10.1103/PhysRevA.72.063618. (Cited on pages 29 and 30.)

[53] J.-F. Riou. *Étude des propriétés de propagation d'un laser à atomes (Propagation on an atom laser)*. PhD thesis, Institut D'Optique, 2006. URL http://tel.archives-ouvertes.fr/docs/00/13/84/50/PDF/These_Jean-Felix_Riou.pdf. (Cited on pages 31, 49, 51, 52, and 66.)

[54] N. P. Robins, A. K. Morrison, J. J. Hope, and J. D. Close. Limits to the flux of a continuous atom laser. *Phys. Rev. A*, 72(3):031606–+, September 2005. doi: 10.1103/PhysRevA.72.031606. (Cited on page 30.)

[55] G. M. Moy, J. J. Hope, and C. M. Savage. Atom laser based on Raman transitions. *Phys. Rev. A*, 55(5):3631–3638, May 1997. doi: 10.1103/PhysRevA.55.3631. URL http://prola.aps.org/abstract/PRA/v55/i5/p3631_1. (Cited on pages 32 and 60.)

[56] J.-F. Riou, Y. Le Coq, F. Impens, W. Guerin, C. J. Bordé, A. Aspect, and P. Bouyer. Theoretical tools for atom-laser-beam propagation. *Physical Review A (Atomic, Molecular, and Optical Physics)*, 77(3):033630, 2008. doi: 10.1103/PhysRevA.77.033630. URL http://link.aps.org/abstract/PRA/v77/e033630. (Cited on pages 35 and 50.)

[57] Mattias Johnsson, Simon Haine, Joseph Hope, Nick Robins, Cristina Figl, Matthew Jeppesen, Julien Dugué, and John Close. Semiclassical limits to the linewidth of an atom laser. *Physical Review A*, 75(4):043618, 2007. doi: 10.1103/PhysRevA.75.043618. URL http://link.aps.org/abstract/PRA/v75/e043618. (Cited on page 35.)

[58] F. Gerbier, P. Bouyer, and A. Aspect. Quasicontinuous atom laser in the presence of gravity. *Physical Review Letters*, 86(21), 2001. URL http://link.aps.org/doi/10.1103/PhysRevLett.86.4729. (Cited on page 36.)

[59] R. G. Dall, L. J. Byron, A. G. Truscott, G. R. Dennis, M. T. Johnsson, M. Jeppesen, and J. J. Hope. Observation of transverse interference fringes on an atom laser beam. *Opt. Express*, 15(26):17673–17680, 2007. URL http://www.opticsexpress.org/abstract.cfm?URI=oe-15-26-17673. (Cited on page 36.)

[60] F. Dalfovo, L. Pitaevskii, and S. Stringari. Order parameter at the boundary of a trapped bose gas. *Phys. Rev. A*, 54(5):4213–4217, Nov 1996. doi: 10.1103/PhysRevA.54.4213. URL http://prola.aps.org/abstract/PRA/v54/i5/p4213_1. (Cited on pages 38 and 39.)

[61] K. Dieckmann. *Bose-Einstein Condensation with High Atom Number in a Deep Magentic Trap.* PhD thesis, Amsterdam, 2001. URL `http://www.amolf.nl/publications/theses/dieckmann/dieckmann.html`. (Cited on page 40.)

[62] C. J. Bordé. Theoretical tools for atom optics and interferometry. *C. R. Acad. Sci. Paris*, 4:509–530, 2001. (Cited on page 47.)

[63] T. Kramer, C. Bracher, and M. Kleber. Matter waves from quantum sources in a force field. *Journal of Physics A Mathematical General*, 35:8361–8372, October 2002. (Cited on page 47.)

[64] C. J. Bordé. Propagation of laser beams and of atomic systems. In J. Dalibard, editor, *Fundamental Systems in Quantum Optics.* Elsevier, 1991. (Cited on page 49.)

[65] Y. Le Coq. *Bose-Einstein condensates and atom lasers.* PhD thesis, Laboratoire Charles Fabry, 2002. (Cited on pages 49 and 50.)

[66] L. D. Landau and E. M. Lifchitz. *Course of Theoretical Physics: Quantum Mechanics*, volume 3. Pergamon Press, 1971. (Cited on page 50.)

[67] J. E. Lye. *Bose-Einstein Condensates.* PhD thesis, Australian National University, 2002. (Cited on page 55.)

[68] N. P. Robins. *Bose-Einstein condensation and the atom laser.* PhD thesis, Australian National University, 2004. (Cited on page 55.)

[69] K. Dieckmann, R. J. C. Spreeuw, M. Weidemüller, and J. T. M. Walraven. Two-dimensional magneto-optical trap as a source of slow atoms. *Phys. Rev. A*, 58(5):3891, 1998. (Cited on page 55.)

[70] W. Wohllebena, F. Chevy, K. Madison, and J. Dalibard. An atom faucet. *The European Physical Journal D*, 15:237–244, 2001. (Cited on page 55.)

[71] J. Schoser, R. Löw A. Batär, V. Schweikhard, A. Grabowski, Yu. B. Ovchinnikov, and T. Pfau. Intense source of cold Rb atoms from a pure two-dimensional magneto-optical trap. *Physical Review A*, 66:23410, 2002. (Cited on page 55.)

[72] Z. T. Lu, K. L. Corwin, M. J. Renn, M. H. Anderson, E. A. Cornell, and C. E. Wieman. Low-velocity intense source of atoms from a magneto-optical trap. *Phys. Rev. Lett.*, 77(16):3331–3334, Oct

1996. doi: 10.1103/PhysRevLett.77.3331. URL http://dxi.doi.org/10.1103/PhysRevLett.77.3331. (Cited on page 55.)

[73] J. Söding, D. Guéry-Odelin, P. Desbiolles, G. Ferrari, and J. Dalibard. Giant spin relaxation of an ultracold cesium gas. *Phys. Rev. Lett.*, 80(9):1869–1872, Mar 1998. doi: 10.1103/PhysRevLett.80.1869. URL http://prola.aps.org/abstract/PRL/v80/i9/p1869_1. (Cited on page 58.)

[74] Kendall B. Davis, Marc-Oliver Mewes, Michael A. Joffe, Michael R. Andrews, and Wolfgang Ketterle. Evaporative cooling of sodium atoms. *Phys. Rev. Lett.*, 74(26):5202–5205, Jun 1995. doi: 10.1103/PhysRevLett.74.5202. (Cited on page 58.)

[75] Wolfgang Petrich, Michael H. Anderson, Jason R. Ensher, and Eric A. Cornell. Stable, tightly confining magnetic trap for evaporative cooling of neutral atoms. *Phys. Rev. Lett.*, 74(17):3352–3355, Apr 1995. doi: 10.1103/PhysRevLett.74.3352. (Cited on page 58.)

[76] C. V. Sukumar and D. M. Brink. Spin-flip transitions in a magnetic trap. *Phys. Rev. A*, 56(3):2451–2454, Sep 1997. doi: 10.1103/PhysRevA.56.2451. URL http://dx.doi.org/10.1103/PhysRevA.56.2451. (Cited on page 58.)

[77] H. J. Lewandowski, D. M. Harber, D. L. Whitaker, and E. A. Cornell. Simplified System for Creating a Bose–Einstein Condensate. *Journal of Low Temperature Physics*, 132(5):309–367, 2003. URL http://dx.doi.org/10.1023/A:1024800600621. (Cited on page 58.)

[78] Markus Greiner, Immanuel Bloch, Theodor W. Hänsch, and Tilman Esslinger. Magnetic transport of trapped cold atoms over a large distance. *Phys. Rev. A*, 63(3):031401, Feb 2001. doi: 10.1103/PhysRevA.63.031401. (Cited on page 58.)

[79] W. Ketterle, D. S. Durfee, and D. M. Stamper-Kurn. Making, probing and understanding Bose-Einstein condensates. *ArXiv Condensed Matter e-prints*, April 1999. URL http://arxiv.org/abs/cond-mat/9904034v1. (Cited on pages 60, 80, 84, and 95.)

[80] M. Kozuma, L. Deng, E. W. Hagley, J. Wen, R. Lutwak, K. Helmerson, S. L. Rolston, and W. D. Phillips. Coherent Splitting of Bose-Einstein Condensed Atoms with Optically Induced Bragg Diffraction. *Physical Review Letters*, 82:871–875, February 1999. doi: 10.1103/PhysRevLett.82.871. (Cited on page 71.)

[81] Tino Weber, Jens Herbig, Michael Mark, Hanns-Christoph Nägerl, and Rudolf Grimm. Bose-Einstein Condensation of Molecules. *Science*, 302(5653):2101–2103, 2003. doi: 10.1126/science.1093280. URL http://www.sciencemag.org/cgi/content/abstract/302/5653/2101. (Cited on page 71.)

[82] M. Fattori, C. D'Errico, G. Roati, M. Zaccanti, M. Jona-Lasinio, M. Modugno, M. Inguscio, and G. Modugno. Atom Interferometry with a Weakly Interacting Bose-Einstein Condensate. *Physical Review Letters*, 100(8):080405, 2008. doi: 10.1103/PhysRevLett.100.080405. URL http://link.aps.org/abstract/PRL/v100/e080405. (Cited on page 71.)

[83] N. P. Robins, C. M. Savage, J. J. Hope, J. E. Lye, C. S. Fletcher, S. A. Haine, and J. D. Close. Fluctuations and flux: The limits of multistate atom lasers. *Phys. Rev. A*, 69(5):051602, May 2004. URL http://link.aps.org/abstract/PRA/v69/e051602. (Cited on page 71.)

[84] J. Dugué, N. P. Robins, C. Figl, M. Jeppesen, P. Summers, M. T. Johnsson, J. J. Hope, and J. D. Close. Investigation and comparison of multistate and two-state atom laser-output couplers. *Phys. Rev. A*, 75(5):053602–+, May 2007. doi: 10.1103/PhysRevA.75.053602. URL http://scitation.aip.org/getabs/servlet/GetabsServlet?prog=normal&id=PLRAAN000075000005053602000001&idtype=cvips&gifs=yes. (Cited on page 71.)

[85] L. Xia, F. Yang, X. Xu, X. Zhou, and X. Chen. The inherent fluctuations of the pulsed atom laser produced in the $F = 2$ manifold. *ArXiv e-prints*, February 2008. URL http://arxiv.org/abs/0802.0833. (Cited on page 71.)

[86] Anton Öttl, Stephan Ritter, Michael Kohl, and Tilman Esslinger. Hybrid apparatus for Bose-Einstein condensation and cavity quantum electrodynamics: Single atom detection in quantum degenerate gases. *Review of Scientific Instruments*, 77(6):063118, 2006. URL http://link.aip.org/link/?RSI/77/063118/1. (Cited on page 71.)

[87] W. Guerin, J.-F. Riou, J. P. Gaebler, V. Josse, P. Bouyer, and A. Aspect. Guided Quasicontinuous Atom Laser. *Physical Review Letters*, 97(20):200402–+, November 2006. doi: 10.1103/PhysRevLett.97.200402. (Cited on pages 76 and 77.)

[88] Y. Le Coq, J. A. Retter, S. Richard, A. Aspect, and P. Bouyer. Coherent matter wave inertial sensors for precision measurements in space. *Applied Physics B: Lasers and Optics*, 84:627–632, September 2006. doi: 10.1007/s00340-006-2363-2. URL http://www.springerlink.com/index/W57400102L33150Q.pdf. (Cited on page 76.)

[89] W. Guerin. *Source atomique cohérente dans des pièges optique et magnétique: réalisation d'un laser à atomes guidé (A coherent atomic source in a optical-magnetic trap: realisation of a guided atom laser).* PhD thesis, Institut D'Optique, 2007. URL http://hal.archives-ouvertes.fr/docs/00/14/63/75/PDF/These_WilliamGuerin.pdf. (Cited on page 77.)

[90] J. Billy, V. Josse, Z. Zuo, W. Guerin, A. Aspect, and P. Bouyer. Guided atom laser : a new tool for guided atom optics. *ArXiv e-prints*, 712, December 2007. URL http://arxiv.org/abs/0712.1482. (Cited on page 77.)

[91] Juliette Billy, Vincent Josse, Zhanchun Zuo, Alain Bernard, Ben Hambrecht, Pierre Lugan, David Clément, Laurent Sanchez-Palencia, Philippe Bouyer, and Alain Aspect. Direct observation of Anderson localization of matter waves in a controlled disorder. *Nature*, 453(7197):891–894, 2008. ISSN 0028-0836. doi: 10.1038/nature07000. URL http://dx.doi.org/10.1038/nature07000. (Cited on page 77.)

[92] Steven Chu, J. E. Bjorkholm, A. Ashkin, and A. Cable. Experimental observation of optically trapped atoms. *Phys. Rev. Lett.*, 57(3):314–317, Jul 1986. doi: 10.1103/PhysRevLett.57.314. (Cited on page 78.)

[93] M. D. Barrett, J. A. Sauer, and M. S. Chapman. All-Optical Formation of an Atomic Bose-Einstein Condensate. *Phys. Rev. Lett.*, 87(1):010404, Jun 2001. doi: 10.1103/PhysRevLett.87.010404. URL http://prola.aps.org/abstract/PRL/v87/i1/e010404. (Cited on page 78.)

[94] M. D. Barrett. *A QUEST for BEC: An all optical alternative.* PhD thesis, Georgia Institute of Technology, 2002. URL http://www.physics.gatech.edu/ultracool/Papers/Murray_Barrett_phd_thesis.pdf. (Cited on page 78.)

[95] B. P. Anderson and M. A. Kasevich. Macroscopic Quantum Interference from Atomic Tunnel Arrays. *Science*, 282(5394):1686–

1689, 1998. doi: 10.1126/science.282.5394.1686. URL http://www.sciencemag.org/cgi/content/abstract/282/5394/1686. (Cited on page 78.)

[96] G. Cennini. *Field-Insensitive Bose-Einstein Condensates and an All-Optical Atom Laser.* PhD thesis, Universität Tübingen, 2004. URL http://deposit.ddb.de/cgi-bin/dokserv?idn=972737421&dok_var=d1&dok_ext=pdf&filename=972737421.pdf. (Cited on pages 79, 87, and 97.)

[97] N. Lundblad, R. J. Thompson, D. C. Aveline, and L. Maleki. Spinor dynamics-driven formation of a dual-beam atom laser. *Opt. Express*, 14(22):10164–10170, 2006. URL http://www.opticsexpress.org/abstract.cfm?URI=oe-14-22-10164. (Cited on pages 79 and 100.)

[98] Nathan Eric Lundblad. *All-optical spinor Bose-Einstein condensation and the spinor dynamics-driven atom laser.* PhD thesis, California Institute of Technology, 2006. URL http://etd.caltech.edu/etd/available/etd-05242006-104400/. (Cited on pages 79 and 100.)

[99] T. Lahaye, Z. Wang, G. Reinaudi, S. P. Rath, J. Dalibard, and D. Guéry-Odelin. Evaporative cooling of a guided rubidium atomic beam. *Physical Review A (Atomic, Molecular, and Optical Physics)*, 72(3):033411, 2005. doi: 10.1103/PhysRevA.72.033411. URL http://link.aps.org/abstract/PRA/v72/e033411. (Cited on pages 79, 108, 111, and 130.)

[100] G. Reinaudi, T. Lahaye, A. Couvert, Z. Wang, and D. Guéry-Odelin. Evaporation of an atomic beam on a material surface. *Physical Review A (Atomic, Molecular, and Optical Physics)*, 73(3):035402, 2006. doi: 10.1103/PhysRevA.73.035402. URL http://link.aps.org/abstract/PRA/v73/e035402. (Cited on pages 79 and 108.)

[101] G. Reinaudi, Z. Wang, A. Couvert, T. Lahaye, and D. Guéry-Odelin. A moving magnetic mirror to slow down a bunch of atoms. *The European Physical Journal D - Atomic, Molecular, Optical and Plasma Physics*, 40(3):405–410, 2006. URL http://dx.doi.org/10.1140/epjd/e2006-00244-6. (Cited on page 79.)

[102] K. Bongs, S. Burger, S. Dettmer, D. Hellweg, J. Arlt, W. Ertmer, and K. Sengstock. Waveguide for Bose-Einstein condensates. *Phys. Rev. A*, 63(3):031602, Feb 2001. doi: 10.1103/PhysRevA.63.031602. URL

http://prola.aps.org/abstract/PRA/v63/i3/e031602. (Cited on page 79.)

[103] M. Key, I. G. Hughes, W. Rooijakkers, B. E. Sauer, E. A. Hinds, D. J. Richardson, and P. G. Kazansky. Propagation of cold atoms along a miniature magnetic guide. *Phys. Rev. Lett.*, 84(7):1371–1373, Feb 2000. doi: 10.1103/PhysRevLett.84.1371. URL http://prola.aps.org/abstract/PRL/v84/i7/p1371_1. (Cited on page 80.)

[104] A. E. Leanhardt, A. P. Chikkatur, D. Kielpinski, Y. Shin, T. L. Gustavson, W. Ketterle, and D. E. Pritchard. Propagation of Bose-Einstein Condensates in a Magnetic Waveguide. *Phys. Rev. Lett.*, 89(4):040401, Jul 2002. doi: 10.1103/PhysRevLett.89.040401. URL http://prola.aps.org/abstract/PRL/v89/i4/e040401. (Cited on page 80.)

[105] N. H. Dekker, C. S. Lee, V. Lorent, J. H. Thywissen, S. P. Smith, M. Drndić, R. M. Westervelt, and M. Prentiss. Guiding neutral atoms on a chip. *Phys. Rev. Lett.*, 84(6):1124–1127, Feb 2000. doi: 10.1103/PhysRevLett.84.1124. URL http://prola.aps.org/abstract/PRL/v84/i6/p1124_1. (Cited on page 80.)

[106] M. J. Renn, D. Montgomery, O. Vdovin, D. Z. Anderson, C. E. Wieman, and E. A. Cornell. Laser-guided atoms in hollow-core optical fibers. *Phys. Rev. Lett.*, 75(18):3253–3256, Oct 1995. doi: 10.1103/PhysRevLett.75.3253. URL http://prola.aps.org/pdf/PRL/v75/i18/p3253_1. (Cited on page 80.)

[107] S. Kuhr, W. Alt, D. Schrader, M. Müller, V. Gomer, and D. Meschede. Deterministic Delivery of a Single Atom. *Science*, 293:278–281, July 2001. doi: 10.1126/science.1062725. (Cited on page 81.)

[108] M. H. Anderson, W. Petrich, J.R. Ensher, and E. A. Cornell. Reduction of light-assisted collisional loss rate from a low-pressure vapor-cell trap. *Physical Review A*, 50:3597–+, November 1994. doi: 10.1103/PhysRevA.50.R3597. (Cited on page 83.)

[109] W. Ketterle, K. B. Davis, M. A. Joffe, A. Martin, and D. E. Pritchard. High densities of cold atoms in a dark spontaneous-force optical trap. *Physical Review Letters*, 70:2253–2256, April 1993. doi: 10.1103/PhysRevLett.70.2253. (Cited on page 83.)

[110] K. M. O'Hara, M. E. Gehm, S. R. Granade, and J. E. Thomas. Scaling laws for evaporative cooling in time-dependent optical

traps. *Phys. Rev. A*, 64(5):051403, Oct 2001. doi: 10.1103/PhysRevA.64.051403. URL http://prola.aps.org/abstract/PRA/v64/i5/e051403. (Cited on page 84.)

[111] M.-S. Chang, Q. Qin, W. Zhang, L. You, and M. S. Chapman. Coherent spinor dynamics in a spin-1 Bose condensate. *Nature Physics*, 1: 111–116, November 2005. doi: 10.1038/nphys153. URL http://www.nature.com/nphys/journal/v1/n2/abs/nphys153.html. (Cited on page 87.)

[112] M.-S. Chang. *Coherent Spin Dynamics of a Spin-1 Bose-Einstein Condensate.* PhD thesis, Georgia Institute of Technology, 2006. URL http://www.physics.gatech.edu/ultracool/Papers/Ming-Shien_Chang_phd_thesis.pdf. (Cited on page 87.)

[113] Tobias Kramer and Marcos Moshinsky. Tunnelling out of a time-dependent well. *Journal of Physics A: Mathematical and General*, 38(26):5993–6003, 2005. URL http://stacks.iop.org/0305-4470/38/5993. (Cited on page 92.)

[114] J. Kobayashi, Y. Izumi, M. Kumakura, and Y. Takahashi. Stable all-optical formation of Bose–Einstein condensate using pointing-stabilized optical trapping beams. *Applied Physics B: Lasers and Optics*, 83(1):21–25, 2006. URL http://dx.doi.org/10.1007/s00340-006-2140-2. (Cited on page 100.)

[115] B. Fröhlich, T. Lahaye, B. Kaltenhäuser, H. Kübler, S. Müller, T. Koch, M. Fattori, and T. Pfau. Two-frequency acousto-optic modulator driver to improve the beam pointing stability during intensity ramps. *Review of Scientific Instruments*, 78(4):043101, 2007. doi: 10.1063/1.2720725. URL http://link.aip.org/link/?RSI/78/043101/1. (Cited on page 100.)

[116] Gaël Reinaudi. *Vers l'obtention d'un laser à atomes continu (Towards a continuous atom laser).* PhD thesis, École Normale Superieure, 2008. URL http://www.cinephys.com/These_Reinaudi.pdf. (Cited on page 108.)

[117] Y. Castin, R. Dum, E. Mandonnet, A. Minguzzi, and I. Carusotto. Coherence properties of a continuous atom laser. *Journal of Modern Optics*, 47:2671–2695, January 2000. URL http://www.ingentaconnect.com/content/tandf/tmop/2000/00000047/F0020014/art00015. (Cited on page 109.)

[118] S. Dettmer, D. Hellweg, P. Ryytty, J. J. Arlt, W. Ertmer, K. Sengstock, D. S. Petrov, G. V. Shlyapnikov, H. Kreutzmann, L. Santos, and M. Lewenstein. Observation of phase fluctuations in elongated bose-einstein condensates. *Phys. Rev. Lett.*, 87(16):160406, Oct 2001. doi: 10.1103/PhysRevLett.87.160406. (Cited on page 110.)

[119] A. P. Chikkatur, Y. Shin, A. E. Leanhardt, D. Kielpinski, E. Tsikata, T. L. Gustavson, D. E. Pritchard, and W. Ketterle. A Continuous Source of Bose-Einstein Condensed Atoms. *Science*, 296:2193–2195, 2002. (Cited on pages 111 and 125.)

[120] S. Schmid, G. Thalhammer, K. Winkler, F. Lang, and J. Hecker Denschlag. Long-distance transport of ultracold atoms using a 1D optical lattice. *New. J. Phys.*, 8(159), 2006. (Cited on page 111.)

[121] F. Lattimore. Honours thesis, Australian National University, 2007. (Cited on page 111.)

[122] C. J. Myatt, E. A. Burt, R. W. Ghrist, E. A. Cornell, and C. E. Wieman. Production of Two Overlapping Bose-Einstein Condensates by Sympathetic Cooling. *Phys. Rev. Lett.*, 78(4):586–589, Jan 1997. doi: 10.1103/PhysRevLett.78.586. URL `http://prola.aps.org/abstract/PRL/v78/i4/p586_1`. (Cited on page 112.)

[123] Yutaka Yoshikawa, Toshiaki Sugiura, Yoshio Torii, and Takahiro Kuga. Observation of superradiant Raman scattering in a Bose-Einstein condensate. *Phys. Rev. A*, 69(4):041603, Apr 2004. doi: 10.1103/PhysRevA.69.041603. (Cited on page 113.)

[124] Dominik Schneble, Gretchen K. Campbell, Erik W. Streed, Micah Boyd, David E. Pritchard, and Wolfgang Ketterle. Raman Amplification of Matter Waves. *Phys. Rev. A*, 69(4):041601, Apr 2004. doi: 10.1103/PhysRevA.69.041601. (Cited on page 113.)

[125] Naomi S. Ginsberg, Sean R. Garner, and Lene Vestergaard Hau. Coherent control of optical information with matter wave dynamics. *Nature*, 445(7128):623–626, 2007. URL `http://dx.doi.org/10.1038/nature05493`. (Cited on page 113.)

[126] K. M. R. van der Stam, E. D. van Ooijen, R. Meppelink, J. M. Vogels, and P. van der Straten. Large atom number bose-einstein condensate of sodium. *Review of Scientific Instruments*, 78(1):013102, 2007. doi: 10.1063/1.2424439. URL `http://link.aip.org/link/?RSI/78/013102/1`. (Cited on page 130.)

[127] Mark Kasevich and Steven Chu. Laser cooling below a photon recoil with three-level atoms. *Phys. Rev. Lett.*, 69(12):1741–1744, Sep 1992. doi: 10.1103/PhysRevLett.69.1741. (Cited on page 130.)

[128] S. A. Haine, M. K. Olsen, and J. J. Hope. Generating Controllable Atom-Light Entanglement with a Raman Atom Laser System. *Physical Review Letters*, 96(13):133601–+, April 2006. doi: 10.1103/PhysRevLett.96.133601. (Cited on page 131.)

[129] H.-A. Bachor and T. C. Ralph. *A Guide to Experiments in Quantum Optics*. Wiley, 2003. (Cited on page 131.)

[130] S. A. Haine and J. J. Hope. Outcoupling from a bose-einstein condensate with squeezed light to produce entangled-atom laser beams. *Phys. Rev. A*, 72(3):033601, Sep 2005. doi: 10.1103/PhysRevA.72.033601. (Cited on page 131.)

[131] Mattias T. Johnsson and Simon A. Haine. Generating quadrature squeezing in an atom laser through self-interaction. *Physical Review Letters*, 99(1):010401, 2007. doi: 10.1103/PhysRevLett.99.010401. URL `http://link.aps.org/abstract/PRL/v99/e010401`. (Cited on page 131.)

[132] S. A. Haine and M. T. Johnsson. A dynamic scheme for generating number squeezing in Bose-Einstein condensates through nonlinear interactions. *ArXiv e-prints*, December 2008. (Cited on page 131.)

INDEX

COLOPHON

This thesis was typeset with LaTeX using Robert Slimbach's *Minion* typeface from Adobe. The layout is based upon André Miede's `classicthesis` template, with a few additions.

Final Version as of January 5, 2010.